

Air Force Institute of Technology

AFIT Scholar

Theses and Dissertations

Student Graduate Works

12-1983

Stochastic Estimation Applied to the Land Speed of Sound Record Attempt by a Rocket Car

David A. Reinholz

Follow this and additional works at: <https://scholar.afit.edu/etd>



Part of the [Aerospace Engineering Commons](#), and the [Applied Mathematics Commons](#)

Recommended Citation

Reinholz, David A., "Stochastic Estimation Applied to the Land Speed of Sound Record Attempt by a Rocket Car" (1983). *Theses and Dissertations*. 5675.

<https://scholar.afit.edu/etd/5675>

This Thesis is brought to you for free and open access by the Student Graduate Works at AFIT Scholar. It has been accepted for inclusion in Theses and Dissertations by an authorized administrator of AFIT Scholar. For more information, please contact AFIT.ENWL.Repository@us.af.mil.

AFIT/GAE/AA/83D-19

STOCHASTIC ESTIMATION APPLIED TO THE
LAND SPEED OF SOUND RECORD ATTEMPT
BY A ROCKET CAR

THESIS

David A. Reinholz
Captain, USAF

AFIT/GAE/AA/83D - 19

A. T. INSTITUTE OF TECHNOLOGY
ACADEMIC LIBRARY
TOLSON LANE HALL
AFIT/ID B-640 Area B
Wright-Patterson AFB, OH 45433

Approved for public release; distribution unlimited

Acknowledgments

I wish to thank several individuals who were instrumental in helping me complete this project. Dr. Peter S. Maybeck provided the motivation to use filtering theory in a practical application. His sequence of courses and textbooks on Stochastic Estimation and Control gave me a solid foundation in the subject. Captain James K. Hodge and Major David R. Audley were the first to interest me in the Budweiser Rocket Car and helped provide guidance throughout my work. The person with the most "corporate knowledge" about the rocket car tests at Edwards AFB is Captain David E. Hamilton, without whose help this report would not have been possible. Mr. Stan Musick of the Air Force Avionics Laboratory at Wright-Patterson AFB provided unlimited support and encouragement. Stan provided much practical guidance on developing a proper filter algorithm and implementation of available software. Thanks are due to Mrs. Sharon Maruna for her patience and excellence in typing the final copy of this report. Finally, I wish to thank my loving wife and family, without whose support and patience I could not have completed this work.

David A. Reinholz

Table of Contents

	<u>Page</u>
Acknowledgments	ii
List of Figures	v
List of Tables	ix
Abstract	x
I. Introduction	1
Filtering Theory	1
Application of Theory	3
Description of Rocket Car Test	3
Method of Analysis	10
II. Background Theory	11
Linear Kalman Filter	11
Extended Kalman Filter	14
Fixed-Interval Smoother	19
III. Modeling Techniques	22
System Model	22
Measurement Model	35
IV. Development and Performance Analysis of the Extended Kalman Filter	41
Accelerometer Calibration	43
Calculation of Measurement Noise Variance	53
Check of Filter Implementation	64
Extended Kalman Filter Performance Analysis	75
Results of One Iteration of the Extended Kalman Filter	79
V. Optimal Smoother Results	92
One Iteration of Smoother	93
Second Iteration of Smoother	107

Table of Contents

	Page
VI. Hypothesis Testing.	121
Development of Scalar Speed	
Standard Deviation.	121
Calculation of Peak Scalar Speed	
and Standard Deviation.	126
Hypothesis Test of Peak Speed	
and Confidence Level.	131
VII. Conclusions and Recommendations	133
Conclusions	133
Recommendations	139
Appendix A: Plots from Second Iteration of	
Extended Kalman Filter	142
Appendix B: Optimal Smoother Computer Program.	154
Bibliography.	170
Vita.	171

List of Figures

Figure	Page
i. Rocket Car.	xi
1.1 Rodgers Dry Lake Test Area.	5
3.1 Coordinate Frames of Reference.	23
3.2 Accelerometer Time History.	26
4.1 Extended Kalman filter estimate of x-position and standard deviation with accelerometer model for x velocity (no measurements).	45
4.2 Extended Kalman filter estimate of y-position and standard deviation with accelerometer model for x velocity (no measurements).	46
4.3 Extended Kalman filter estimate of x-velocity and standard deviation with accelerometer model for x velocity (no measurements).	47
4.4 Extended Kalman filter estimate of y-velocity and standard deviation with accelerometer model for x velocity (no measurements).	48
4.5 Extended Kalman filter estimate of accelerometer error and standard deviation with accelerometer model for x velocity (no measurements).	49
4.6 Extended Kalman filter estimate of range bias error and standard deviation with accelerometer model for x velocity (no measurements).	50
4.7 Extended Kalman filter estimate of azimuth bias error and standard deviation with accelerometer model for x velocity (no measurements).	51
4.8 Extended Kalman filter estimate of scalar speed converted to Mach (no measurements)	52
4.9 Residual range measurement based on a track heading of 180° true.	56
4.10 Residual azimuth measurement based on track heading of 180° true.	57

Figure		Page
4.10(a)	Corrected coordinate frames of reference. . . .	61
4.11	Residual range measurement based on a track heading of 179° true.	62
4.12	Residual azimuth measurement based on a track heading of 179° true.	63
4.13	Extended Kalman filter estimate of x-position with random walk model for x-velocity	67
4.14	Extended Kalman filter estimate of y-position with random walk model for x-velocity	69
4.15	Extended Kalman filter estimate of x-velocity with random walk model for x-velocity	71
4.16	Extended Kalman filter estimate of y-velocity with random walk model for x-velocity	73
4.17	Extended Kalman filter estimate of x-position and standard deviation incorporating range and azimuth measurements (first iteration).	80
4.18	Extended Kalman filter estimate of y-position and standard deviation incorporating range and azimuth measurements (first iteration).	81
4.19	Extended Kalman filter estimate of x-velocity and standard deviation incorporating range and azimuth measurements (first iteration).	82
4.20	Extended Kalman filter estimate of y-velocity and standard deviation incorporating range and azimuth measurements (first iteration).	83
4.21	Extended Kalman filter estimate of accelerometer error and standard deviation incorporating range and azimuth measurements (first iteration).	84
4.22	Extended Kalman filter estimate of range bias error and standard deviation incorporating range and azimuth measurements (first iteration).	85
4.23	Extended Kalman filter estimate of azimuth bias error and standard deviation incorporating range and azimuth measurements (first iteration).	86

Figure		Page
4.24	Residual measurements and residual standard deviations for first iteration of extended Kalman filter.	87
4.25	Extended Kalman filter estimate of scalar speed converted to Mach (first iteration). . . .	88
5.1	Smoother estimate and variance of x-position after one iteration.	94
5.2	Smoother estimate and variance of y-position after one iteration.	95
5.3	Smoother estimate and variance of x-velocity after one iteration.	96
5.4	Smoother estimate and variance of y-velocity after one iteration.	97
5.5	Smoother estimate and variance of accelerometer error after one iteration.	98
5.6	Smoother estimate and variance of range bias error after one iteration.	99
5.7	Smoother estimate and variance of azimuth bias error after one iteration.	100
5.8	Smoother estimate and variance of x-position after two iterations	108
5.9	Smoother estimate and variance of y-position after two iterations	109
5.10	Smoother estimate and variance of x-velocity after two iterations	110
5.11	Smoother estimate and variance of y-velocity after two iterations	111
5.12	Smoother estimate and variance of accelerometer error after two iterations	112
5.13	Smoother estimate and variance of range bias error after two iterations	113
5.14	Smoother estimate and variance of azimuth bias error after two iterations	114

Figure		Page
5.15	Vehicle trajectory in earth-fixed coordinate frame of reference after two iterations of the smoother.	115
6.1	Velocity vector and one sigma ellipse of constant likelihood	122
A.1	Residual range measurement based on track heading of 179.209° true.	144
A.2	Extended Kalman filter state estimate and standard deviation of x-position after two iterations.	145
A.3	Extended Kalman filter state estimate and standard deviation of y-position after two iterations.	146
A.4	Extended Kalman filter state estimate and standard deviation of x-velocity after two iterations.	147
A.5	Extended Kalman filter state estimate and standard deviation of y-velocity after two iterations.	148
A.6	Extended Kalman filter state estimate and standard deviation of accelerometer error after two iterations.	149
A.7	Extended Kalman filter state estimate and standard deviation of range bias error after two iterations.	150
A.8	Extended Kalman filter state estimate and standard deviation of azimuth bias error after two iterations.	151
A.9	Residual measurements and standard deviations after two iterations of extended Kalman filter.	152
A.10	Scalar speed estimate converted to Mach number after two iterations of the extended Kalman filter.	153

List of Tables

Table	Page
I. Filter Performance Analysis.	78
II. Comparison of First and Second Smoother Iterations	116
III. Speed Estimate at FIM Trap (18.65 seconds)	135
IV. Peak Scalar Speed Estimates.	135

Abstract

Optimal linear smoothing theory is applied to the data from the Speed of Sound record attempt of a three-wheeled rocket car on 17 December 1979. A forward-backward estimation method is used which employs a seven state forward-running extended Kalman filter and a Meditch-form backward recursive "fixed-interval" smoothing algorithm. Data for this analysis is supplied by a longitudinal accelerometer mounted on the vehicle and tracking radar measurements of range, azimuth, and elevation. States of interest include two components of vehicle position and velocity, accelerometer time-correlated error, and radar range and azimuth bias errors.

Two iterations of the forward-backward smoothing algorithm provide excellent convergence of state estimates and error variance. Based on this analysis a peak speed estimate of 1082.028 ft/sec or 1.008 Mach is obtained at 16.85 seconds from the start of the high speed run. After two iterations of the smoother the standard deviation of the peak speed estimate is reduced to 1.055 ft/sec. We conclude with a confidence level of nearly one, based on the assumptions and modeling techniques employed in this analysis, that the rocket car did, in fact, exceed the reference speed of sound on 17 December 1979.

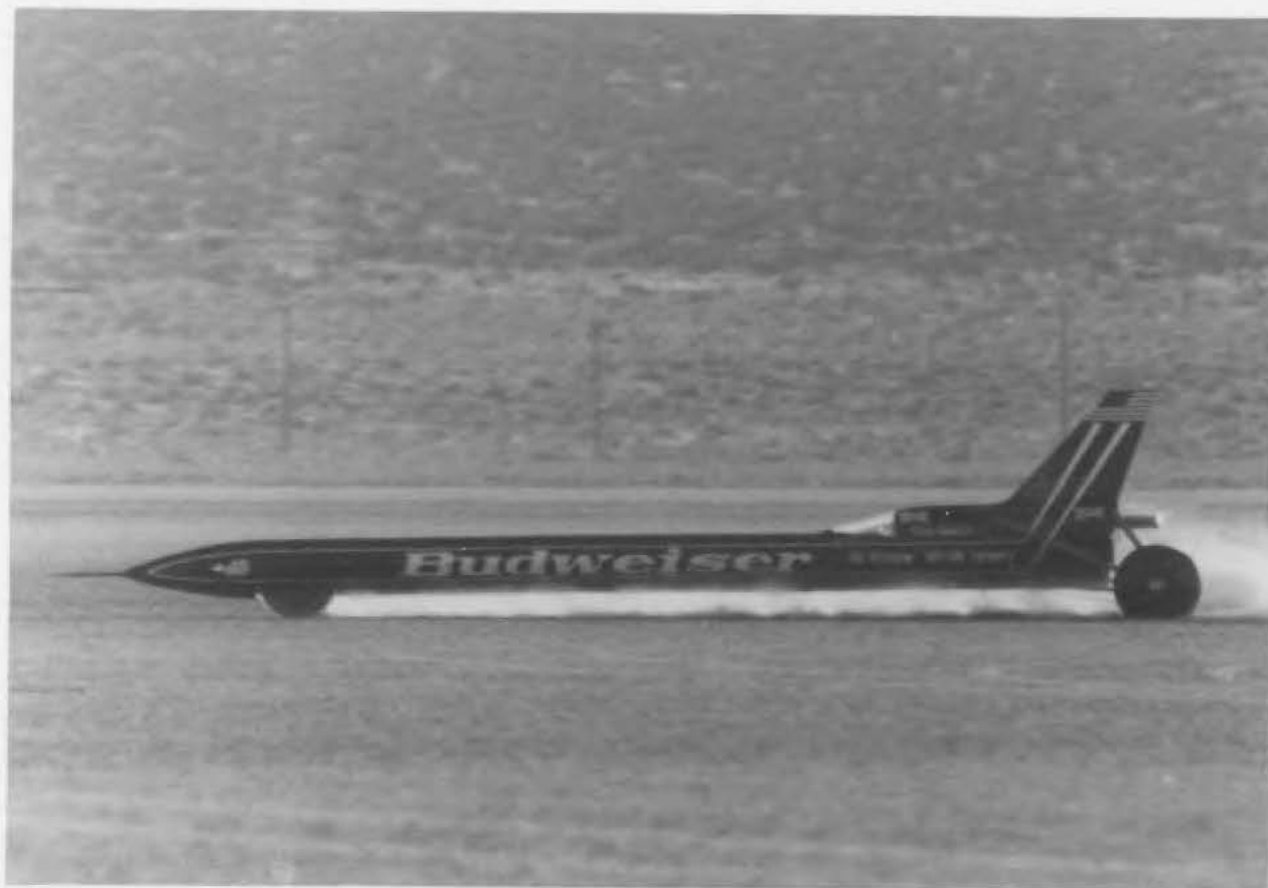


Fig. i - Rocket Car (Courtesy Mr. Ray VanAken)

STOCHASTIC ESTIMATION APPLIED TO THE
LAND SPEED OF SOUND RECORD ATTEMPT
BY A ROCKET CAR

I. Introduction

Filtering Theory

Any engineering problem inherently involves the use of measured or calculated information. The engineer bases his decisions on a variety of issues by using mathematical models of the "real world" to predict results obtained by experimentation. The mathematical models seldom describe every factor impacting a particular issue, but are simplifications in order to describe the most important characteristics of the problem and maintain tractability. Likewise, no measurement device can be considered "perfect", no matter what accuracy is claimed. How, then, does the engineer meet the ever-increasing demand for accuracy when he must rely on imperfect models and measurement devices?

One method for obtaining better answers is to model the important characteristics of a system and include the effects of model simplifications and measurement imperfections. This is the basic idea behind filtering theory, developed by several individuals, most notably Kalman. Filtering theory is concerned with estimating the "state" or status of a system of interest at any time, t_i , by incorporating the time

history of measurements up through time t_i . Another method of estimation, called the predictor algorithm, computes a state estimate at any time, t_i , based on the time history of measurements received before time, t_i . The "Kalman filter" algorithm combines both prediction of the state estimate before time t_i and correction of this predicted value based on the measurements received up through time t_i . With the advent of high-speed digital computers, the "Kalman filter" has proven to be very suitable in a number of applications most frequently in guidance and control problems. In this implementation, state estimates are generated in an "on-line" manner utilizing the measurement time history up through the time at which an estimate of state values is required. When the entire time history of measurements over a particular time interval of interest has been recorded, "off-line" estimation methods can be implemented. In this case, a "smoother" algorithm can be employed to generate state estimates based on all of the measurements, before and after any time t_i . Since the smoother algorithm has more information available for state estimation, it is the preferred method for post-run data analysis.

The Kalman filter algorithm requires a linear model to describe the dynamics of a particular system and a linear relationship between available measurements and the states of interest. More often than not, the system model or observation relationships are non-linear. This requires linearization about some reference values for the states as in the

"linearized Kalman filter", or re-linearization about the current state estimate provided by the "extended Kalman filter". The extended Kalman filter is most appropriate when the nominal (reference) state trajectory is unknown or when deviations from the nominal trajectory may become severe.

Application of Theory

The purpose of this report is to apply estimation theory in post-run data analysis of the "Budweiser Rocket Car" speed of sound attempt. The method used is to develop an extended Kalman filter to describe the vehicle dynamics and available measurements of vehicle position provided by a tracking radar. The events leading up to this unique event have been well documented in many publications, most notably Road and Track Magazine, April 1980. It is not my purpose here to provide a historical account of the "Budweiser Rocket Car" or to analyze Air Force involvement in this project. However, some brief background information may be helpful.

Description of Rocket Car Test

In the summer of 1979 a company known as Speed of Sound, Inc. (SOS) requested and received permission from the Air Force to use Rodgers Dry Lake at Edwards Air Force Base. Their purpose was to drive a rocket-powered land vehicle at the reference speed of sound. If successful, their rocket car would be the first to attain such a speed on land. The "Budweiser Rocket Car" was not designed for high sustained speeds due to very limited fuel storage capability and short

duration thrust augmentation (Sidewinder motor). The SOS plan was to reach peak speed very quickly and then slow to a stop. For these reasons, an official "land speed record" attempt would not be made. The Air Force Flight Test Center (AFFTC) provided a safe test area for conducting high speed runs. The speed runs were not allowed to impact in any way with normal operations at the base, and the government was reimbursed. At the request of SOS, the AFFTC provided computer analysis of the final high speed run.

The test track used for all the high speed runs at Edwards AFB began at the northwest corner of Rodgers Dry Lake (Fig. 1.1). The starting position varied but was located approximately 200 feet from the lake shore. The course followed a straight line on a heading of nearly true south from remote camera site A8 to the intersection of lakebed runways 17/35 and 15/33. From here it made a 12 degree turn to the right and followed runway 17 to the end. This turn began at about the seven mile point and had a radius of five miles. Use of the curve was required to take full advantage of the length of the lake and would only be used if the normal deceleration systems on the vehicle (parachute and brakes) failed. Every quarter mile along the course there were a pair of yellow flags mounted 30 feet either side of centerline to help guide the driver. Special red flags were used to signal the driver when to fire the thrust augmentation system. Approximately two miles from the starting position was a photoelectric "speed trap" system erected by the Federation Internationale

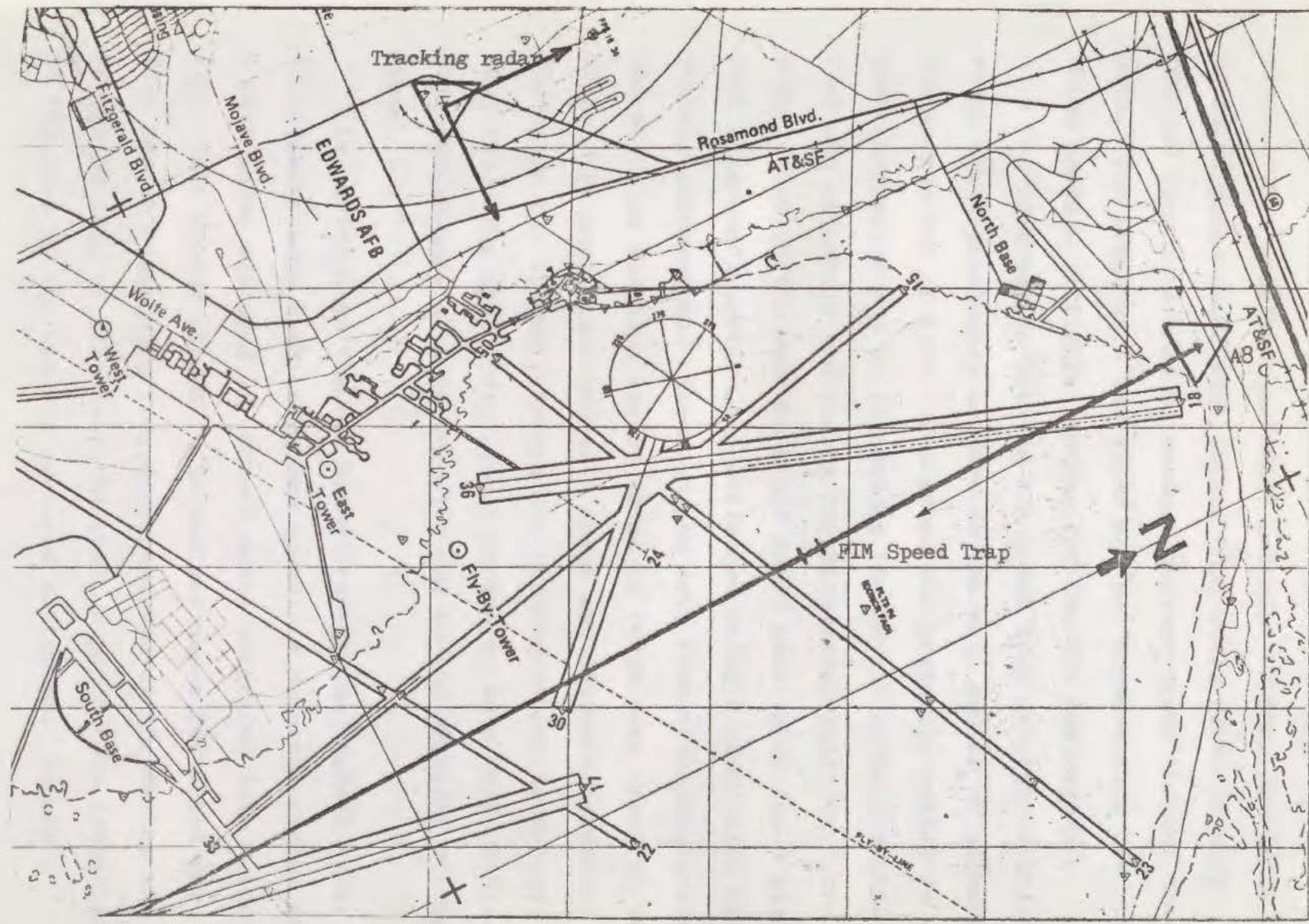


Fig. 1.1 Rodgers Dry Lake Test Area

des Motorcyclistes (FIM), official speed recorder for the event. The "trap" was actually a series of four precisely measured gates lined with lights that would flash at very precise time intervals to measure average speed through the gate. The traps were installed and not moved during the runs, which posed a difficult problem for the SOS engineers.

The idea was to hit the FIM speed trap at peak velocity which would presumably be just as the main engine or augmented system ran out of fuel. The speed was gradually raised on each successive run by increasing the amount of main engine fuel and adjusting the timing for Sidewinder ignition. The point at which the vehicle would reach peak speed for a given fuel load/configuration was estimated using a simulation of vehicle performance. Based on the data from this simulation, the starting position was adjusted to reach peak speed at the traps. In most cases the peak speed was seldom achieved at the traps but slightly before due to underestimated vehicle drag (3). The speed trap system proved to be a very unreliable measurement of peak velocity due to the problems stated above.

In addition to the FIM speed trap system several other instruments were used to record speed. A magnetic pickup on a rear wheel was used to convert wheel rotations into velocity. This device proved to be useless above 500 miles per hour due to inadequate frequency response of the device and a severe buildup of dirt over the run. A pitot tube installed on the nose of the vehicle measured air speed. Due to

compressibility errors near Mach one and the unknown influence of ground effect this device was not considered reliable (3). Longitudinal and lateral accelerations were measured by a set of accelerometers installed on the vehicle. Accelerometer data was not used to find velocity by the SOS engineers, only as a check on the number of acceleration units (g's) the driver was exposed to. Data from these devices were recorded via frequency modulated (FM) telemetry. An Air Force tracking radar was used to track the car and provide a backup of vehicle performance. This radar coverage was considered training for the operators and in no way impacted on any mission requirements at Edwards.

On the final day of the high speed runs, the fuel load on the vehicle was increased to maximum capacity and a Side-winder motor was installed. The run was set for early morning to take advantage of light winds and lower temperatures. Radar coverage was provided by a tracking radar located approximately 4.5 miles from the starting position on a hill overlooking Rodgers Dry Lake (Fig. 1.1). Temperature at the speed trap was recorded by an FIM official as 20 degrees Fahrenheit. Using the familiar relationship for the calculation of the reference speed of sound, a ,

$$a = \sqrt{\gamma RT} \quad (1-1)$$

where

γ ratio of specific heats for air = 1.4

R gas constant = 1715 ft²/sec²-R

T temperature in degrees Rankine = 479.66 R

we find

$$a = 1073.536213 \text{ ft/sec} = 931.956 \text{ mph}$$

The speed of sound depends primarily on the temperature of the air. The value at a given temperature can also vary due to changes in relative humidity. For this analysis, we have no information on the accuracy of the FIM temperature recording system, or relative humidity. Since the run was made in desert conditions we assume any changes to the calculated speed of sound due to relative humidity can be ignored. We also assume that the recorded temperature of 20 degrees is exact. The calculated speed of sound is used as a reference velocity to compare rocket car performance. A peak speed of 931.956 mph, therefore, was the goal of SOS people.

At 0726 Pacific Standard time the main rocket engine ignited, followed 12 seconds later by ignition of the Side-winder. The vehicle ran out of fuel about a fifth of a mile prior to the speed traps and thus was already decelerating as it passed through them. The four traps showed the vehicle speed to be 666.234 mph, 646.725 mph, 640.112 mph, and 632.522 mph, respectively (3). Since the speed trap measurements were made after the vehicle had reached peak speed they could not be used. The radar measurements would have to provide the estimate of top speed. Unfortunately, the radar range broke lock at the critical point during the run and followed a larger vehicle running parallel to the test track and approximately 1500 feet beyond the rocket car. After two seconds the radar again picked up the car. The Air Force

radar became the only check of actual vehicle performance with the FIM speed trap system unavailable and unreliable wheel speed and air speed indicators. The radar azimuth and elevation data were considered valid for the following reasons (3). The Air Force radar operator used a television monitor aligned with the axis of the radar dish and manually adjusted azimuth and elevation tracking rates. Using a set of "cross-hairs" on the monitor, the operator kept the car centered on the television screen. To attempt to correct the erroneous range data, another vehicle was driven over the tracks of the rocket car. The same tracking radar followed this vehicle and measured range and azimuth. Azimuth data from the rocket car and this second vehicle were aligned and a corrected range measurement for the rocket car was found. Based on this corrected range data, Air Force computer analysis showed three data points above the reference speed of sound, 731.96 mph. Speed of Sound, Inc. averaged these three points and claimed a maximum speed of 739.66 mph or 1.0106 Mach.

Speed of Sound, Inc. elected not to make any more high speed runs as the engineers felt they could get no more performance from the vehicle and the driver had complained of stability problems. Thus, the speed of 739.66 mph became the "official" figure that was claimed as the top speed of the "Budweiser Rocket Car".

Method of Analysis

The data available for this analysis includes raw radar range, azimuth, and elevation sampled at 20 points per second. Also we have the data from the longitudinal accelerometer which measured specific force continuously. The telemetry data for the accelerometer is digitized at 250 samples per second. Using these data sources, a model for the dynamics of the vehicle is developed and put in proper form for use in an extended Kalman filter algorithm. A measurement model for the radar measurements is used to relate the states of interest to the available measurements. To find the best estimate of vehicle performance with the lowest achievable error, a "fixed-interval" smoother algorithm is used. The filtering theory used in this analysis and specific modeling methods are developed in the next two chapters. Chapter IV will present the results of the extended Kalman filter, while Chapter V details two iterations of the extended Kalman filter-fixed interval smoother estimation scheme. Finally, Chapter VI will present a hypothesis test of the peak velocity estimate and give a confidence level for this estimate.

II. Background Theory

The problem as defined in Chapter I is to obtain better estimates of vehicle position and velocity by proper modeling of vehicle dynamics and measurement devices. By combining data from all measurement sources and including the effects of identifiable errors and noise through the use of a Kalman filter, one hopes to get improved state estimates. The standard form for the model to describe the dynamics of a problem for which a Kalman filter is to be developed is a first order vector differential equation. Generally, a discrete-time (sampled data) measurement model is used to relate observations to the states of interest. The basic Kalman filter equations will be presented here with little explanation. It is assumed that the reader is generally familiar with Kalman filtering. An excellent text on this subject is available by Maybeck (4).

Linear Kalman Filter

The basic equation to describe system dynamics has the following continuous-time form:

$$\dot{\underline{x}}(t) = \underline{f}[\underline{x}(t), \underline{u}(t), t] + \underline{G}(t)\underline{w}(t) \quad (2-1)$$

where

$\underline{x}(t)$ - n-state vector

$\underline{u}(t)$ - r-input vector (controls)

\underline{f} - dynamics vector (possibly non-linear)

$\underline{Q}(t)$ - time dependent coefficient matrix (n-by-s)

$\underline{w}(t)$ - zero-mean, white Gaussian noise s-vector of strength $\underline{Q}(t)$ such that

$$E[\underline{w}(t)\underline{w}(t+\tau)^T] = \underline{Q}(t)\delta(\tau) \quad (s\text{-by-}s) \quad (2-2)$$

where $\delta(\tau)$ is the Dirac delta function. Available discrete-time measurements are modeled by the following relation

$$\underline{z}(t_i) = \underline{h}[\underline{x}(t_i), t_i] + \underline{v}(t_i) \quad (2-3)$$

where

t_i - discrete measurement time

$\underline{z}(t_i)$ - m-vector of discrete measurements

\underline{h} - measurement model vector function (possibly non-linear)

$\underline{x}(t_i)$ - n-state vector

$\underline{v}(t_i)$ - zero mean, white, Gaussian discrete-time m-vector noise process, independent of system noise and of covariance $\underline{R}(t_i)$, i.e. such that

$$E[\underline{v}(t_i)\underline{v}(t_j)^T] = \underline{R}(t_i)\delta_{ij} \quad (m\text{-by-}m) \quad (2-4)$$

The initial condition on the state is only known with some uncertainty, and is modeled as a Gaussian random n-vector, assumed independent of $\underline{w}(t)$ and $\underline{v}(t_i)$, with mean and covariance:

$$E[\underline{x}(t_0)] = \hat{\underline{x}}_0 \quad (2-5)$$

$$E[(\underline{x}(t_0) - \hat{\underline{x}}_0)(\underline{x}(t_0) - \hat{\underline{x}}_0)^T] = \underline{P}_0 \quad (2-6)$$

The Kalman filter algorithm is most easily generated when the dynamics and measurement models are linear relationships. If the vectors \underline{f} and \underline{h} are linear combinations of the states, the dynamics model and measurement relation become linear relationships:

$$\dot{\underline{x}}(t) = \underline{F}(t)\underline{x}(t) + \underline{B}(t)\underline{u}(t) + \underline{G}(t)\underline{w}(t) \quad (2-7)$$

$$\underline{z}(t_i) = \underline{H}(t_i)\underline{x}(t_i) + \underline{v}(t_i) \quad (2-8)$$

where $\underline{F}(t)$ and $\underline{H}(t_i)$ become time-dependent (or possibly time invariant) coefficient matrices of dimensions n-by-n and m-by-n, respectively, and $\underline{B}(t)$ is an n-by-r matrix relating control inputs to the dynamics model.

The Kalman filter incorporates measurement updates using the following relations:

$$\underline{K}(t_i) = \underline{P}(t_i^-)\underline{H}^T(t_i)[\underline{H}(t_i)\underline{P}(t_i^-)\underline{H}^T(t_i) + \underline{R}(t_i)]^{-1} \quad (2-9)$$

$$\hat{\underline{x}}(t_i^+) = \hat{\underline{x}}(t_i^-) + \underline{K}(t_i)[\underline{z}_i - \underline{H}(t_i)\hat{\underline{x}}(t_i^-)] \quad (2-10)$$

$$\underline{P}(t_i^+) = \underline{P}(t_i^-) - \underline{K}(t_i)\underline{H}(t_i)\underline{P}(t_i^-) \quad (2-11)$$

where

t_i^- - before measurement update at time t_i

t_i^+ - after measurement update at time t_i

$\underline{K}(t_i)$ - Kalman filter gain matrix (m-by-n)

$\hat{\underline{x}}(t_i)$ - n-state estimate vector

\underline{z}_i - m vector of measurements

$\underline{P}(t_i)$ - error covariance matrix (n-by-n)

The state estimate and covariance are propagated forward to the next sample time from the initial condition, $\hat{\underline{x}}(t_{i-1}^+)$ and $\underline{P}(t_{i-1}^+)$ at time t_{i-1} , by integrating

$$\dot{\hat{\underline{x}}}(t/t_{i-1}) = \underline{F}(t)\hat{\underline{x}}(t/t_{i-1}) + \underline{B}(t)\underline{u}(t) \quad (2-12)$$

$$\begin{aligned} \dot{\underline{P}}(t/t_{i-1}) = & \underline{F}(t)\underline{P}(t/t_{i-1}) + \underline{P}(t/t_{i-1})\underline{F}^T(t) \\ & + \underline{G}(t)\underline{Q}(t)\underline{G}(t)^T \end{aligned} \quad (2-13)$$

where t/t_{i-1} , indicates integration forward from the previous measurement update time, t_{i-1} .

Extended Kalman Filter

The case where either the vector of dynamics relations, \underline{f} , or the measurement equation vector, \underline{h} , is non-linear in the states requires special consideration. The method most commonly used when system dynamics or measurement non-linearities exist is the "extended Kalman filter". The approach used in this method is to relinearize the dynamics and/or measurement equations about the most recent estimate of the state, $\hat{\underline{x}}(t_i^-)$, at update time, or $\hat{\underline{x}}(t/t_{i-1})$ in the ensuing sample period. Thus, the matrices \underline{F} , \underline{H} , \underline{K} , and \underline{P} are evaluated by knowing the most recent estimate of the nominal (reference) state trajectory.

The system matrix, $\underline{F}(t)$, in (2-13) and observation matrix, $\underline{H}(t_i)$ in (2-9) and (2-11) become partial derivative matrices in the extended Kalman filter:

$$\underline{F}[t; \hat{\underline{x}}(t/t_{i-1})] = \frac{\partial \underline{f}[\underline{x}(t); \underline{u}(t), t]}{\partial \underline{x}} \bigg|_{\underline{x} = \hat{\underline{x}}(t/t_{i-1})} \quad (2-14)$$

$$\underline{H}[t_i; \hat{\underline{x}}(t_i^-)] = \frac{\partial \underline{h}[\underline{x}(t_i), t_i]}{\partial \underline{x}} \bigg|_{\underline{x} = \hat{\underline{x}}(t_i^-)} \quad (2-15)$$

In equations (2-14) and (2-15) the differentiation is done so that the derivative of a scalar with respect to a column vector is a row vector. The matrices resulting from this differentiation have dimensions n-by-n and m-by-n, respectively. These matrices relate small perturbations in the state vector, $\underline{x}(t)$, to changes in the equations for $\dot{\underline{x}}(t)$ and $\underline{z}(t_i)$. The \underline{F} matrix is called the "filter dynamics partial matrix" and the \underline{H} matrix the "measurement sensitivity matrix". Defining the perturbation of the state, $\underline{x}(t)$, from its current estimate, $\hat{\underline{x}}(t_i^-)$ as

$$\delta \underline{x}(t) \triangleq \underline{x}(t) - \hat{\underline{x}}(t_i^-) \quad (2-16)$$

the perturbation $\delta \underline{x}(t)$ is called the error state while $\underline{x}(t)$ is the full state.

We expand equations (2-1) for $\dot{\underline{x}}(t)$ and (2-3) for $\underline{z}(t_i)$ in a Taylor series about the current state estimate in powers of $\delta \underline{x}(t)$. Since $\delta \underline{x}(t)$ is assumed small, powers of $\delta \underline{x}(t)$ higher than one are ignored. We arrive at the following linearized perturbation equations in $\delta \underline{x}(t)$:

$$\dot{\delta \underline{x}}(t) = \underline{F}[t; \hat{\underline{x}}(t/t_{i-1})] \delta \underline{x}(t) + \underline{G}(t) \underline{w}(t) \quad (2-17)$$

$$\underline{\delta z}(t_i) = \underline{H}[t_i; \hat{\underline{x}}(t_i^-)] \underline{\delta x}(t_i) + \underline{v}(t_i) \quad (2-18)$$

where \underline{F} and \underline{H} are defined as in (2-14) and (2-15), respectively.

Equations (2-17) and (2-18) are in the proper form for use in a conventional filter. Thus, an estimate $\hat{\underline{\delta x}}(t_i^+)$ of the error state $\underline{\delta x}(t)$ can be made from perturbation measurements, $\underline{\delta z}(t_i)$, using equations (2-9) through (2-11). The measurement difference $\underline{\delta z}(t_i)$ is called the residual. It is formed by subtracting the predicted measurements $\hat{\underline{z}}(t_i)$ from the actual measurements $\underline{z}(t_i)$:

$$\underline{\delta z}(t_i) = \underline{z}_i - \underline{h}[\hat{\underline{x}}(t_i^-), t_i] \quad (2-19)$$

Equation (2-10) provides an updated estimate of the error state, $\hat{\underline{\delta x}}(t_i^+)$. By using equation (2-16) we can obtain an updated estimate of the whole value state, $\hat{\underline{x}}(t_i^+)$:

$$\hat{\underline{x}}(t_i^+) = \hat{\underline{x}}(t_i^-) + \hat{\underline{\delta x}}(t_i^+) \quad (2-20)$$

This equation places all of the available information into the whole-value state estimate. This allows $\hat{\underline{\delta x}}(t_i^+)$ to be reset to zero for propagation of the state estimate to the next update time. At any time, t_i , $\underline{\delta x}(t)$ has a conditional mean, $\hat{\underline{\delta x}}(t_i)$, and conditional covariance $\underline{P}_\delta(t_i)$ such that:

$$E[\underline{\delta x}(t_i) | \underline{z}(t_i)] = \hat{\underline{\delta x}}(t_i) \quad (2-21)$$

and

$$E[\underline{\delta x}(t_i) - \hat{\underline{\delta x}}(t_i) [\underline{\delta x}(t_i) - \hat{\underline{\delta x}}(t_i)]^T | \underline{Z}(t_i)] = \underline{P}_\delta(t_i) \quad (2-22)$$

where $\underline{Z}(t_i)$ is defined as the entire measurement history up through time t_i . If we assume a zero mean initial condition on the error state,

$$\hat{\underline{\delta x}}(t_0) = \underline{0} \quad (2-23)$$

then $\hat{\underline{\delta x}}(t)$ will be zero over the entire interval between updates such that:

$$\hat{\underline{\delta x}}(t) = 0 \quad \text{for} \quad t_{i-1} \leq t \leq t_i \quad (2-24)$$

With $\hat{\underline{\delta x}}(t_i^-)$ zero, the error state update equation from (2-10)

$$\hat{\underline{\delta x}}(t_i^+) = \hat{\underline{\delta x}}(t_i^-) + \underline{K}(t_i) \underline{\delta z}(t_i) \quad (2-25)$$

simplifies to

$$\hat{\underline{\delta x}}(t_i^+) = \underline{K}(t_i) \underline{\delta z}(t_i) \quad (2-26)$$

which upon substitution into the full state update equation (2-20) produces

$$\hat{\underline{x}}(t_i^+) = \hat{\underline{x}}(t_i^-) + \underline{K}(t_i) \underline{\delta z}(t_i) \quad (2-27)$$

where $\underline{\delta z}(t_i)$ is given by (2-19).

Consider the conditional covariance, $\underline{P}_\delta(t_i)$ of the error state, $\underline{\delta x}(t)$, given by (2-21). We wish to relate this conditional covariance to the conditional covariance, $\underline{P}(t_i)$ of the whole state, $\underline{x}(t)$. From (2-21)

$$\begin{aligned} \underline{P}_\delta(t_i) &= E[\underline{\delta x} - \hat{\underline{\delta x}}][\underline{\delta x} - \hat{\underline{\delta x}}]^T | \underline{Z}(t_i)] \\ &= E[\underline{\delta x}][\underline{\delta x}]^T | \underline{Z}(t_i)] \quad \text{from (2-24)} \end{aligned}$$

$$\begin{aligned}
&= E[\underline{\hat{x}} - \underline{x}][\underline{\hat{x}} - \underline{x}]^T | \underline{z}(t_i)] \quad \text{from (2-16)} \\
&= \underline{P}(t_i)
\end{aligned}$$

Thus, the error covariance of $\underline{x}(t)$ is identical to that of $\underline{\delta x}(t)$. Equations (2-13) and (2-11) describe the propagation and update of the error state covariance, $\underline{P}(t)$, with $\underline{F}(t)$ and $\underline{H}(t)$ in these equations replaced by equations (2-14) and (2-15), respectively.

The extended Kalman filter algorithm is summarized here. The measurement vector at time $t_i, \underline{z}(t_i)$, is incorporated using

$$\begin{aligned}
\underline{K}(t_i) &= \underline{P}(t_i^-) \underline{H}^T[t_i; \underline{\hat{x}}(t_i^-)] \times \\
&\quad [\underline{H}[t_i; \underline{\hat{x}}(t_i^-)] \underline{P}(t_i^-) \underline{H}^T[t_i; \underline{\hat{x}}(t_i^-)] + \underline{R}(t_i)]^{-1} \quad (2-28)
\end{aligned}$$

$$\underline{\hat{x}}(t_i^+) = \underline{\hat{x}}(t_i^-) + \underline{K}(t_i) [\underline{z}_i - \underline{h}[\underline{\hat{x}}(t_i^-), t_i]] \quad (2-29)$$

$$\underline{P}(t_i^+) = \underline{P}(t_i^-) - \underline{K}(t_i) \underline{H}[t_i; \underline{\hat{x}}(t_i^-)] \underline{P}(t_i^-) \quad (2-30)$$

The estimate is propagated forward to the update time, t_i , from the previous update time, t_{i-1} , by integrating

$$\dot{\underline{\hat{x}}}(t/t_{i-1}) = \underline{f}[\underline{\hat{x}}(t/t_{i-1}), \underline{u}(t), t] \quad (2-31)$$

and

$$\begin{aligned}
\dot{\underline{P}}(t/t_{i-1}) &= \underline{F}[t; \underline{\hat{x}}(t/t_{i-1})] \underline{P}(t/t_{i-1}) + \underline{P}(t/t_{i-1}) \underline{F}^T[t; \underline{\hat{x}}(t/t_{i-1})] \\
&\quad + \underline{G}(t) \underline{Q}(t) \underline{G}(t)^T \quad (2-32)
\end{aligned}$$

from time t_{i-1} to t_i , using the initial conditions provided by:

1. The first step is to identify the problem. This involves understanding the current situation and what needs to be changed.

[illegible]

LEVEL SHOOT

[illegible]

\mathcal{L}

\mathcal{L}

the combined forward/backward filter scheme can

$\underline{P}(t_i)$

$= \underline{P}$

the smoothed estimate is generated backward in time using

$$\hat{\underline{x}}(t_i/t_f) = \hat{\underline{x}}(t_i^-) + \underline{A}(t_i) [\hat{\underline{x}}(t_{i+1}/t_f) - \hat{\underline{x}}(t_{i+1}^-)] \quad (2-39)$$

where the "smoothing estimator gain matrix" $\underline{A}(t_i)$ is given by

$$\underline{A}(t_i) = \underline{P}(t_i^+) \underline{\Phi}^T(t_{i+1}, t_i) \underline{P}^{-1}(t_{i+1}^-) \quad (2-40)$$

and $\underline{\Phi}(t_{i+1}, t_i)$ is the state transition matrix for propagating adjoint system quantities backward in time (4).

The covariance of the zero mean Gaussian estimation error $[\underline{x}(t_i) - \hat{\underline{x}}(t_i/t_f)]$ can be generated backward from the boundary condition by

$$\underline{P}(t_i/t_f) = \underline{P}(t_i^+) + \underline{A}(t_i) [\underline{P}(t_{i+1}/t_f) - \underline{P}(t_{i+1}^-)] \underline{A}^T(t_i) \quad (2-41)$$

The method of analysis chosen to analyze available data from the rocket car is to develop such a "fixed-interval smoother" algorithm based on the state trajectory (time history) generated from an extended Kalman filter. The extended Kalman filter will be shown as the appropriate choice due to non-linear measurement relations. The amount of pseudo-noise is adjusted to achieve optimum filter performance in a "tuning" process described more fully in Chapter IV. The next chapter describes the methods used to model vehicle dynamics, errors to be estimated, and available measurements for implementation in an extended Kalman filter.

III. Modeling Techniques

System Model

The test track described in Chapter I has no surveyed positions from which to reference vehicle position. The best information on the starting position is provided by the radar which was set on the vehicle for several minutes before the start of the high speed run. It is this position provided by the radar to which changes in vehicle position are referenced.

The coordinate system for the dynamics of the rocket car is chosen as a Cartesian system fixed at the starting point of the run. This system is shown in Fig. 3.1 and has the x-axis aligned with the straight portion of the test track (true south) and the y-axis aligned with true east. The time interval of interest is the first 24 seconds of the run, as the vehicle achieved its maximum velocity at approximately 17 seconds into the run. Thus, the velocity and position along the x and y axis is taken with respect to a fixed position on the earth corresponding to an inexact starting position. The elevation of the car is ignored due to minimal change in vertical displacement (± 20 feet). Therefore, the coordinate frame we are concerned with becomes planar or two-dimensional. Post-run inspection of the test track indicated that the vehicle deviated very little from track centerline (3). Therefore, y components of position and velocity are minimal with the motion restricted to the x-axis almost entirely.

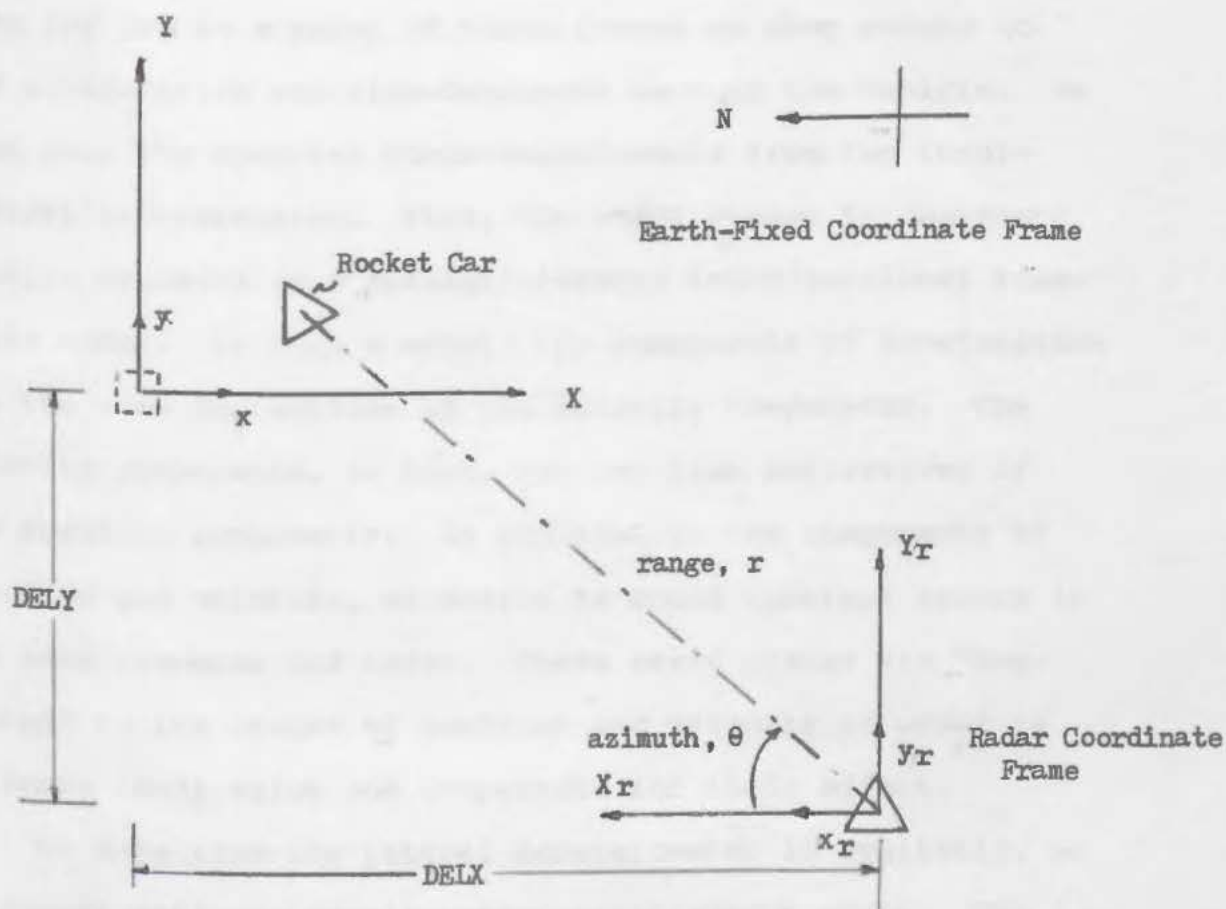


Fig. 3-1(a). Top View of Coordinate Systems

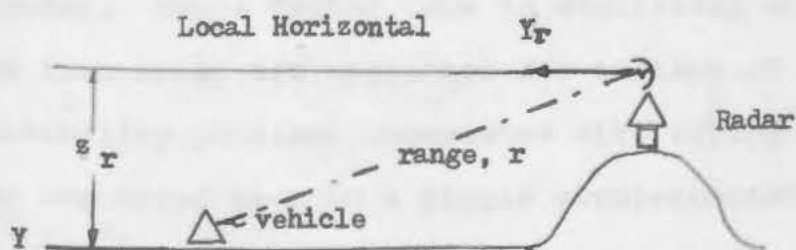


Fig. 3-1(b). Side View of Coordinate Systems

the only assumed inaccuracies in these measurements. Thus, the additional states to be estimated include one error state for the accelerometer, and two error states for the radar. Lack of additional measurements and resulting observability problems precluded the identification of any other errors. It will be shown in the next chapter that even these states are only weakly observable.

The states to be estimated become:

- x_1 - position component along x-axis
- x_2 - position component along y-axis
- x_3 - velocity along x-axis
- x_4 - velocity along y-axis
- x_5 - longitudinal accelerometer time-correlated error
- x_6 - radar range bias error
- x_7 - radar azimuth bias error

The first four states are related by deterministic means (i.e., velocity is the first derivative of position, etc.). The error states are modeled as stochastic processes in the following manner.

The time-correlated error of the accelerometer is modeled as a first order Gauss-Markov process, the output of a first order lag, which is driven by white, Gaussian noise. Figure 3.2 shows the output of the longitudinal accelerometer indicating the extreme fluctuations in specific force sensed by this device. Such rapid fluctuations are due to extreme vibrations caused by rough ground and engine "pulsing" (3). Conceivably, the accelerometer error state can also vary

[REDACTED]

[illegible]

ce

WC

The first order differential vector dynamics model for the propagation of the seven states of interest plus additive "driving" noise becomes:

$$\dot{x}_1(t) = x_3$$

$$\dot{x}_2(t) = x_4$$

$$\dot{x}_3(t) = a_x + x_5(t)$$

$$\dot{x}_4(t) = w_4(t)$$

$$\dot{x}_5(t) = -1/T x_5(t) + w_5(t)$$

$$\dot{x}_6(t) = w_6(t)$$

$$\dot{x}_7(t) = w_7(t)$$

Here $\underline{w}(t)$ is a white Gaussian vector noise process of strength $\underline{Q}(t)$ over the time interval $[t_o, t_f]$. Off-line "tuning" of the system noise matrix, $\underline{Q}(t)$, can be used to match the available data as closely as desired. This was not done in this analysis. Instead, the noise matrix, $\underline{Q}(t)$ is adjusted "on-line" in a performance analysis in order to achieve lowest possible variance in the state estimates. The results of this tuning process are detailed in the next chapter.

In the system model presented above the longitudinal accelerometer output a_x is used to "drive" the propagation of the x component of velocity. The output of the accelerometer is corrupted by a time correlated error which is expected to vary frequently during the run. With no lateral accelerometer data available, we assume the y velocity component, x_4 , is well modeled as a constant with zero value. A

[illegible][illegible]

1/T 5

_____ $\frac{n}{y}$ _____ $\frac{n}{y}$ _____

The first of these is the fact that the

 second of these is the fact that the

 third of these is the fact that the

 fourth of these is the fact that the

 fifth of these is the fact that the

 sixth of these is the fact that the

 seventh of these is the fact that the

 eighth of these is the fact that the

 ninth of these is the fact that the

 tenth of these is the fact that the

$$E_L = -\frac{m}{x} \left(\frac{1}{x} - \frac{1}{x_0} \right)$$

m

ψ

$n_x(0)$

$n_x(0)$

$$e^{-[t_1-t_2]/T}$$

ca

ψ_{xx}

[illegible][illegible]

[REDACTED] at [REDACTED]

$$+q_5 T/2[1-e^{-2(t-t_0)/T}];$$

The only information available on the longitudinal accelerometer is calibration data taken before and after the high speed run of the rocket car. This data indicates that the accelerometer calibration varied by an average of .003 g's between the two calibration checks. With no more information on the inherent errors in the accelerometer, we are forced to refer to information on comparable models. We desire a comparable accelerometer which has a specified bias error on the order of .003 g's. The model chosen in this case is a Honeywell solid-state low-cost accelerometer. The specified RMS error for this model is listed at .005g. Thus, we use this specified error as the steady-state deviation in error of the accelerometer actually used in this test run. Obviously, we need to vary this value in order to check filter performance, but .005g will serve as a "first-guess". We now can solve for the driving noise, q_5

$$P_5(\infty) = (.005g)^2 = q_5 T / 2 \quad (3-13c)$$

and

$$q_5(t) = 2(.005g)^2 = .0518 \text{ (ft/sec}^2\text{)}^2/\text{sec} \quad (3-13d)$$

Choosing the initial variance, $P_5(0)$, to be equal to the steady-state variance, $P_5(\infty)$, results in a "stationary" process (4) for the accelerometer error state, x_5 . This stationary characteristic is, in fact, implemented in the system model for the rocket car.

The initial condition of the state vector at the start of the run is known only with some uncertainty and is

modeled as a Gaussian random variable of zero-mean and covariance, \underline{P}_0 , such that:

$$E[\underline{x}(t_0)] = \hat{\underline{x}}_0 = \underline{0} \quad (3-14)$$

$$E[(\underline{x}(t_0) - \hat{\underline{x}}_0)(\underline{x}(t_0) - \hat{\underline{x}}_0)^T] = \underline{P}_0 \quad (3-15)$$

Initially, our uncertainty in the state values is very high.

We choose the following values for \underline{P}_0 :

$$\underline{P}_0 = \begin{bmatrix} 10000 & & & & & & \\ & 10000 & & & & & \\ & & 100 & \underline{0} & & & \\ & & 100 & & & & \\ \underline{0} & & & .0259 & & & \\ & & & & 225 & & \\ & & & & & .25E-6 & \end{bmatrix} \quad (3-16)$$

The initial guess on the last three diagonal elements is obtained by using specified Root Mean Squared (RMS) errors for the accelerometer, range, and azimuth respectively:

$$P_{05} = (.005g)^2 = .0259 \text{ [ft/sec}^2\text{]}^2$$

$$P_{06} = (15 \text{ ft})^2 = 225 \text{ ft}^2$$

$$P_{07} = (.0005 \text{ rad})^2 = .25E - 6 \text{ rad}^2$$

The initial variances of the first four states are subjective values based on relatively high uncertainty in state values. Having developed the dynamics model for propagating the states of interest, it is now necessary to relate these

[illegible]

1998

[The following text is heavily blurred and illegible.]

[REDACTED]
 [REDACTED]
 [REDACTED]
 [REDACTED]
 [REDACTED]

[REDACTED]
[REDACTED]
[REDACTED]
[REDACTED] 1 [REDACTED] [REDACTED] [REDACTED]
[REDACTED] et [REDACTED] [REDACTED]
[REDACTED]
[REDACTED]

[REDACTED]
[REDACTED]
[REDACTED]
[REDACTED] 9 [REDACTED]
[REDACTED]
[REDACTED]

[REDACTED]
[REDACTED]
[REDACTED]

[REDACTED]
[REDACTED]
[REDACTED] li [REDACTED]
[REDACTED] la [REDACTED]
[REDACTED] r [REDACTED]

[REDACTED] i [REDACTED]
[REDACTED] ry [REDACTED]
[REDACTED]

th

$$\leq$$

I+

2

ef

5

H

 $(1,6)$

УГ

1

Thus, the extended Kalman filter incorporates the measurements at time, t_i by using:

$$\underline{K}(t_i) = \underline{P}(t_i^-) \underline{H}^T [\underline{H} \underline{P}(t_i^-) \underline{H}^T + \underline{R}(t_i)]^{-1} \quad (3-25)$$

$$\hat{\underline{x}}(t_i^+) = \hat{\underline{x}}(t_i^-) + \underline{K}(t_i) \delta \underline{z}(t_i) \quad (3-26)$$

$$\underline{P}(t_i^+) = \underline{P}(t_i^-) - \underline{K}(t_i) \underline{H} \underline{P}(t_i^-) \quad (3-27)$$

where $\delta \underline{z}(t_i)$ is given by:

$$\delta \underline{z}(t_i) = \begin{bmatrix} \delta z_1(t_i) \\ \delta z_2(t_i) \end{bmatrix} = \begin{bmatrix} z_1 - [[(\text{DELX} - \hat{x}_1^-)^2 + (\text{DELY} + \hat{x}_2^-)^2 + z_r^2] + \hat{x}_6^-] \\ z_2 - [\arctan [(\text{DELY} + \hat{x}_2^-) / (\text{DELX} - \hat{x}_1^-)] + \hat{x}_7^-] \end{bmatrix} \quad (3-28)$$

The state estimate at time t_{i-1} is propagated forward to the next sample time t_i by integrating:

$$\dot{\hat{\underline{x}}}(t/t_{i-1}) = \begin{bmatrix} \hat{x}_3(t/t_{i-1}) \\ \hat{x}_4(t/t_{i-1}) \\ \hat{x}_5(t/t_{i-1}) + a_x \\ 0 \\ -1/Tx_5(t/t_{i-1}) \\ 0 \\ 0 \end{bmatrix} \quad (3-29)$$

The error covariance $\underline{P}(t/t_{i-1})$ is propagated forward by integrating equation (2-32) in which

$$\underline{E}[\underline{\hat{x}}(t/t_{i-1})] = \begin{bmatrix} 0 & 0 & 1 & 0 & 0 & 0 & 0 \\ 0 & 0 & 0 & 1 & 0 & 0 & 0 \\ 0 & 0 & 0 & 0 & 1 & 0 & 0 \\ 0 & 0 & 0 & 0 & 0 & 0 & 0 \\ 0 & 0 & 0 & 0 & 0 & -1/T & 0 \\ 0 & 0 & 0 & 0 & 0 & 0 & 0 \\ 0 & 0 & 0 & 0 & 0 & 0 & 0 \end{bmatrix} \quad \text{by} \quad (2-14)$$

The initial value for the system noise matrix in (2-32) is chosen as:

$$\underline{Q}(t) = \begin{bmatrix} 0 & & & & & & \\ & 0 & & & & & \\ & & 0 & & & & \\ & & & .01 & & & \\ & 0 & & .0518 & & & \\ & & & & 1 & & \\ & & & & & 0.1E-7 & \end{bmatrix} \quad (3-30)$$

The initial values for the diagonal elements of $\underline{Q}(t)$ are chosen to indicate our relative uncertainty of the behavior of the corresponding states over the time interval of interest. The initial value for driving noise on the accelerometer error state, x_5 , has been previously calculated (3-13d). The remaining diagonal elements of $\underline{Q}(t)$ are chosen by subjectively deciding how much these states will vary from constant values. By comparing $Q_{44}(t)$, $Q_{66}(t)$ and $Q_{77}(t)$ one can see that we have little doubt that the azimuth bias error, x_7 , is a constant. We are less certain about the behavior of the y velocity, x_4 , and even more uncertain about the range bias error state, x_6 . The initial value for $Q_{44}(t)$ is based on our knowledge of the rocket car trajectory -

described as nearly a straight line along the x-axis (3). We do not expect the y velocity to vary significantly from a constant value of zero. Use of the radar in a "look-down" mode increases our uncertainty in how the range bias state, x_6 , will behave over the 24 second interval. The azimuth bias error is not expected to vary significantly from the behavior of a constant. The initial value for $Q(t)$ presented in (3-30) is adjusted in a "tuning" process to achieve lowest possible variance values for the seven states of interest. This performance analysis is detailed in the next chapter along with the results of the seven state extended Kalman filter developed here.

IV. Development and Performance Analysis of the Extended Kalman Filter

The previous chapters have developed an extended Kalman Filter estimation algorithm for post-run data analysis of the Budweiser Rocket Car. This chapter describes the results obtained by using the seven state filter outlined previously. The amount of computer programming required by this analysis is minimal due to existing software available for the development of a Kalman filter.

The computer software used in this analysis is a Monte Carlo Simulation for Optimal Filter Evaluation (SOFE) available at Wright-Patterson AFB (6,7). The program was developed under contract by the Air Force Avionics Laboratory (AFAL) and is well documented by Musick (6). SOFE is invaluable when designing Kalman Filters. The normal method used is a Monte Carlo analysis (4) whereby a suboptimal (reduced order) Kalman filter is evaluated against a "truth model". The suboptimal filter is adjusted to achieve the best possible performance when compared to a much higher order "truth model". The idea is to track the important characteristics of a physical system adequately using a simpler model. Such a reduced order filter could then be implemented in an operational system where computer capability may be limited.

For the purpose of analyzing the rocket car data, SOFE is used to integrate the dynamics equations and update the

states of interest at measurement times. There is no truth model available for tuning purposes, nor do we have the ability to generate sample statistics. SOFE implements the Kalman filter equations for either the linear or extended Kalman filter presented in Chapter II. The user simply specifies the dynamics and measurement relations for his system. SOFE propagates the state and covariance estimates forward from the specified initial time, using a fifth order Kutta-Merson integration algorithm (6). Updates of state and covariance estimates based on available measurements are provided at user-specified intervals. The user can specify any number of measurements to be incorporated at a given update time. Use of SOFE greatly reduces the amount of computer programming necessary in developing a Kalman filter and allows the user to concentrate on the finer details of his particular problem.

The fifth-order Kutta-Merson integrator implemented in SOFE requires a step-size no greater than approximately two milliseconds for the chosen integration tolerances. The integrator uses a variable step size to automatically maintain the integration error below a specified value. The user can specify a fixed step size mode if exterior factors, such as a high measurement rate, cause the step size to remain small regardless of dynamics. If, in order to handle severe dynamics, the integrator reduces its step size to a minimum specified value without satisfying error tolerances, an integration failure occurs and the program stops. The default

parameters for the integrator are variable step size, error tolerance of .0001, maximum step size of $1.0 \text{ E} + 9$, minimum step size of .0001, and initial step size of .01. We are unsure of exact vehicle dynamics but expect rapid changes in acceleration over a very short time interval. We desire to allow the integrator to automatically adjust its step size in order to reduce integration error and avoid "stepping-over" any fluctuations in the solution. A variable step size also reduces computer time. For these reasons, we interpolate the accelerometer data to .002 second intervals for integration purposes.

SOFE implements user-supplied data records from one external tape and expects the same number of records every time the tape is read. The external data provided for the rocket car includes accelerometer, range, azimuth, and elevation data. This data is interpolated to .002 second intervals using the cubic spline interpolator implemented in SOFE. Thus, accelerometer data for integration purposes is available every .002 seconds while the specified measurement update interval of .05 seconds insures that actual, not interpolated values for the radar measurements are used.

Accelerometer Calibration

The first run through the data using SOFE is made to check the calibration of the accelerometer data. The seven state extended Kalman filter as implemented in SOFE is run without incorporating any radar measurements. Integration

of accelerometer data provides state estimates of x position and velocity. We desire to compare the estimate of x velocity

ch

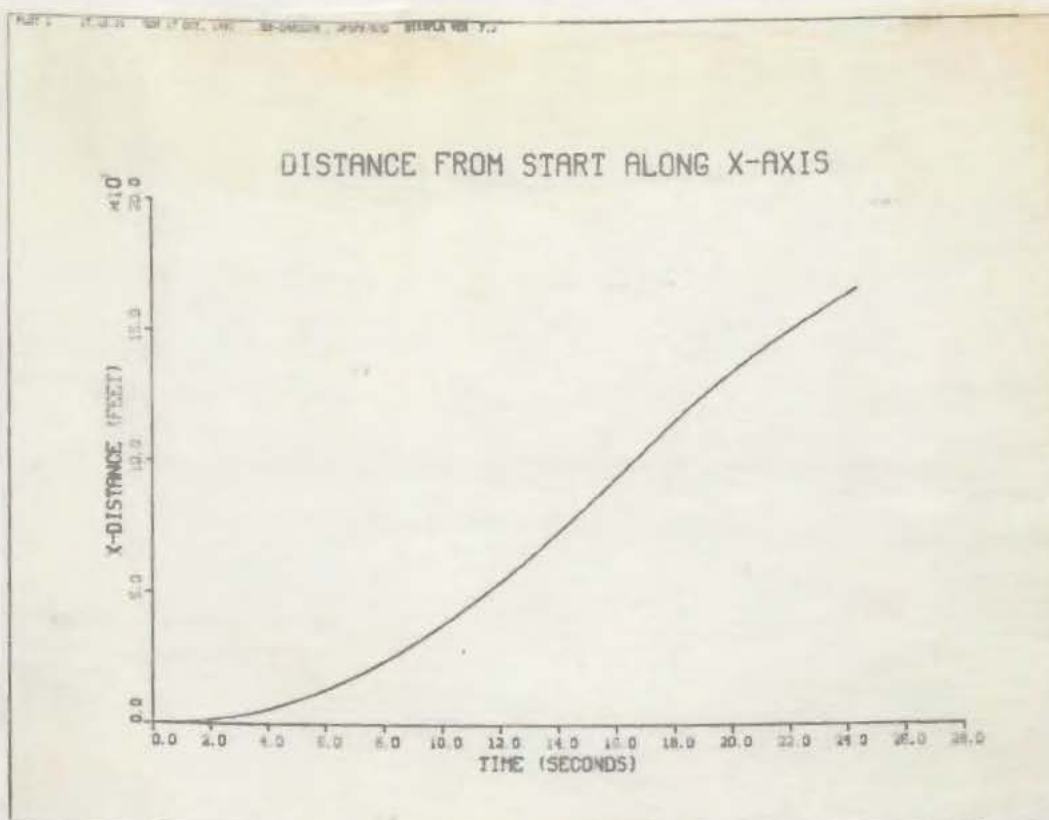
bee

ma

on

el

(a)



(b)

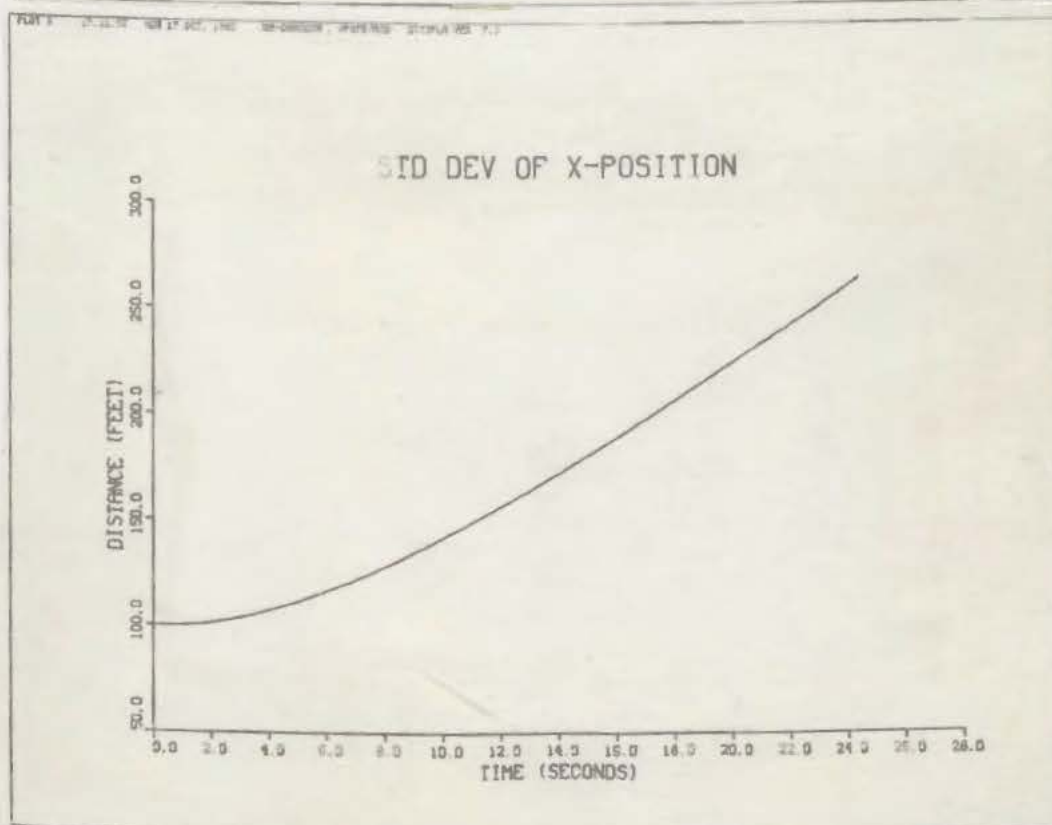
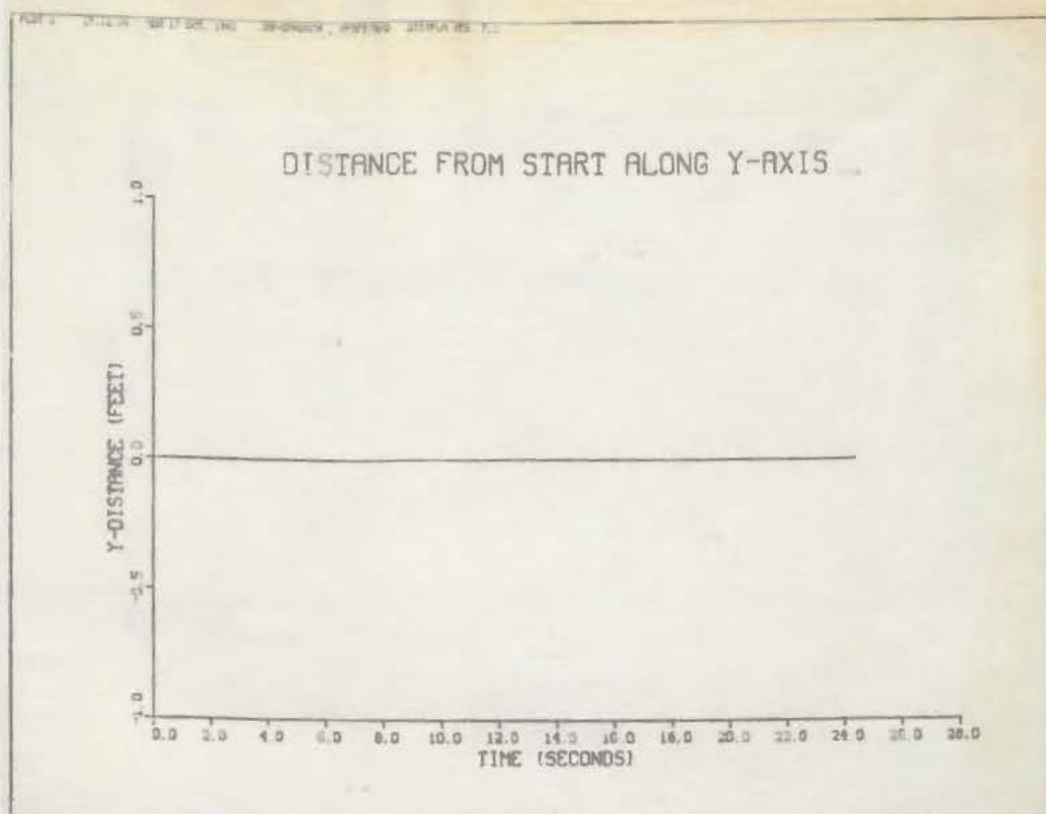


Fig. 4.1(a),(b) Accelerometer model for x_3 - No measurements

(a)



(b)

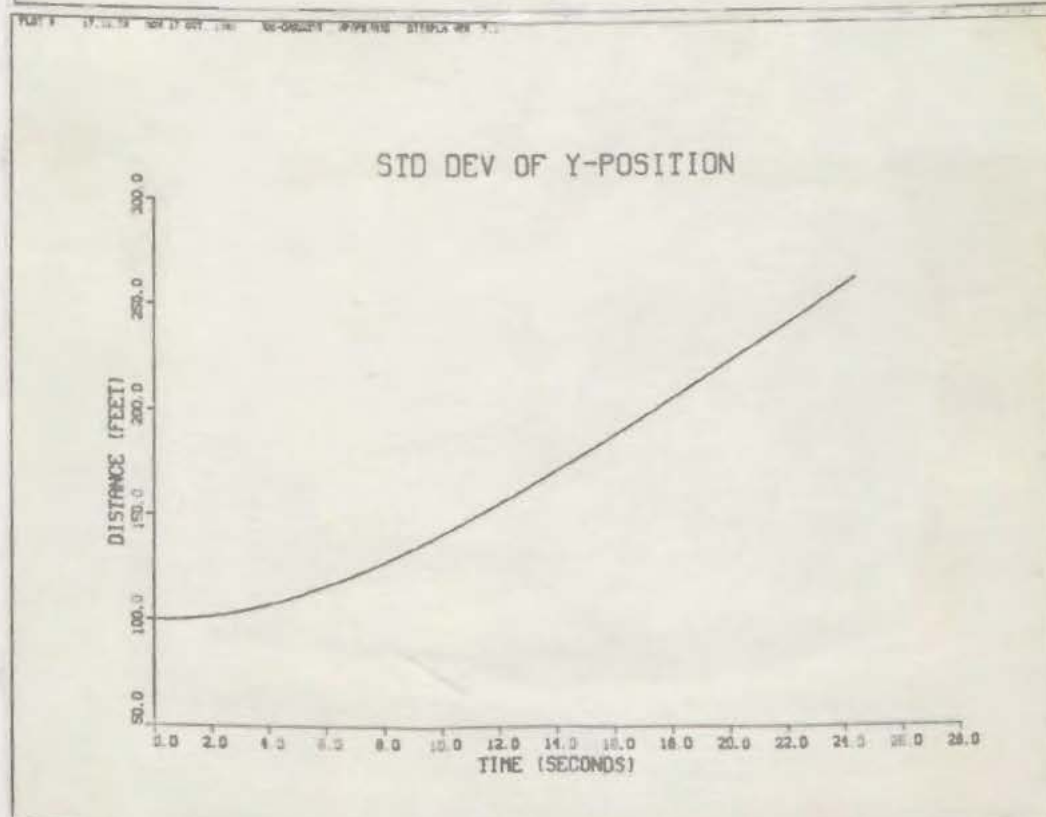
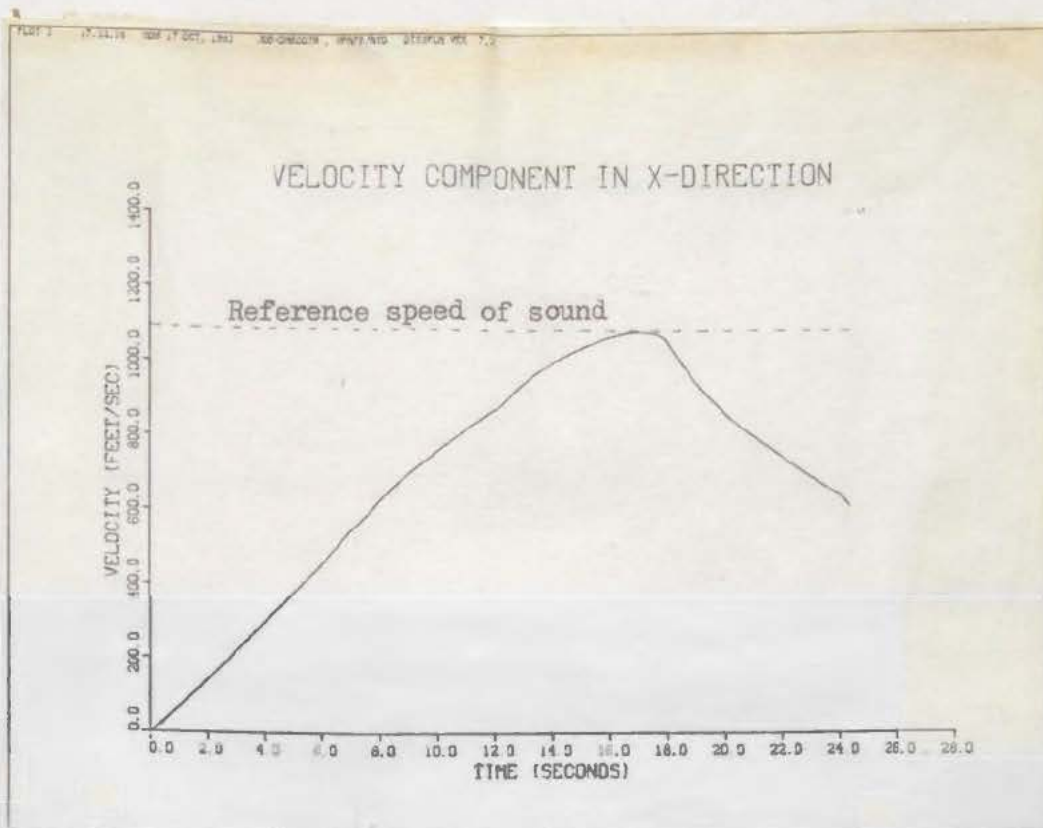


Fig.4.2(a),(b) Accelerometer model for x_3 - No measurements

(a)



(b)

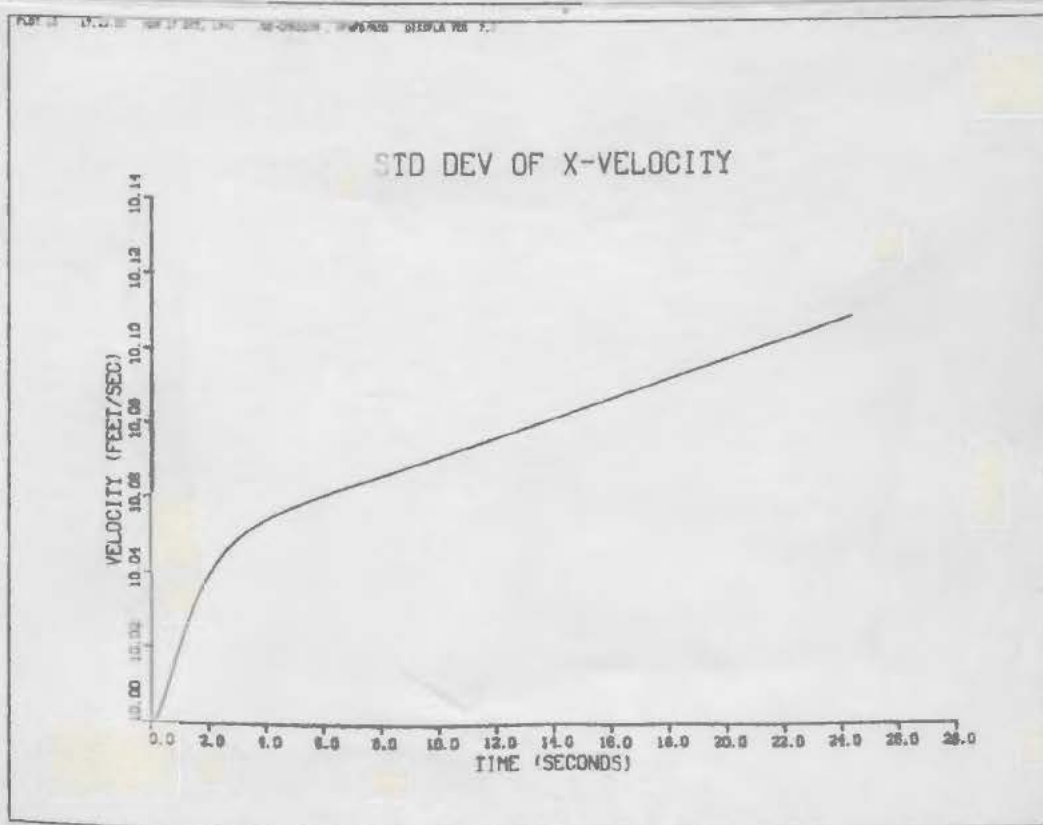
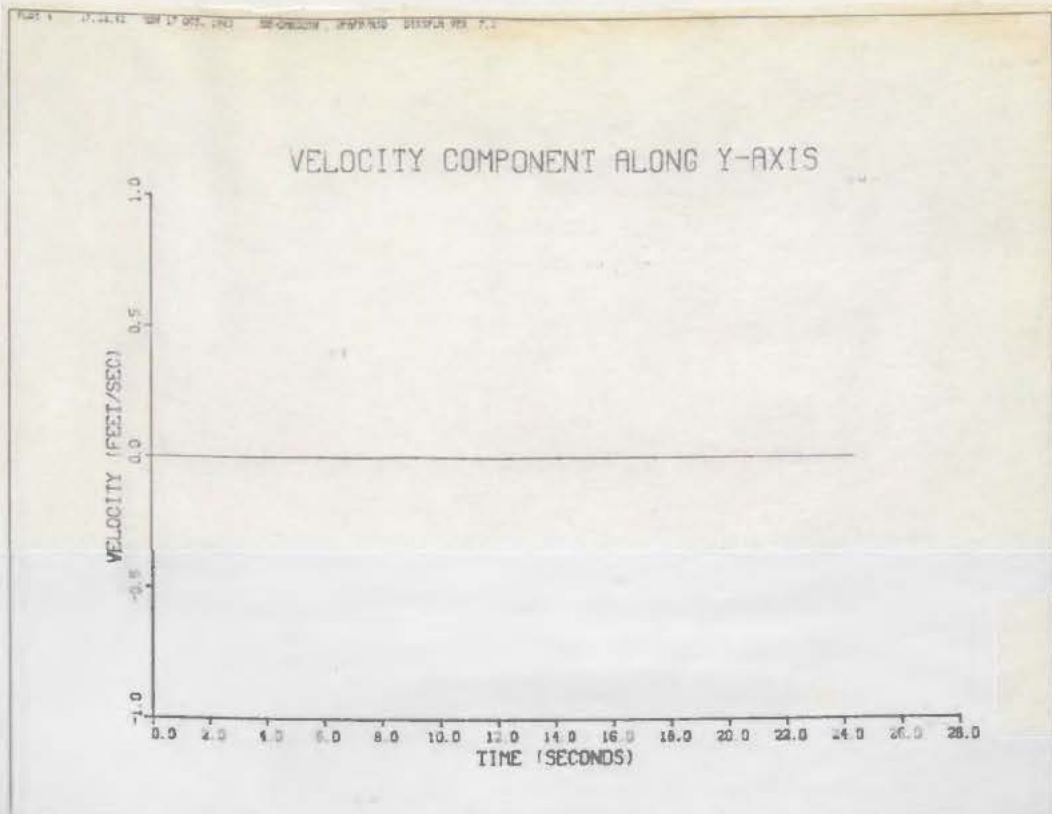


Fig. 4.3(a),(b) Accelerometer model for x_3 - No measurements

(a)



(b)

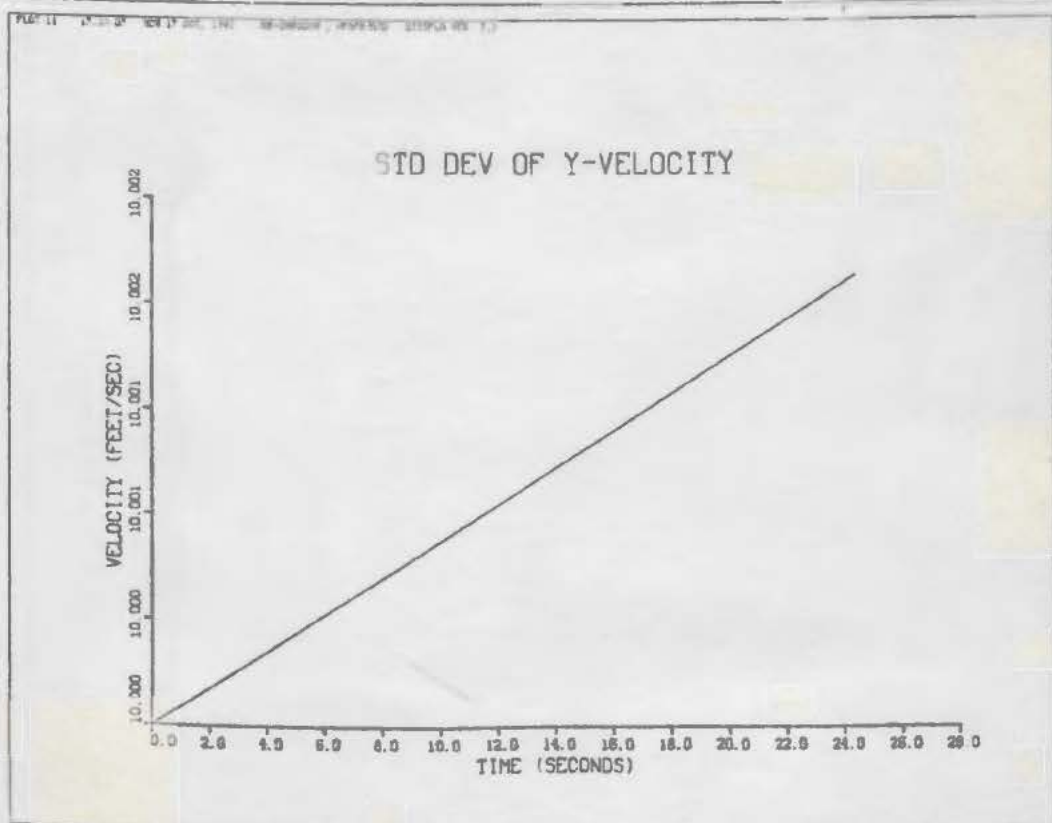
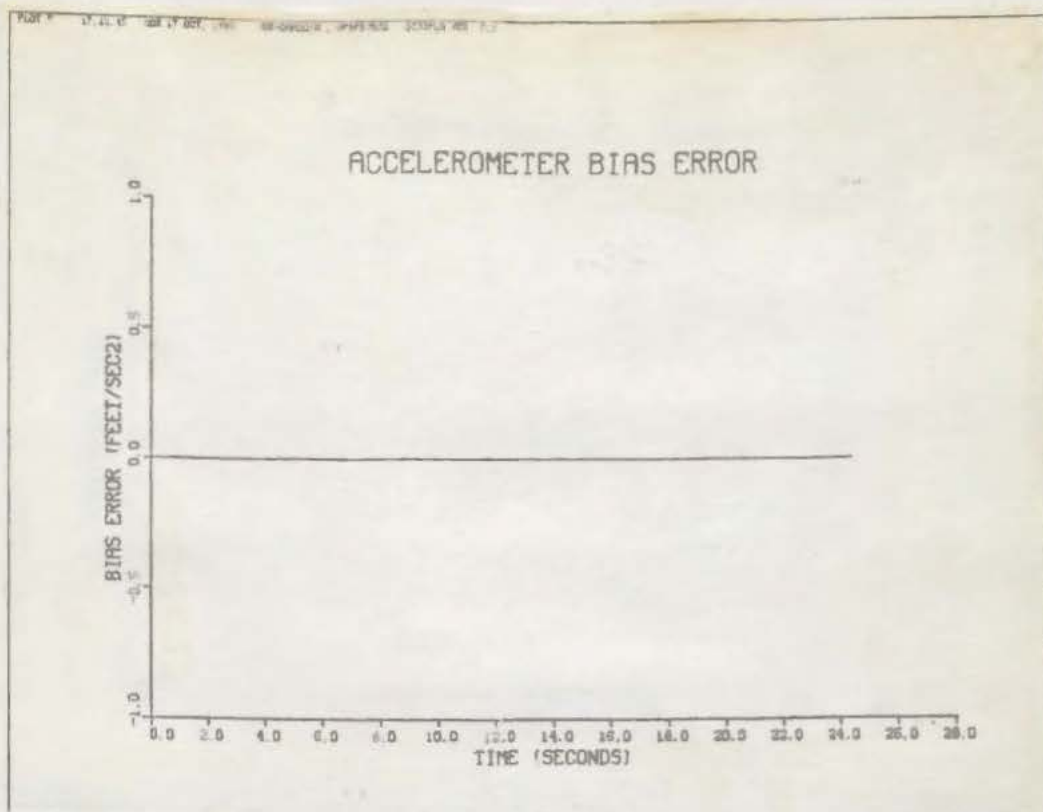


Fig. 4.4(a),(b) Accelerometer model for x_3 - No measurements

(a)



(b)

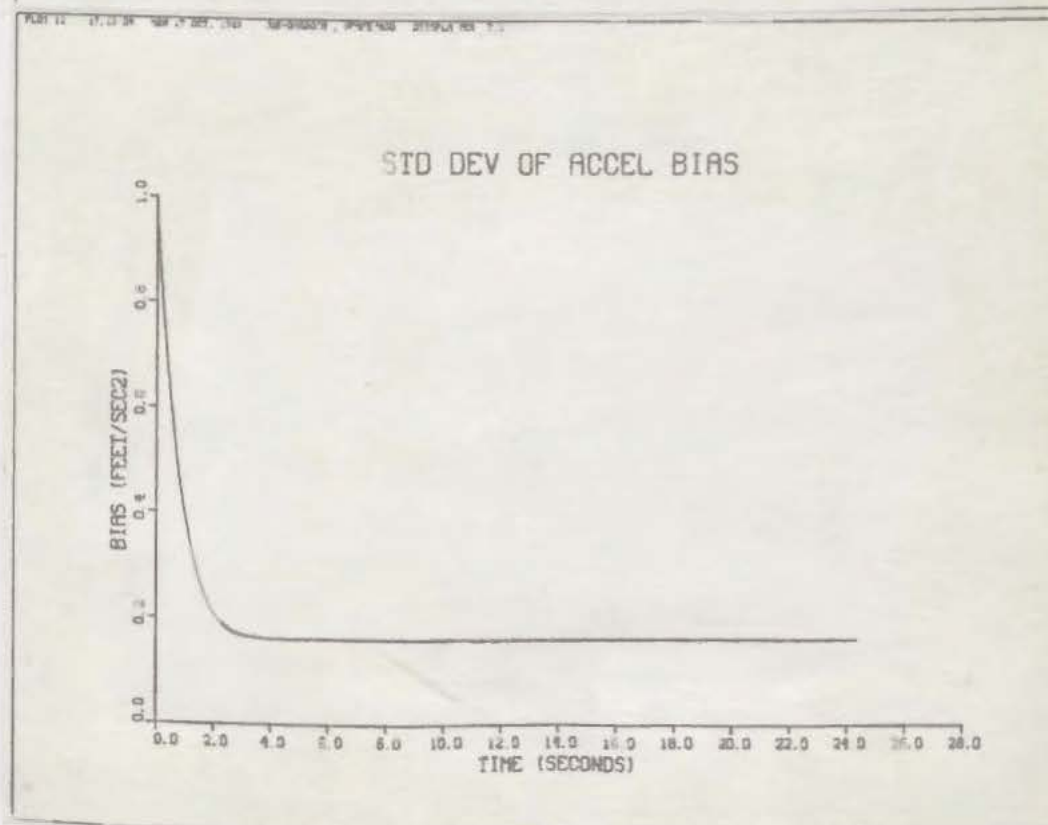
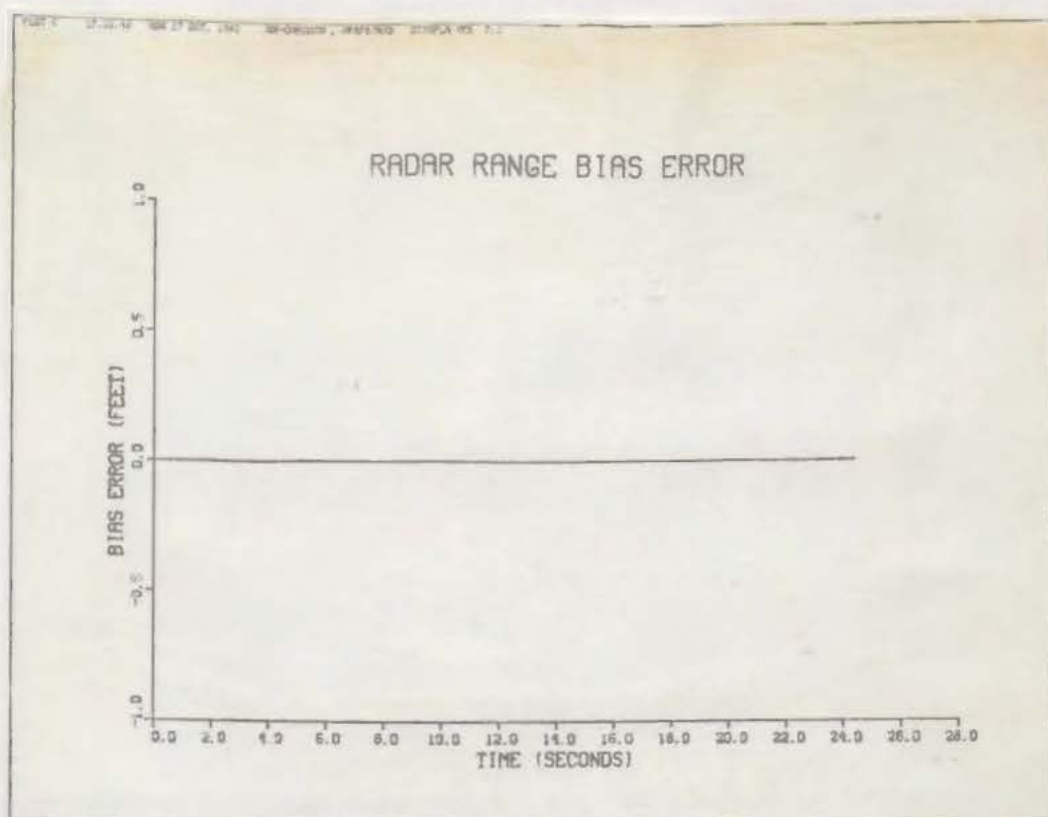


Fig. 4.5(a),(b) Accelerometer model for x_3 - No measurements

(a)



(b)

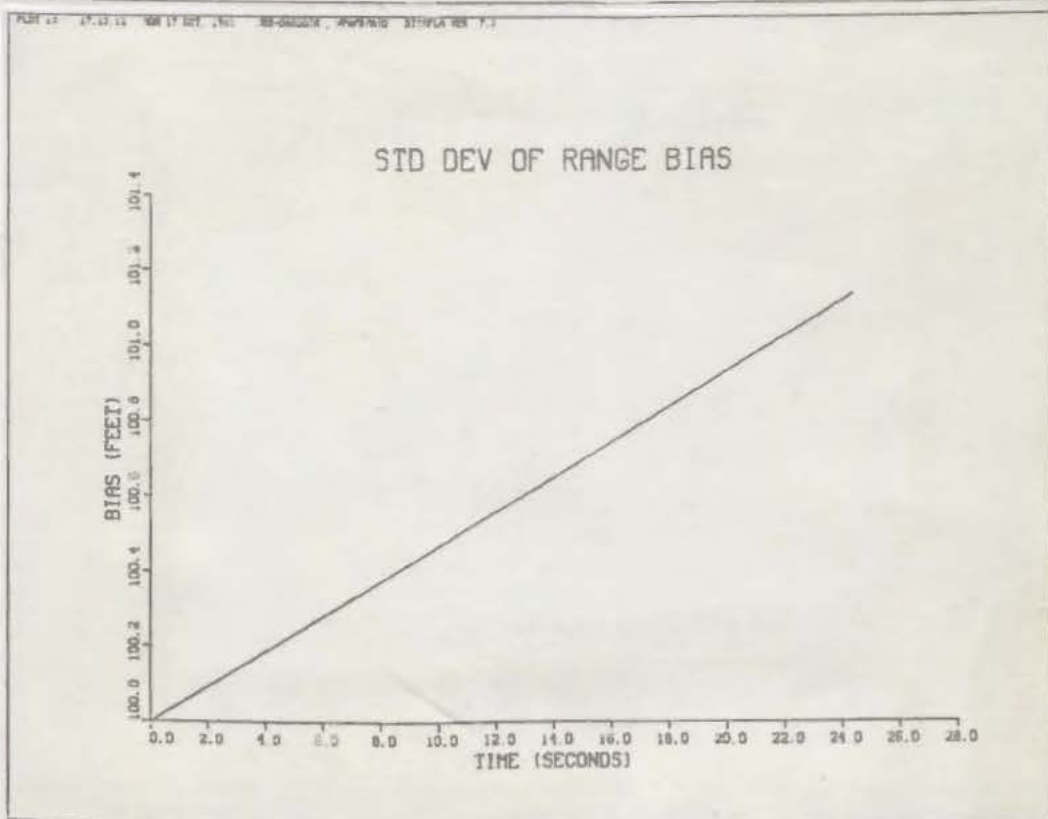


Fig. 4.6(a),(b) Accelerometer model for x_3 - No measurements

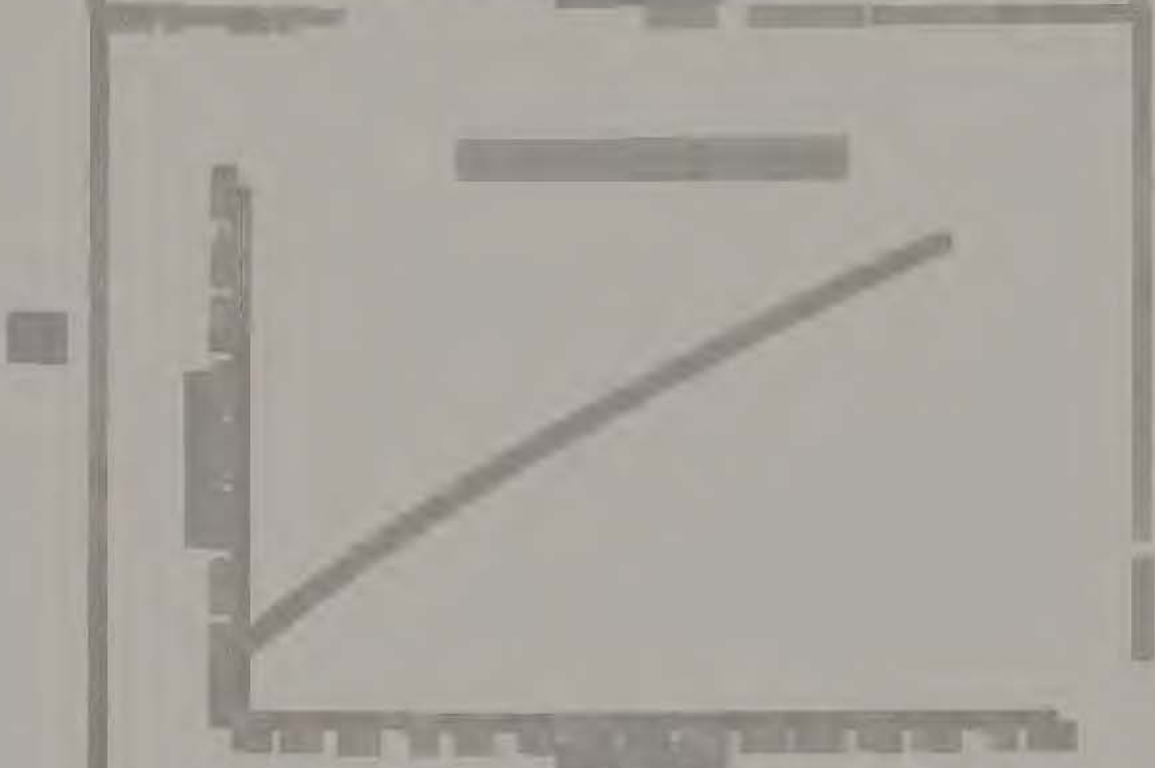
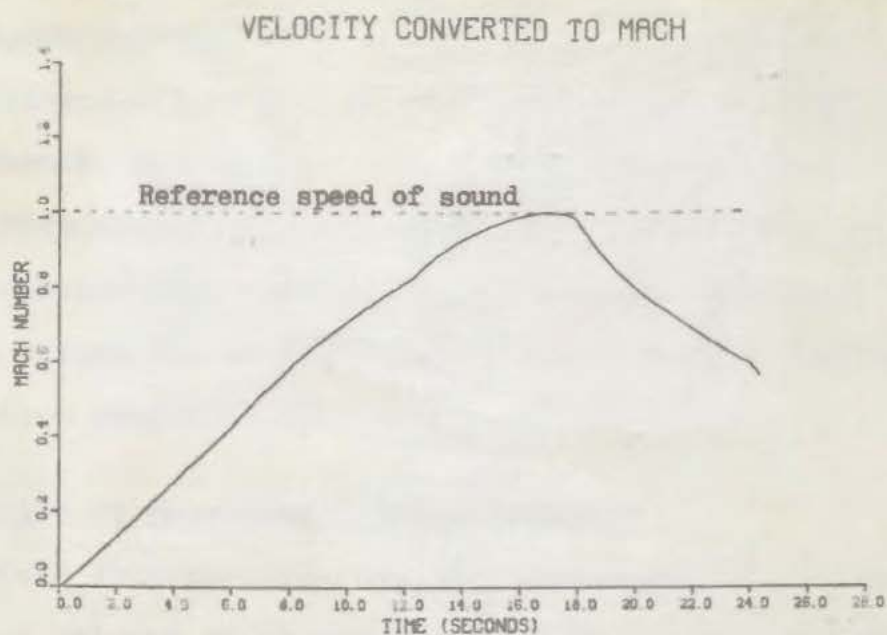


Figure 1: A line graph showing a decreasing trend over time.

(a)



(b)

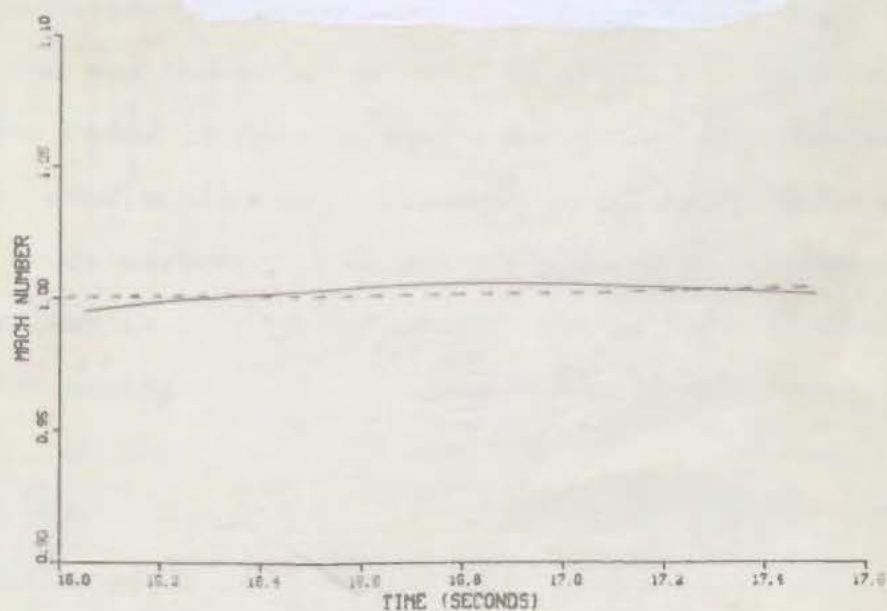


Fig. 4.8(a),(b) Accelerometer model for x_3 - No measurements

the ro

cence

the first of these is the

the second is the

the third is the

the fourth is the

the fifth is the

the sixth is the

the seventh is the

the eighth is the

the ninth is the

the tenth is the

the eleventh is the

the twelfth is the

the thirteenth is the

the fourteenth is the

the fifteenth is the

the sixteenth is the

the seventeenth is the

the eighteenth is the

the nineteenth is the

the twentieth is the

the twenty-first is the

the twenty-second is the

the twenty-third is the

the twenty-fourth is the

the twenty-fifth is the

There is a significant difference between the two groups in the number of children who are overweight or obese. The difference is statistically significant at the 5% level.

The results of the study show that the prevalence of overweight and obesity is significantly higher in the intervention group than in the control group. This finding is consistent with previous research which has shown that interventions aimed at reducing childhood obesity are effective. The results also show that the prevalence of overweight and obesity is significantly higher in the intervention group than in the control group. This finding is consistent with previous research which has shown that interventions aimed at reducing childhood obesity are effective. The results also show that the prevalence of overweight and obesity is significantly higher in the intervention group than in the control group. This finding is consistent with previous research which has shown that interventions aimed at reducing childhood obesity are effective.

the results

The results of the study show that the prevalence of overweight and obesity is significantly higher in the intervention group than in the control group. This finding is consistent with previous research which has shown that interventions aimed at reducing childhood obesity are effective. The results also show that the prevalence of overweight and obesity is significantly higher in the intervention group than in the control group. This finding is consistent with previous research which has shown that interventions aimed at reducing childhood obesity are effective.

The results of the study show that the prevalence of overweight and obesity is significantly higher in the intervention group than in the control group. This finding is consistent with previous research which has shown that interventions aimed at reducing childhood obesity are effective. The results also show that the prevalence of overweight and obesity is significantly higher in the intervention group than in the control group. This finding is consistent with previous research which has shown that interventions aimed at reducing childhood obesity are effective.

only can find the noise strength of the measurements, but check our equations for range and azimuth used in the filter.

Figures 4.9(a) and 4.9(b) are plots of actual range and estimated range. Figure 4.9(a) includes a plot of the difference between these two values for radar range. It is obvious from these plots that between 16 and 18 seconds the range is tracking a larger vehicle beyond the rocket car. It is also apparent from these plots that the range measurement is indeed extremely "noisy" and has significant errors.

The azimuth measurement, however, appears to be much better. Referring to Fig. 4.10, we can see that the actual and estimated azimuth values are very close. This confirms our assumption that the radar operator did a good job of tracking the car in azimuth.

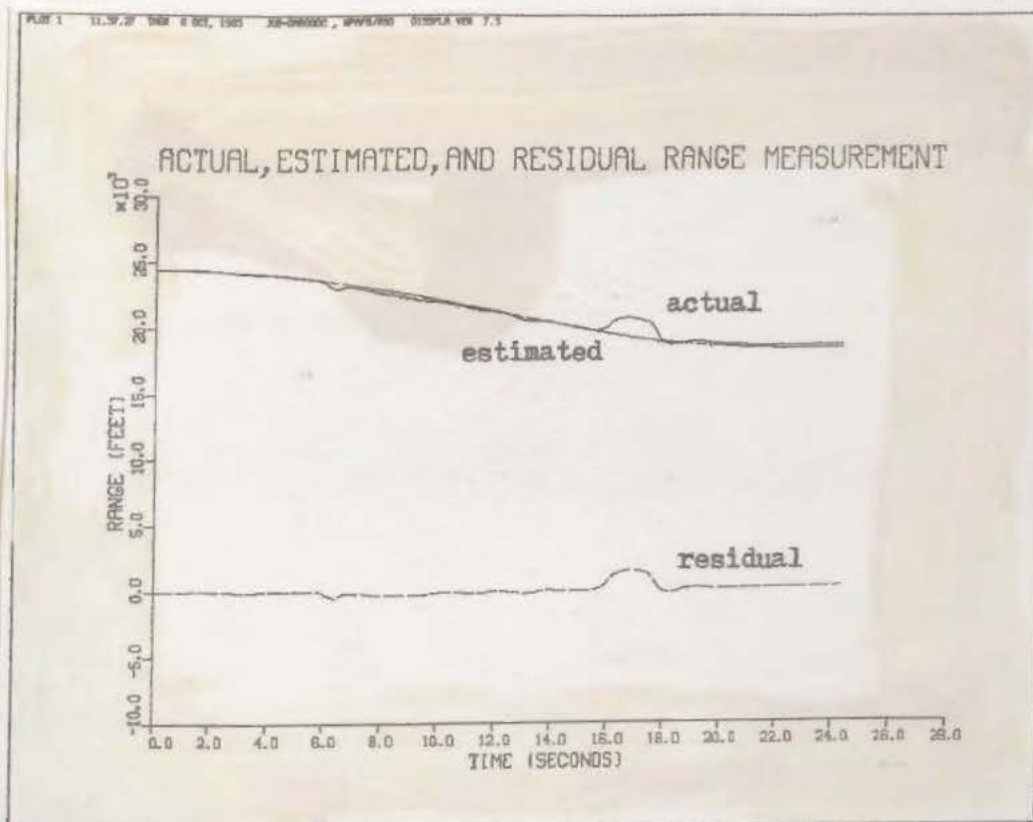
The purpose of comparing actual to estimated measurements is to determine realistic values for the diagonal terms in the measurement noise matrix, $R(t_i)$. To accomplish this, we sum the "residuals", or difference between actual and estimated measurements, over the entire time interval. We then calculate a mean and variance for the residual values using the following equations

$$\text{Mean, } \mu_{\text{res}} = 1/N-1 \sum_{i=1}^N r_i \quad (4-1)$$

$$\text{Variance, } \sigma_{\text{res}}^2 = 1/N-1 \sum_{i=1}^N (r_i^2 - \mu^2) \quad (4-2)$$

where r_i is the residual measurement at a given sample time and N is the number of sample periods used in the calculations.

(a)



(b)

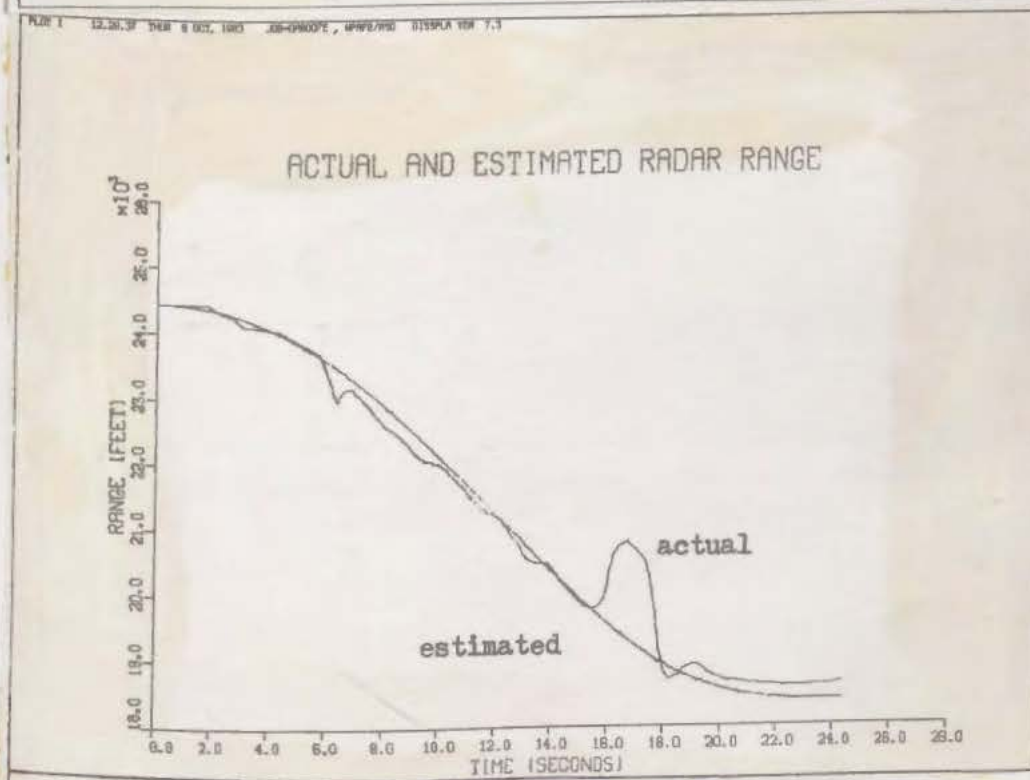


Fig. 4.9(a),(b) Residual range analysis based on an assumed track heading of 180 degrees true.

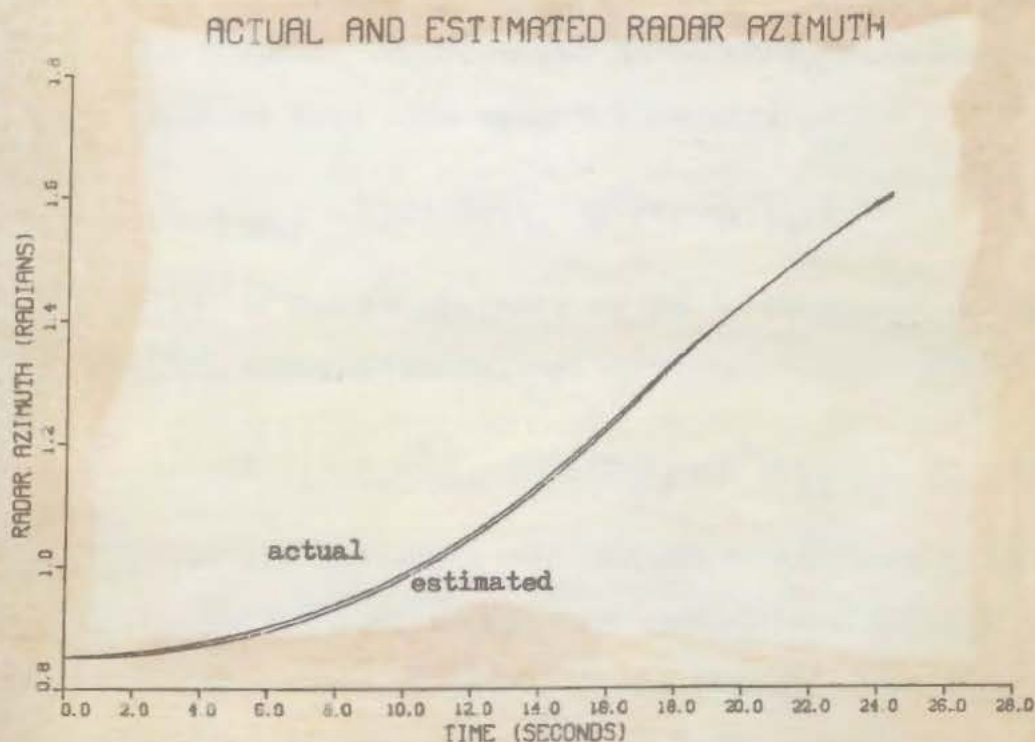


Fig. 4.10 Residual azimuth analysis based on an assumed track heading of 180 degrees true.

1. The first part of the report is a general introduction to the project. It describes the purpose of the study and the objectives that were set at the beginning. It also provides a brief overview of the methodology that was used to collect and analyze the data.

2. The second part of the report is a detailed description of the data that was collected. It includes information about the sample size, the demographic characteristics of the participants, and the specific measures that were used to assess the variables of interest.

3. The third part of the report is a presentation of the results. It includes a series of tables and figures that show the mean scores, standard deviations, and correlations between the different variables. It also includes a series of text descriptions that explain the meaning of the results and how they relate to the research hypotheses.

4. The fourth part of the report is a discussion of the findings. It summarizes the main results of the study and discusses their implications for theory and practice. It also includes a series of conclusions that are based on the evidence that was presented.

5. The final part of the report is a list of references. It includes a list of all the sources that were cited in the report, including books, articles, and other documents.

2. Method

The study was conducted using a cross-sectional design. Data were collected from a sample of 100 participants who were recruited from a local community center. The participants were all adults and were of various ages and ethnicities.

3. Results

The results of the study are presented in a series of tables and figures. Table 1 shows the mean scores and standard deviations for the different variables. Table 2 shows the correlations between the variables. Figure 1 is a line graph that shows the relationship between the variables over time. The results show that there is a significant positive relationship between the variables, and that the relationship is stronger for the older participants.

The findings of the study have several implications for theory and practice. First, they suggest that the relationship between the variables is not just a statistical artifact, but that it has a real-world meaning. Second, they suggest that the relationship is stronger for the older participants, which may be due to a number of factors, including changes in the brain and changes in the environment. Finally, the findings suggest that there may be some practical applications of the results, such as the development of interventions that target the relationship between the variables.

1. The first part of the paper is devoted to a general discussion of the problem.

2. The second part is devoted to a detailed analysis of the case.

3. The third part is devoted to a detailed analysis of the case.

4. The fourth part is devoted to a detailed analysis of the case.

5. The fifth part is devoted to a detailed analysis of the case.

6. The sixth part is devoted to a detailed analysis of the case.

7. The seventh part is devoted to a detailed analysis of the case.

8. The eighth part is devoted to a detailed analysis of the case.

9. The ninth part is devoted to a detailed analysis of the case.

10. The tenth part is devoted to a detailed analysis of the case.

11. The eleventh part is devoted to a detailed analysis of the case.

12. The twelfth part is devoted to a detailed analysis of the case.

13. The thirteenth part is devoted to a detailed analysis of the case.

14. The fourteenth part is devoted to a detailed analysis of the case.

15. The fifteenth part is devoted to a detailed analysis of the case.

16. The sixteenth part is devoted to a detailed analysis of the case.

17. The seventeenth part is devoted to a detailed analysis of the case.

18. The eighteenth part is devoted to a detailed analysis of the case.

19. The nineteenth part is devoted to a detailed analysis of the case.

20. The twentieth part is devoted to a detailed analysis of the case.

21. The twenty-first part is devoted to a detailed analysis of the case.

22. The twenty-second part is devoted to a detailed analysis of the case.

23. The twenty-third part is devoted to a detailed analysis of the case.

24. The twenty-fourth part is devoted to a detailed analysis of the case.

25. The twenty-fifth part is devoted to a detailed analysis of the case.

26. The twenty-sixth part is devoted to a detailed analysis of the case.

27. The twenty-seventh part is devoted to a detailed analysis of the case.

Referring to Fig. 4.10(a), the coordinate translation becomes:

$$x_r = \text{DELX} + (\cos 179^\circ)x_1 + (\sin 179^\circ)x_2 \quad (4-5)$$

$$y_r = \text{DELY} + (\sin 1^\circ)x_1 + (\cos 1^\circ)x_2 \quad (4-6)$$

or

$$x_r = \text{DELX} - .99985x_1 + .01745x_2$$

$$y_r = \text{DELY} + .01745x_1 + .99985x_2$$

When these corrections are applied to (3-22) and (3-23) and the residual plotting and variance calculations are made, the actual and estimated range measurements are much closer. The corrected plots of range and azimuth are shown in Fig. 4.11(a), (b) and 4.12. With these corrections, calculated residual variance for range becomes 16807.66 ft^2 and azimuth variance reduces to $.3573 \times 10^{-4} \text{ rad}^2$. These lower variances result in RMS errors for range and azimuth of 129.88 feet and .005977 radian, respectively. Note that we have calculated an error for the azimuth which matches our initial guess of .006 radian. It is apparent that the one degree correction is closer to the true track heading and reduces the majority of modeling error. Thus, we have computed the estimated measurement noise strength matrix, $\hat{R}(t_i)$:

$$\hat{R}(t_i) = \begin{bmatrix} 16807.66 & 0 \\ 0 & .3573\text{E-}4 \end{bmatrix} \quad (4-7)$$

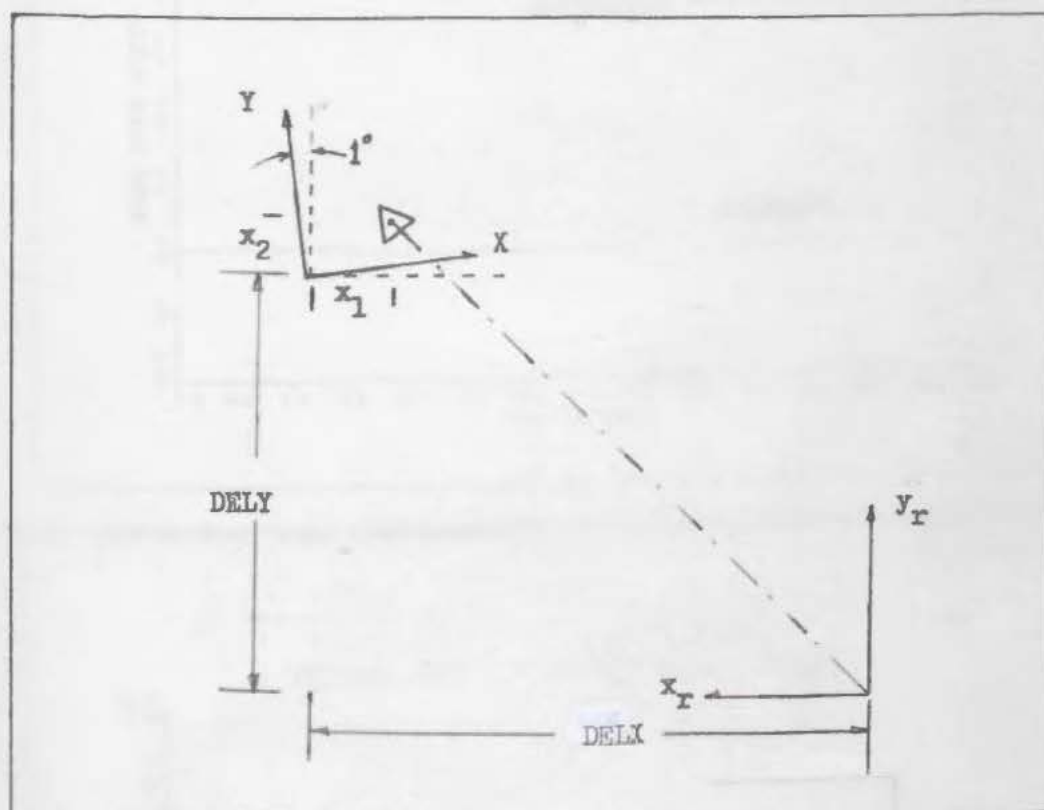
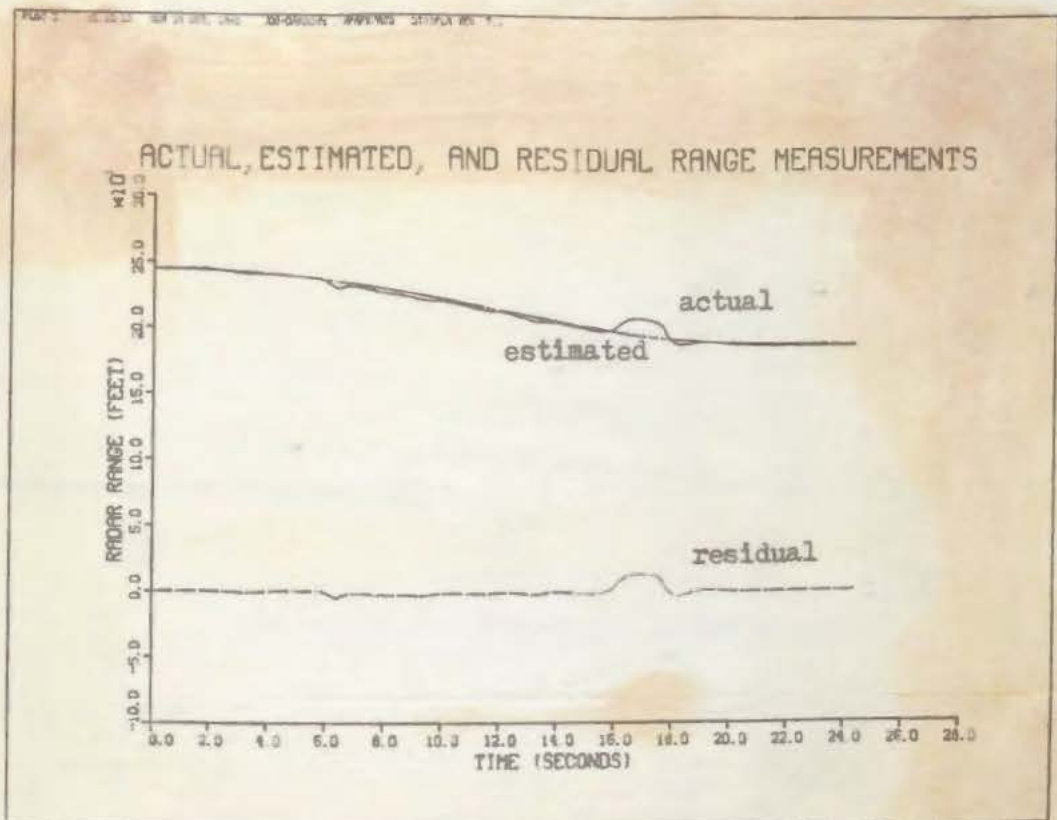


Fig. 4.10 (a) Corrected Coordinate Frame

(a)



(b)

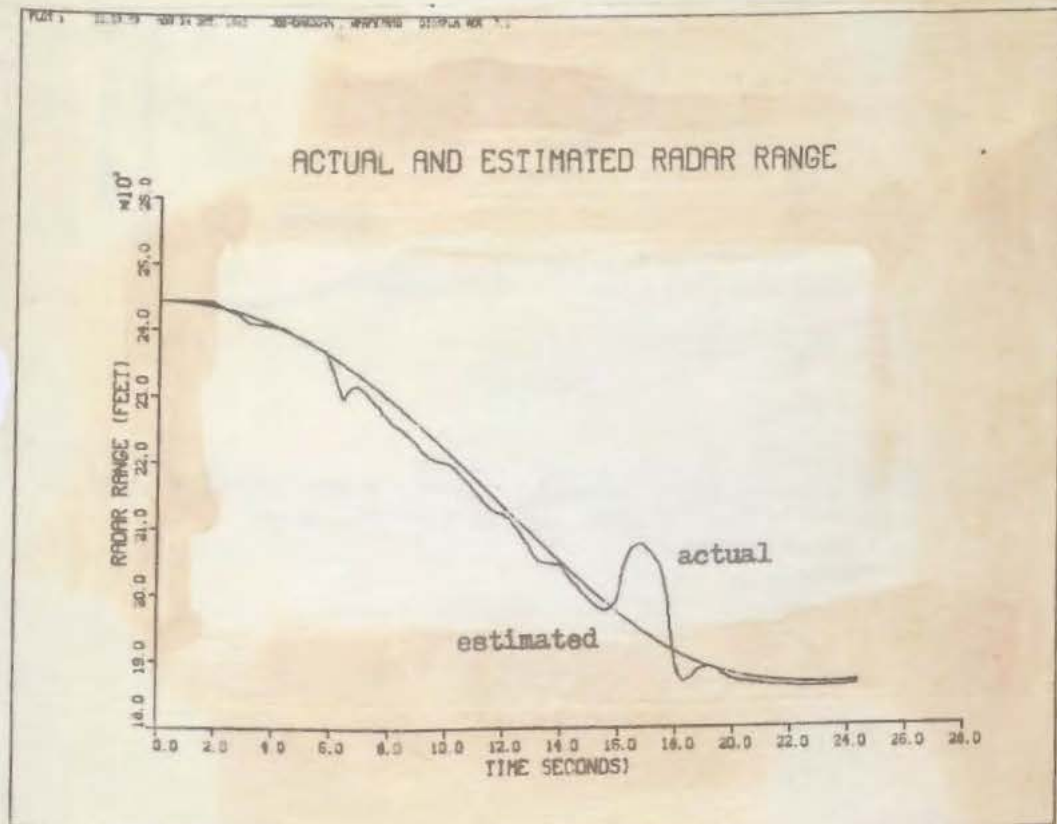


Fig. 4.11(a),(b) Residual range analysis based on assumed track heading of 179 degrees true.

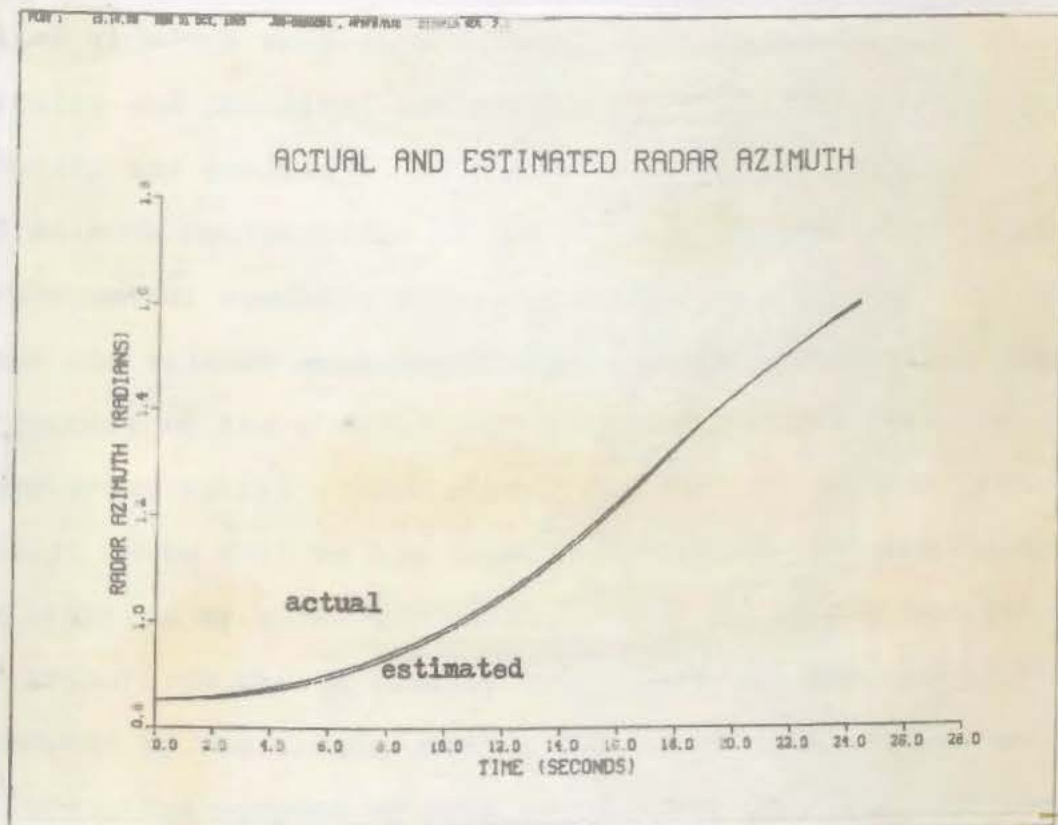


Fig. 4.12 Residual azimuth analysis based on assumed track heading of 179 degrees true.

Introduction

The purpose of this study is to investigate the effects of various factors on the performance of a system. The study is organized as follows: Chapter 1 provides an overview of the research. Chapter 2 describes the methodology used. Chapter 3 presents the results of the experiments. Chapter 4 discusses the implications of the findings. Chapter 5 concludes the study and suggests areas for future research.

The study is divided into two main parts: a theoretical analysis and an experimental investigation. The theoretical part focuses on the development of a model that predicts system performance based on input variables. The experimental part involves the design and execution of a series of tests to validate the model. The results of the experiments are compared with the predictions of the model to assess its accuracy.

The study is organized into five chapters. Chapter 1, the Introduction, outlines the research objectives and the structure of the document. Chapter 2, Methodology, details the experimental setup and the data collection process. Chapter 3, Results, presents the findings of the experiments, including the performance metrics and the statistical analysis. Chapter 4, Discussion, interprets the results and discusses their significance. Chapter 5, Conclusion, summarizes the study and provides recommendations for future work.

The study is organized into five chapters. Chapter 1, the Introduction, outlines the research objectives and the structure of the document. Chapter 2, Methodology, details the experimental setup and the data collection process. Chapter 3, Results, presents the findings of the experiments, including the performance metrics and the statistical analysis. Chapter 4, Discussion, interprets the results and discusses their significance. Chapter 5, Conclusion, summarizes the study and provides recommendations for future work.

The study is organized into five chapters. Chapter 1, the Introduction, outlines the research objectives and the structure of the document. Chapter 2, Methodology, details the experimental setup and the data collection process. Chapter 3, Results, presents the findings of the experiments, including the performance metrics and the statistical analysis. Chapter 4, Discussion, interprets the results and discusses their significance. Chapter 5, Conclusion, summarizes the study and provides recommendations for future work.

$$y = x_1 + x_2$$

$$z_2 = \arctan[(\text{DELY} + .01745x_1 + .99985x_2) / (\text{DELX} - .99985x_1 + .01745x_2)] + x_7 + v_2$$

Applying (2-15) to these equations we form the observation sensitivity matrix, $H[t_i; \hat{x}(t_i^-)]$. It is the model for measurement incorporation, $z(t_i)$, and the calculation of $H[t_i; \hat{x}(t_i^-)]$ that we desire to check. By comparing state trajectories of position and velocity independently obtained from each measurement, we hope to confirm our calculations and modeling techniques.

The primary reason for deviations between measurement trajectories and the accelerometer profile is due to the rather crude model we substitute for the x-velocity state, x_3 . We now choose this state to be modeled as a random walk of the form

$$\dot{x}_3 = w_3(t)$$

where the driving noise, $w_3(t)$, has a relatively high strength to account for our uncertainty in such a model and allow closer tracking of actual data. Modeling this state as we have, the x velocity is considered a constant. Any change to its value based on measurement updates is done in a step-like manner. Therefore, we do not expect to get exact agreement with accelerometer results.

The model for x-velocity is incorporated into a six state extended Kalman filter where accelerometer error, x_5 , has been removed. The filter is run using range measurements

only, azimuth measurements only, and both measurements combined. The results of these three runs of the extended Kalman filter are shown in Fig. 4.13 to 4.16. Plots are made of the estimates of x and y position and velocity. Part (a) of each figure is the depicted state estimate generated using range measurements only. Part (b) is the state estimate generated using azimuth measurements only, while part (c) of each figure shows the result of combining both range and azimuth. We see, in fact, that position and velocity along the x -axis behave as we would expect from the accelerometer trajectory shown in Figs. 4.1 through 4.4. However, the geometry of the radar position to the vehicle is not conducive to accurate estimates of deviations along the earth-fixed y -axis. The range measurement is the only means by which we can hope to estimate position and velocity along the y -axis. The state estimates of these values are subject to any errors in the range measurement and indicate only weak observability of these states. The range measurement is ignored between 16-18 seconds to account for the known error in this measurement during this interval. Due to the geometry of the problem, the range measurement is even less likely to track the vehicle along the x -axis correctly. This can be seen from comparing the plots of x -position and velocity for range only to the plots of these states with azimuth only and both measurements combined. From these plots, it is apparent that the azimuth does a credible job of tracking changes in position and velocity along the x -axis. Conversely, the azimuth

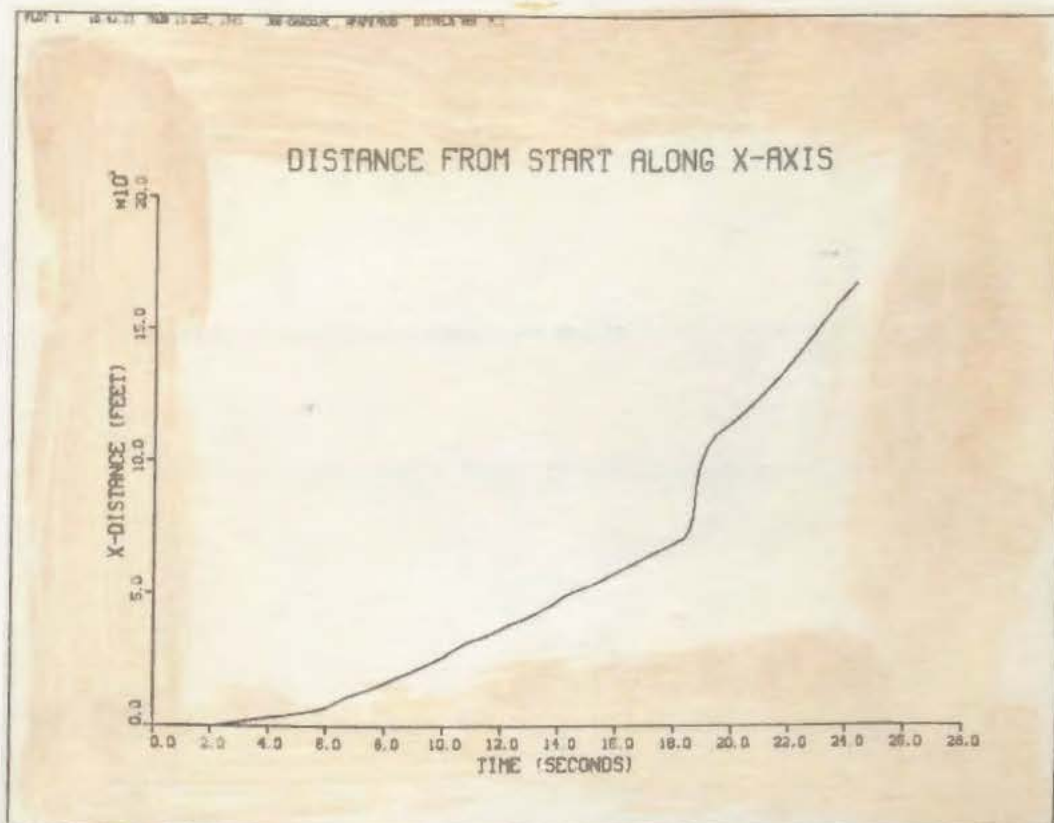


Fig. 4.13(a) Random walk model for x_3 - Range only

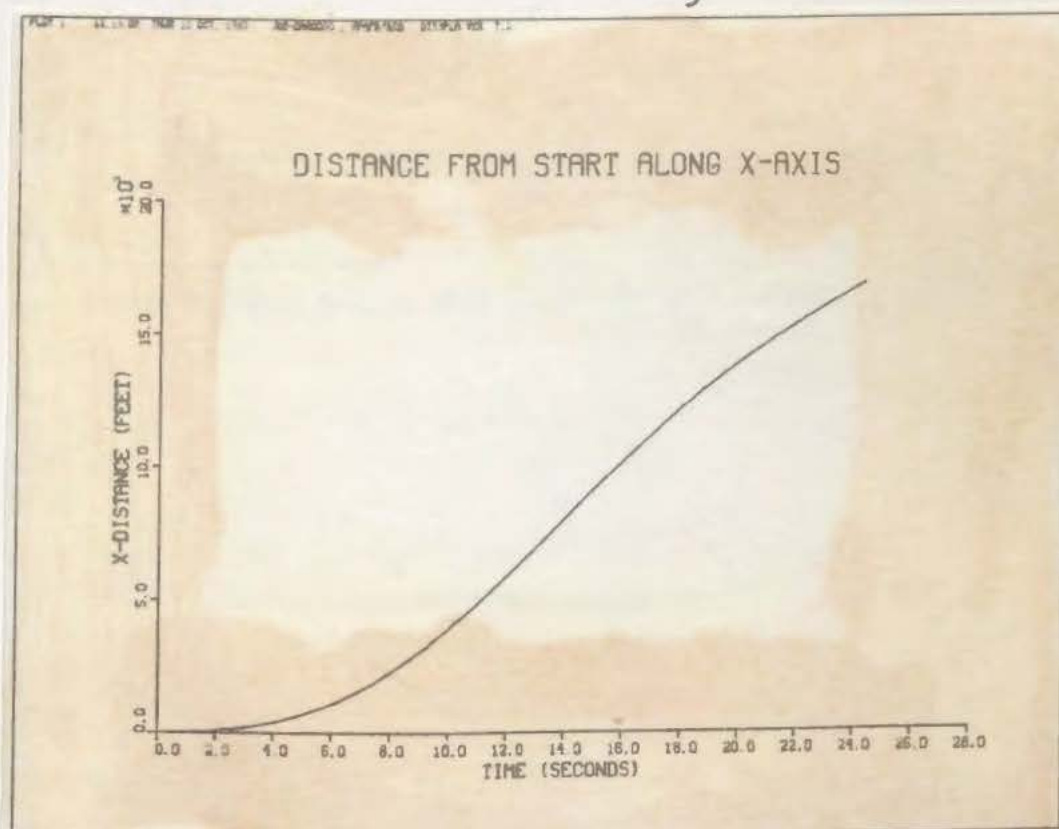


Fig. 4.13(b) Random walk model for x_3 - Azimuth only

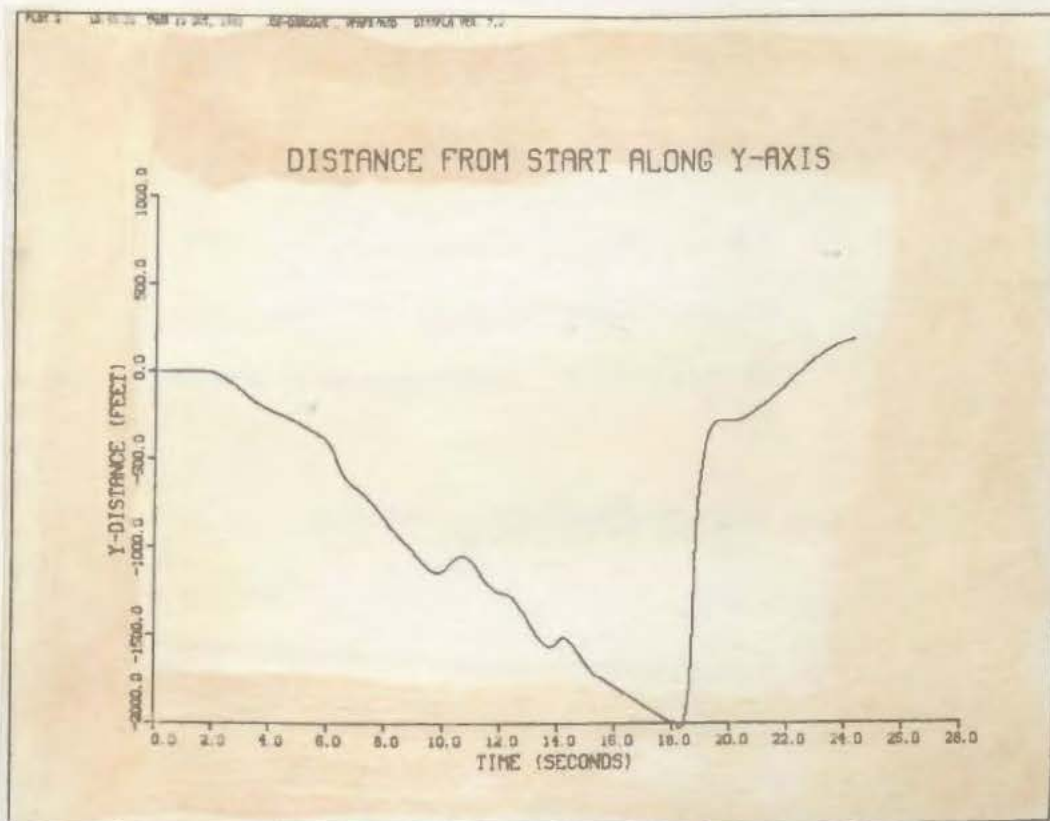


Fig. 4.14(a) Random walk model for x_3 - Range only

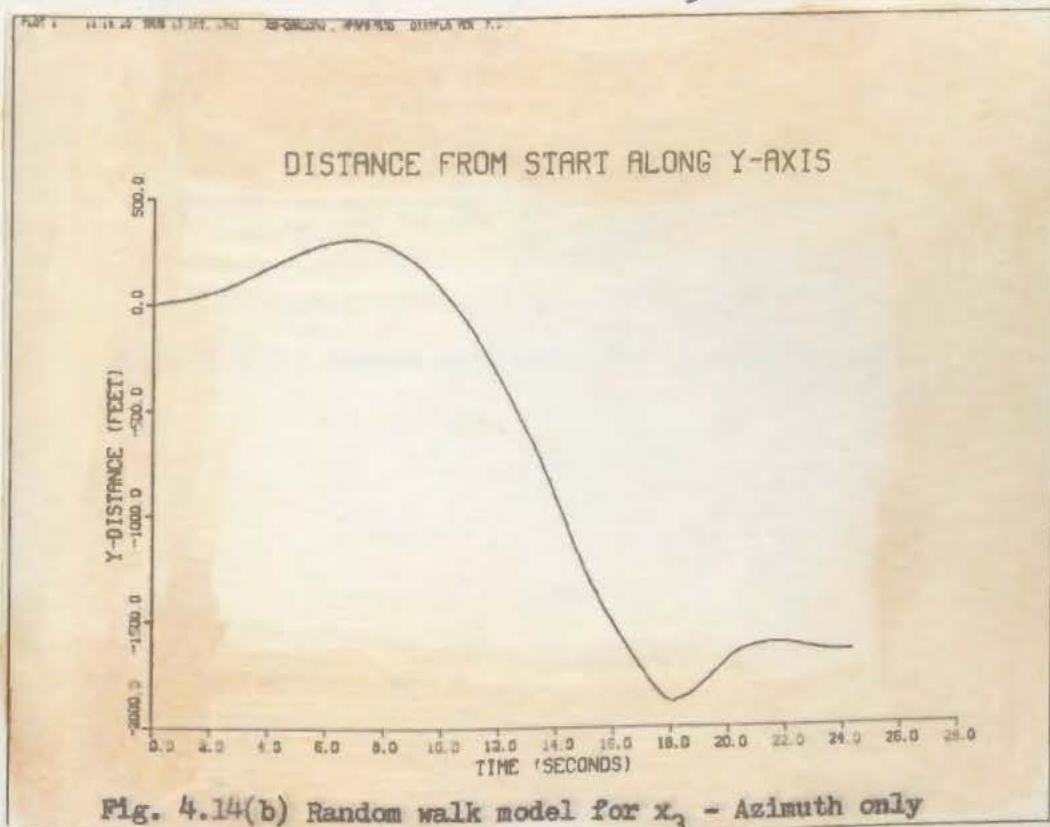


Fig. 4.14(b) Random walk model for x_3 - Azimuth only

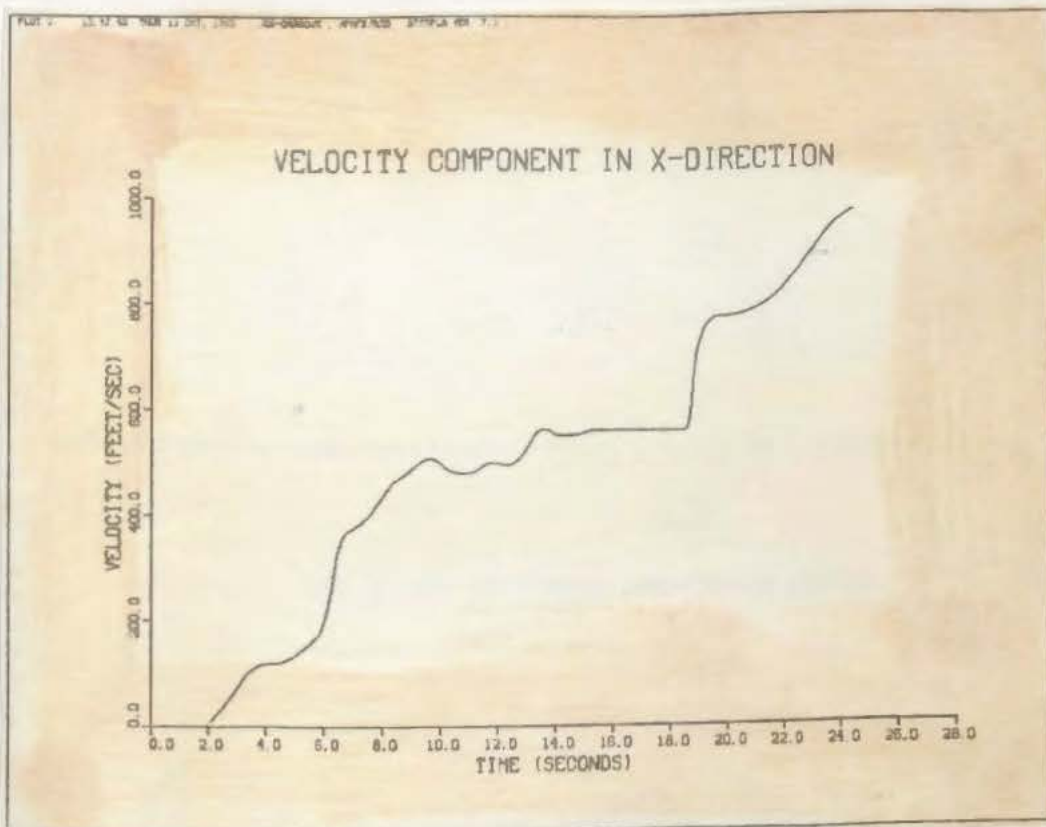


Fig. 4.15(a) Random walk model for x_3 - Range only

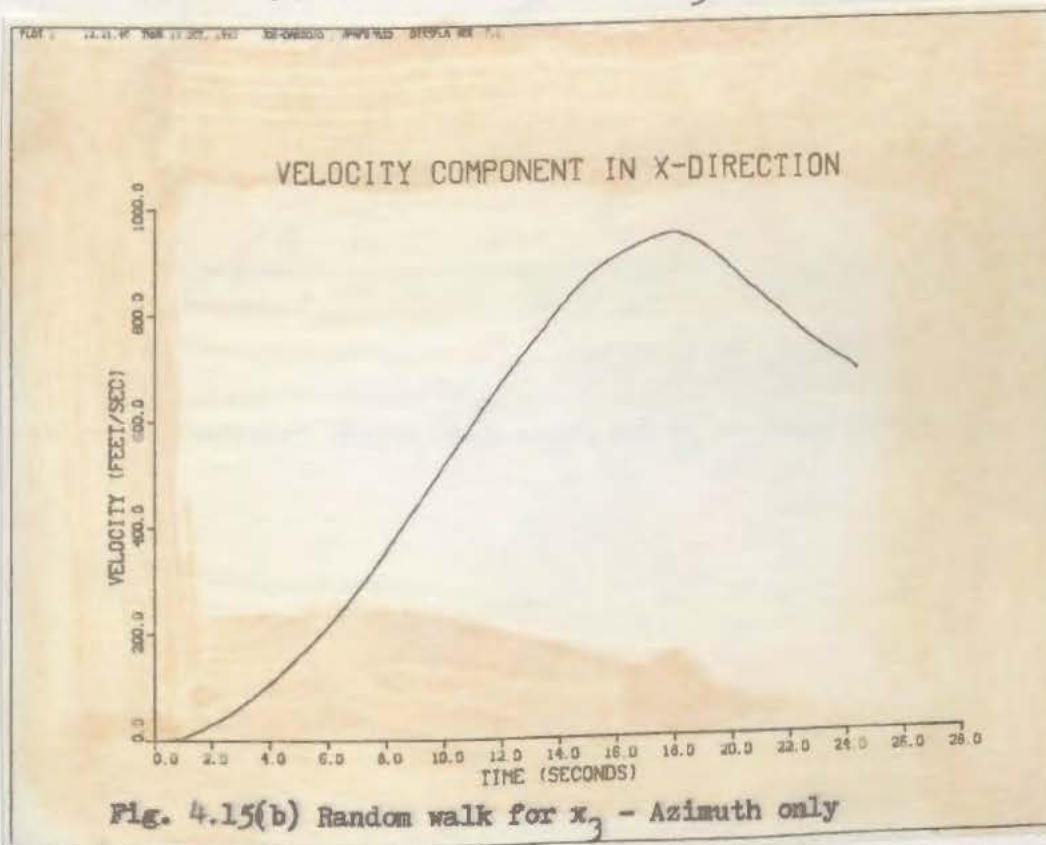


Fig. 4.15(b) Random walk for x_3 - Azimuth only

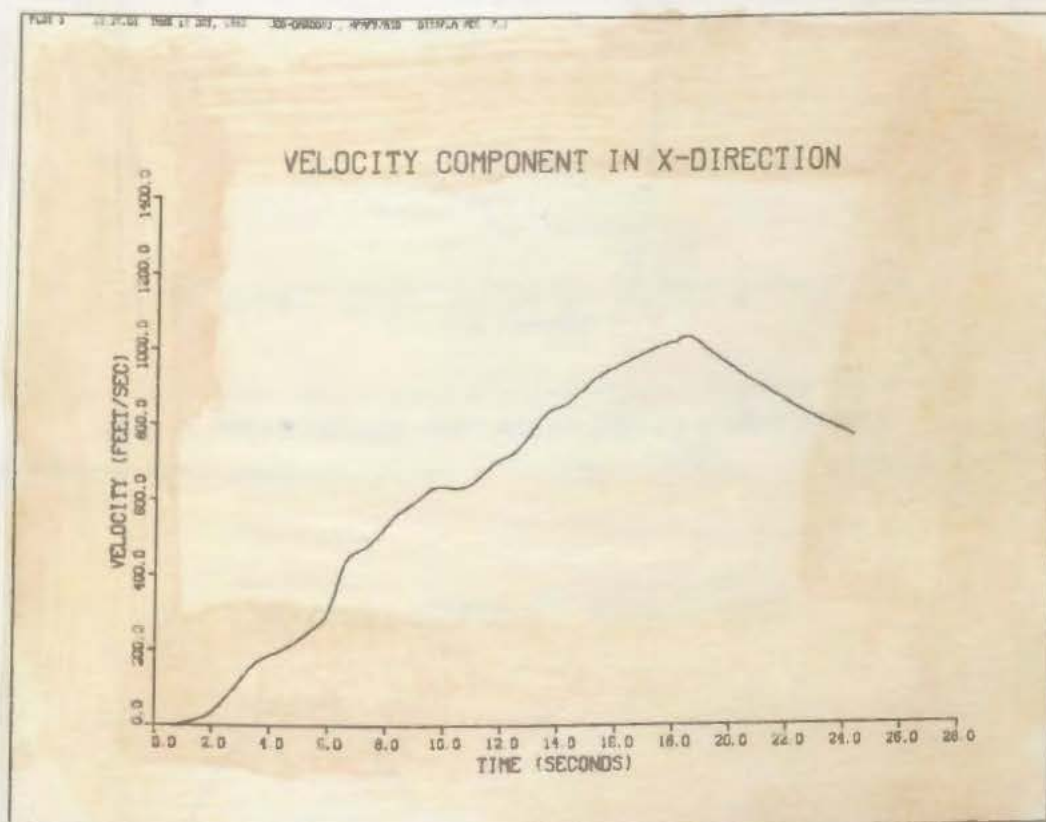


Fig. 4.15(c) Random walk model for x_3 - Range and Azimuth

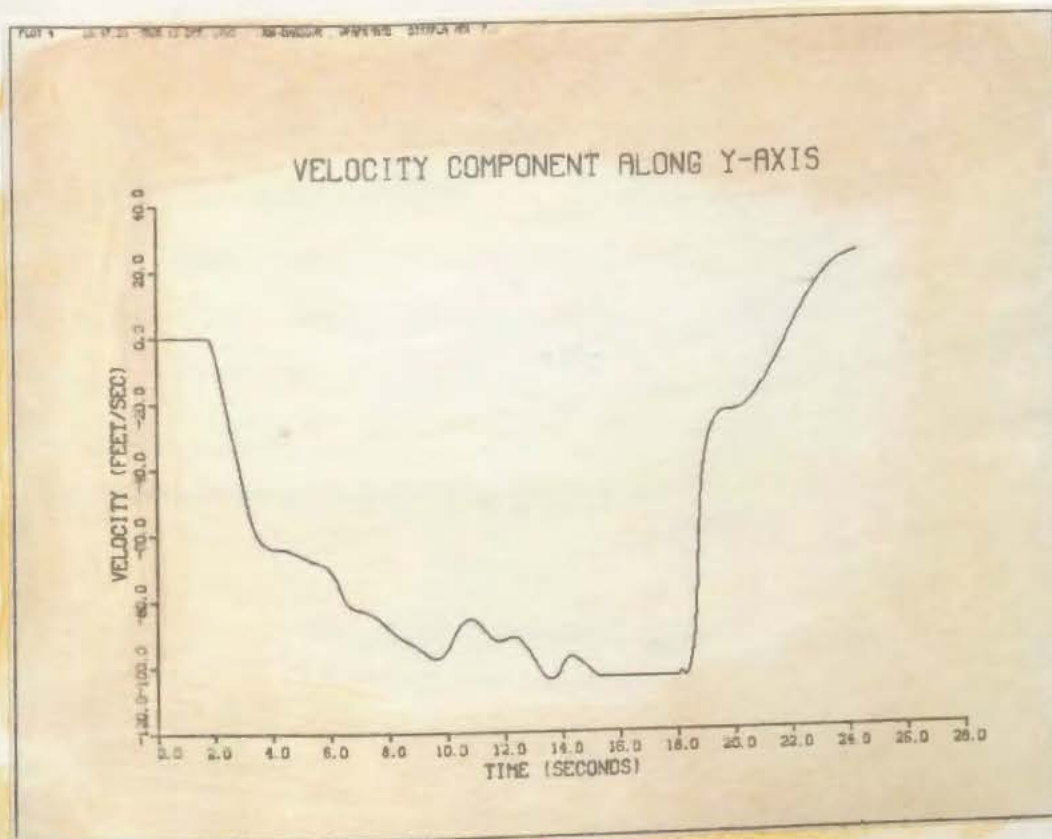


Fig. 4.16(a) Random walk model for x_3 - Range only

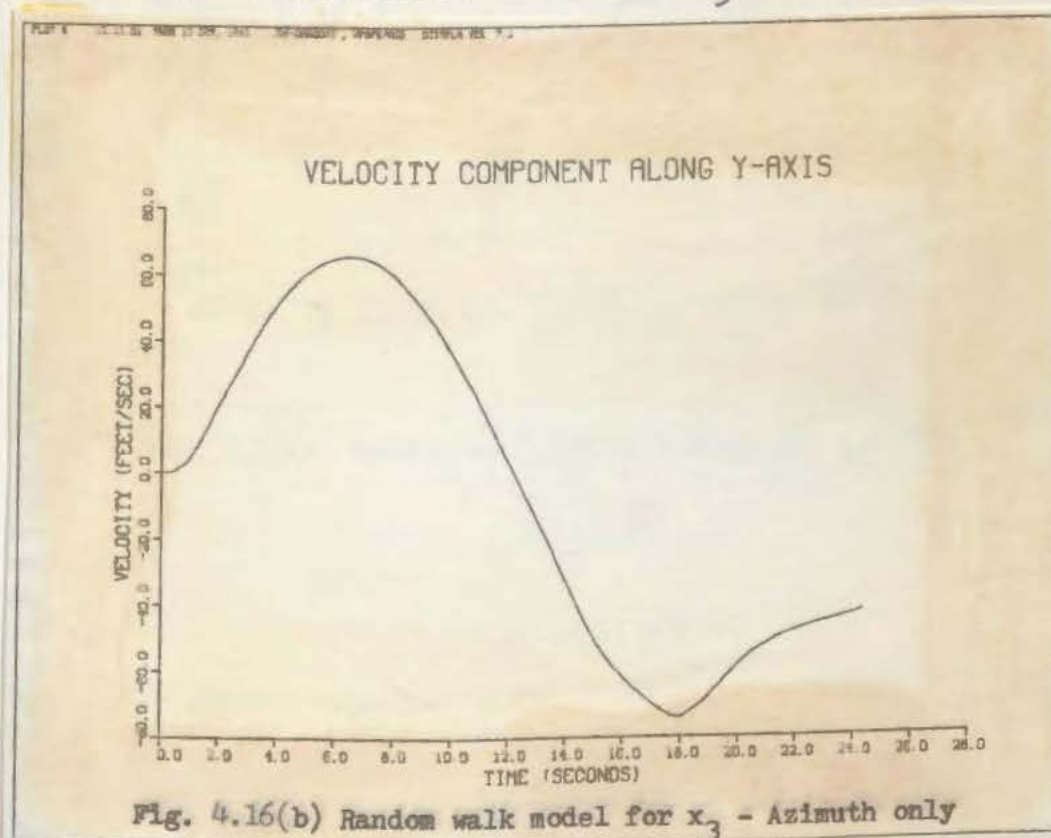


Fig. 4.16(b) Random walk model for x_3 - Azimuth only

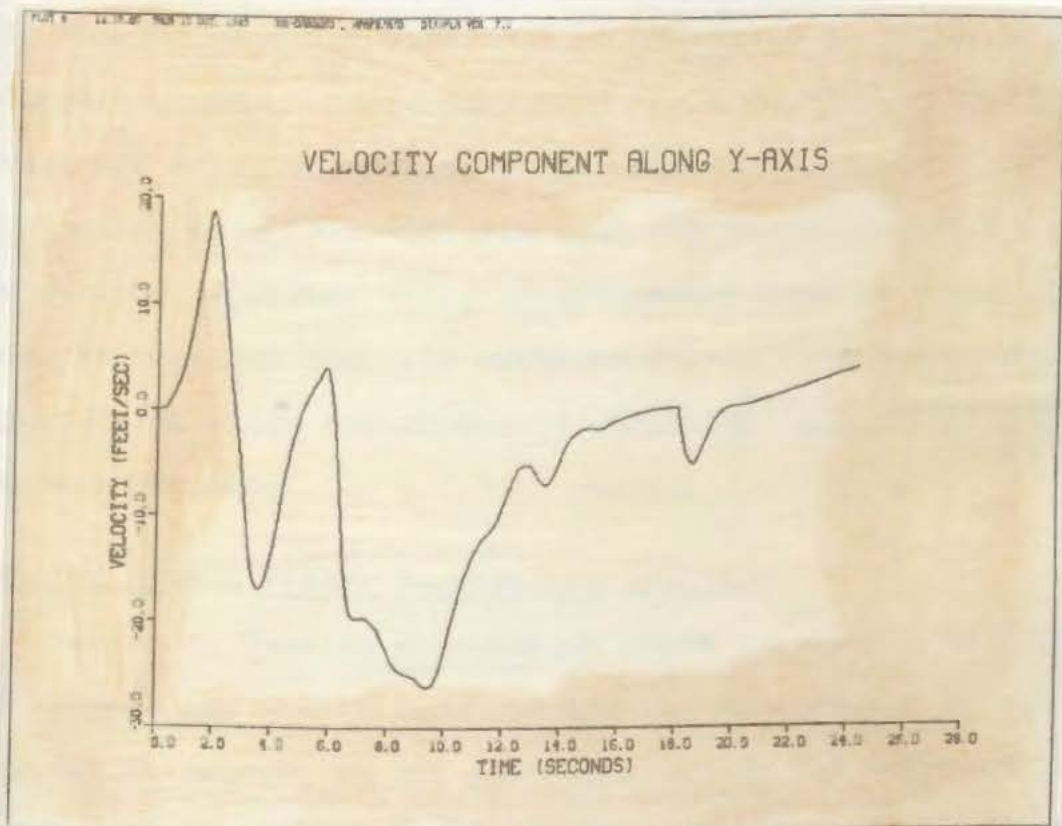


Fig. 4.16(c) Random walk for x_3 - Range and Azimuth

measurement can tell very little about y-axis changes of position and velocity. Again, the geometry of the radar and vehicle track causes this observability problem.

Figures 4.13 (c) through 4.16 (c) are generated by utilizing both azimuth and range measurements. Again, the estimates of x position and velocity are fairly consistent with the estimates of these values generated by using accelerometer data. Deviations from track centerline are less severe but still subject to range measurement errors. It is apparent from this analysis that the basic trajectory of the vehicle generated using accelerometer data is reconfirmed. Thus, we conclude that the extended Kalman filter is correctly calculating the observation matrix, $H[t_i; \hat{x}(t_i^-)]$, and that our model for $\underline{z}(t_i)$ is correct.

Extended Kalman Filter Performance Analysis

Having calculated measurement noise strengths for range and azimuth and also having checked the calculation of the observation matrix, we are now ready to run the extended Kalman filter modeled in Chapter III. The initial condition for the propagation of the state vector is chosen as zero-mean Gaussian random variable with mean

$$E[\underline{x}(t_0)] = \hat{\underline{x}}_0 = \underline{0} \quad (4-8)$$

and covariance

$$E[(\underline{x}(t_0) - \hat{\underline{x}}_0)(\underline{x}(t_0) - \hat{\underline{x}}_0)^T] = \underline{P}_0 \quad (4-9)$$

where the initial covariance matrix from (3-16) is specified as:

$$\underline{P}_0 = \begin{bmatrix} 10000 & & & & & \\ & 10000 & & & & \\ & & 100 & & & \\ & & & 100 & & \\ & & & & .0259 & \\ & & & & & 225 \\ & & & & & & .25E-6 \end{bmatrix} \quad (4-10)$$

The initial values for the diagonal entries of the system noise matrix, $\underline{Q}(t)$, are repeated here for reference:

$$\underline{Q}(t) = \begin{bmatrix} 0 & & & & & \\ & 0 & & & & \\ & & 0 & & & \\ & & & .01 & & \\ & & & & .0518 & \\ & & & & & 1.0 \\ & & & & & & .1E-7 \end{bmatrix} \quad (4-11)$$

The extended Kalman filter as implemented in SOFE is run with several different combinations of $\underline{Q}(t)$, \underline{P}_0 , and $\underline{R}(t_i)$. This analysis is necessary to monitor the behavior of the error variance of each state estimate in order to check filter performance. We desire to obtain the lowest possible error variance on each state after 24 seconds of filter operation, using realistic values of initial covariance, \underline{P}_0 , system noise, $\underline{Q}(t)$, and measurement noise, $\underline{R}(t_i)$. This performance analysis can be thought of as "tuning" the extended Kalman filter. The results obtained from a large number of noise and initial covariance combinations are summarized here.

1. The first part of the document is a letter from the President of the United States to the Congress.

2. The second part is a report from the Secretary of the Treasury on the state of the Union.

3. The third part is a report from the Secretary of the Navy on the state of the Navy.

4. The fourth part is a report from the Secretary of the War on the state of the War.

5. The fifth part is a report from the Secretary of the Interior on the state of the Interior.

6. The sixth part is a report from the Secretary of the Agriculture on the state of the Agriculture.

7. The seventh part is a report from the Secretary of the Commerce on the state of the Commerce.

8. The eighth part is a report from the Secretary of the Education on the state of the Education.

9. The ninth part is a report from the Secretary of the Justice on the state of the Justice.

10. The tenth part is a report from the Secretary of the State on the state of the State.

11. The eleventh part is a report from the Secretary of the War on the state of the War.

12. The twelfth part is a report from the Secretary of the Navy on the state of the Navy.

13. The thirteenth part is a report from the Secretary of the Treasury on the state of the Treasury.

14. The fourteenth part is a report from the Secretary of the Interior on the state of the Interior.

15. The fifteenth part is a report from the Secretary of the Agriculture on the state of the Agriculture.

16. The sixteenth part is a report from the Secretary of the Commerce on the state of the Commerce.

17. The seventeenth part is a report from the Secretary of the Education on the state of the Education.

18. The eighteenth part is a report from the Secretary of the Justice on the state of the Justice.

19. The nineteenth part is a report from the Secretary of the State on the state of the State.

20. The twentieth part is a report from the Secretary of the War on the state of the War.

21. The twenty-first part is a report from the Secretary of the Navy on the state of the Navy.

22. The twenty-second part is a report from the Secretary of the Treasury on the state of the Treasury.

23. The twenty-third part is a report from the Secretary of the Interior on the state of the Interior.

24. The twenty-fourth part is a report from the Secretary of the Agriculture on the state of the Agriculture.

25. The twenty-fifth part is a report from the Secretary of the Commerce on the state of the Commerce.

26. The twenty-sixth part is a report from the Secretary of the Education on the state of the Education.

27. The twenty-seventh part is a report from the Secretary of the Justice on the state of the Justice.

28. The twenty-eighth part is a report from the Secretary of the State on the state of the State.

estimates and associated driving noise strengths and measurement noise is presented in Table I. The initial variance on each state is 100 (ft/sec)^2 , or $\pm 10 \text{ ft/sec}$.

TABLE I
Filter Performance Analysis

Driving Noise q	Measurement Noise, $R(t_i)$	$P(t = 24 \text{ sec})$
$q_4 = .2E-2$	22456/.5388E-4	$P_3 = 2.4$
$q_5 = .0518$	" "	$P_4 = 6.36$
$q_6 = 10.0$	" "	
$q_7 = .5E-5$	" "	
$q_4 = .1E-2$	22456/.5388E-4	$P_3 = 3.193$
$q_5 = .0515$	" "	$P_4 = 6.43$
$q_6 = 1.0$	" "	
$q_7 = .1E-7$	" "	
$q_4 = .1E-3$	22456/.5388E-4	$P_3 = 2.57$
$q_5 = .3E-1$	" "	$P_4 = 6.24$
$q_6 = .10$	" "	
$q_7 = .1E-7$	" "	
$q_4 = .1E-7$	16808/.3573E-4	$P_3 = 2.27$
$q_5 = .3E-1$	" "	$P_4 = 5.92$
$q_6 = .01$	" "	
$q_7 = .1E-7$	" "	

The combination of system noise, initial covariance, and measurement noise chosen as a result of this performance analysis is presented here:

$$\underline{P}_0 = \begin{bmatrix} 10000 & & & & & \\ & 10000 & & & & \\ & & 100 & & & \\ & & & 100 & & \\ & & & & .03 & \\ & & & & & 1600 \\ & & & & & & .5E-4 \end{bmatrix}$$

$$\underline{Q}(t) = \begin{bmatrix} 0 & & & & & \\ & 0 & & & & \\ & & 0 & & & \\ & & & .1E-7 & & \\ & & & & .03 & \\ & & & & & .01 \\ & & & & & & .1E-7 \end{bmatrix}$$

$$\underline{R}(t_i) = \begin{bmatrix} 16808 & 0 \\ 0 & .3573E-4 \end{bmatrix}$$

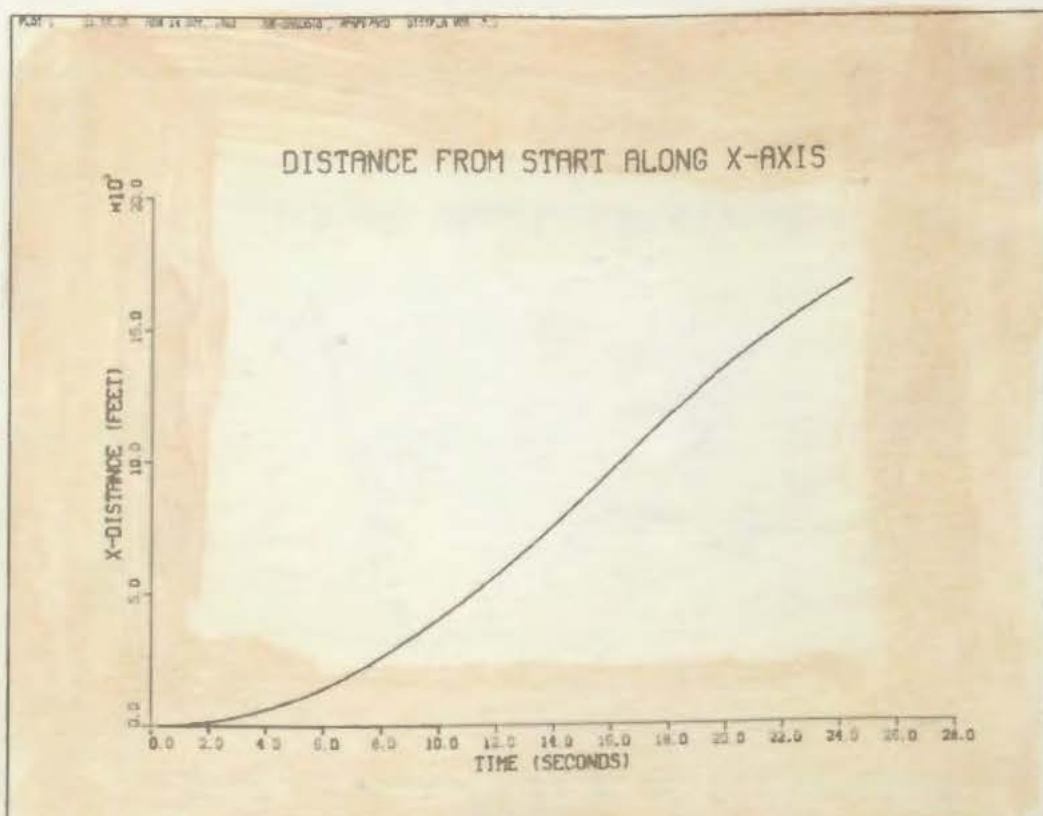
Results of One Iteration of the Extended Kalman Filter

State estimates and error standard deviation in these estimates for the "tuned" extended Kalman filter are presented in Fig. 4.17 through Fig. 4.25. These plots are generated using the values for \underline{P}_0 , $\underline{Q}(t)$, and $\underline{R}(t_i)$, specified above. Figure 4.24(a) is a plot of the range measurement residual bracketed by the residual standard deviation. The azimuth measurement residual and associated residual standard deviation is plotted in Fig. 4.24(b). It should be noted that a "residual monitoring" routine has been included in the basic software for SOFE. This routine calculates the residual standard deviation at each sample time from:

$$\sigma_{res} = [\underline{H}(t_i)\underline{P}(t_i^-)\underline{H}^T(t_i) + \underline{R}(t_i)]^{\frac{1}{2}}$$

and compares the residual measurement to this value for σ_{res} . If the residual measurement, $\delta z(t_i)$, is greater than $3\sigma_{res}$, the measurement is ignored. As a result of residual

(a)



(b)

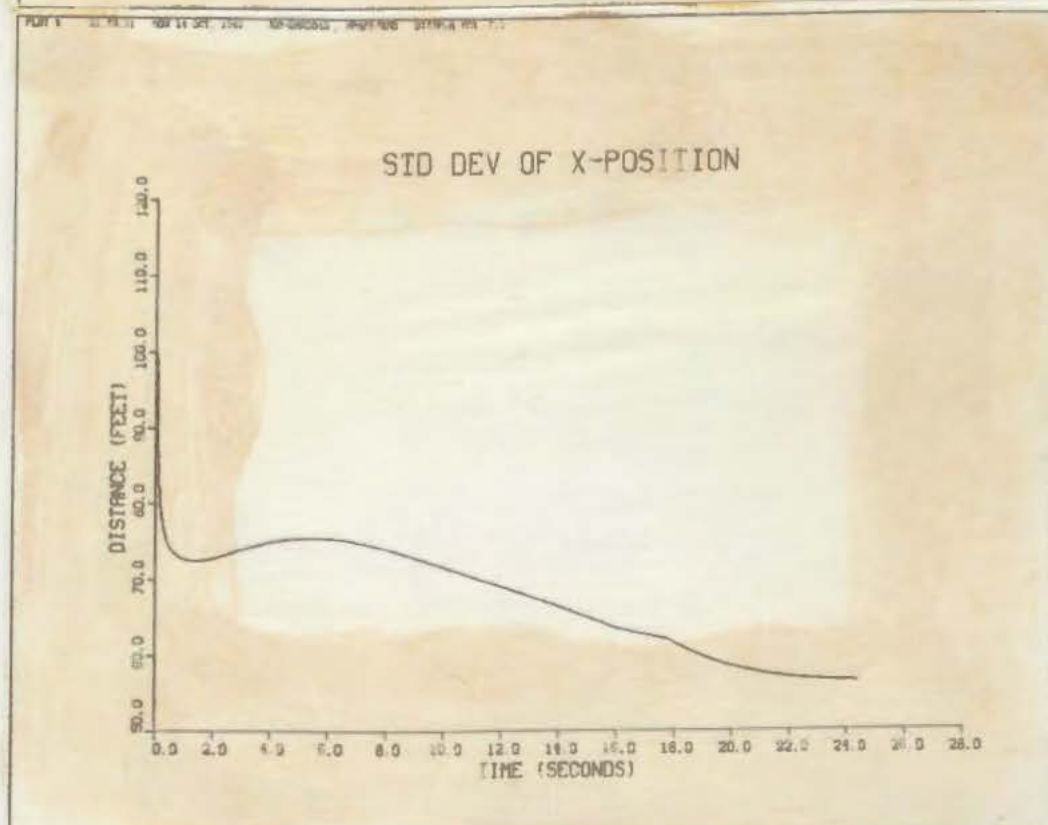
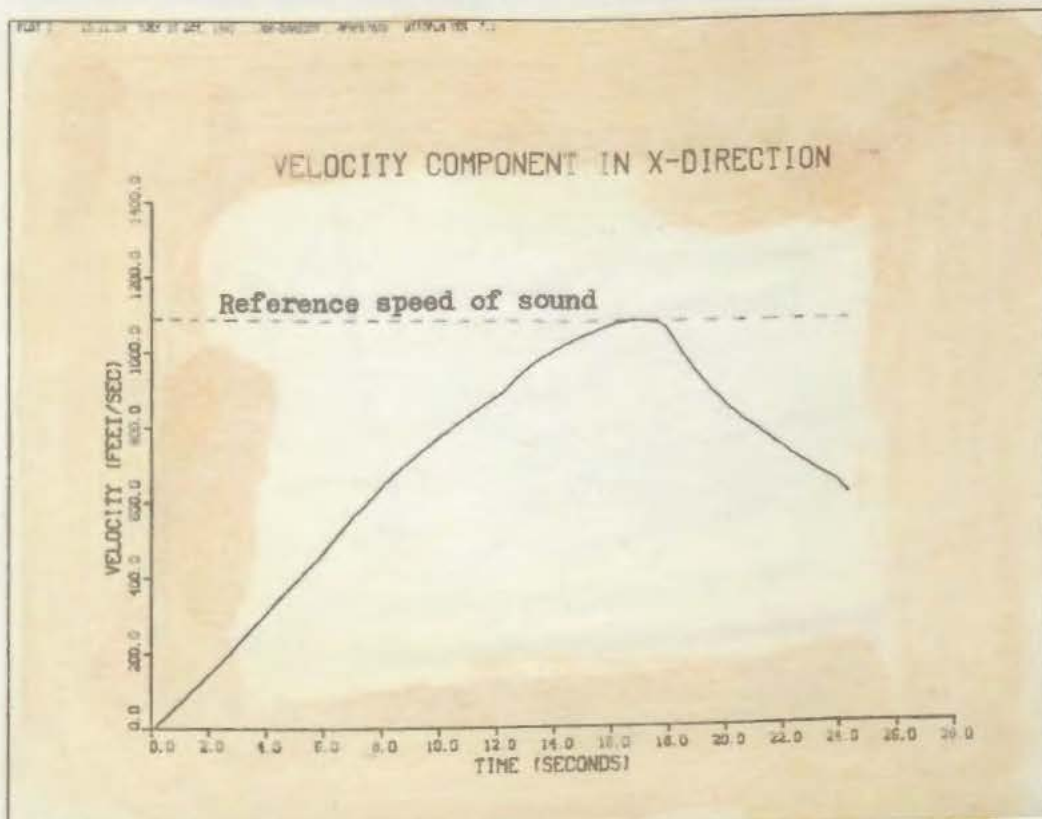


Fig. 4.17(a),(b) Extended Kalman filter - Range and azimuth

(a)



(b)

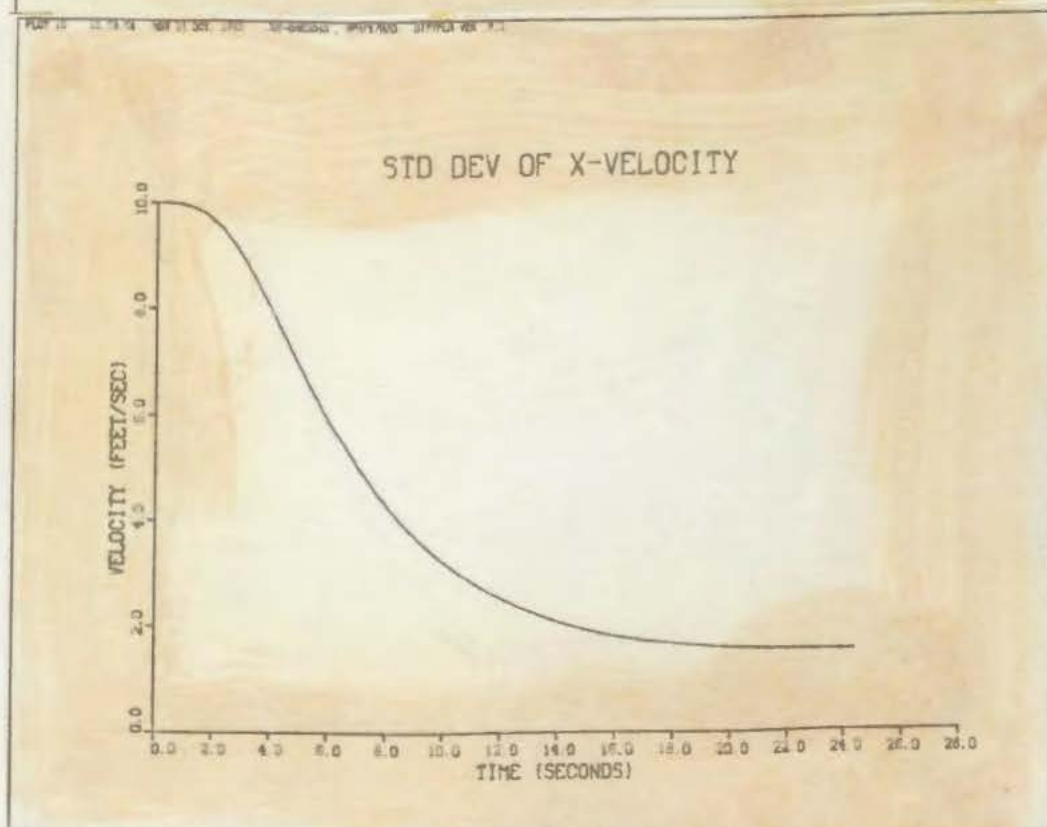
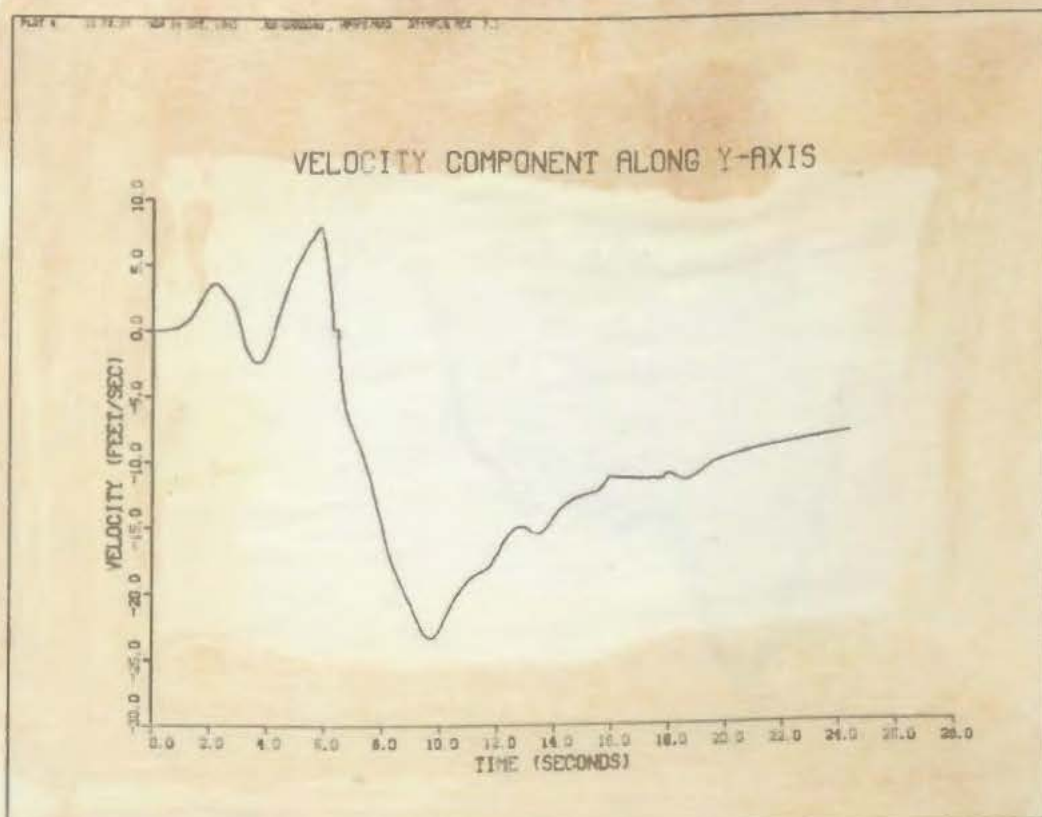


Fig. 4.19(a),(b) Extended Kalman filter - Range and Azimuth

(a)



(b)

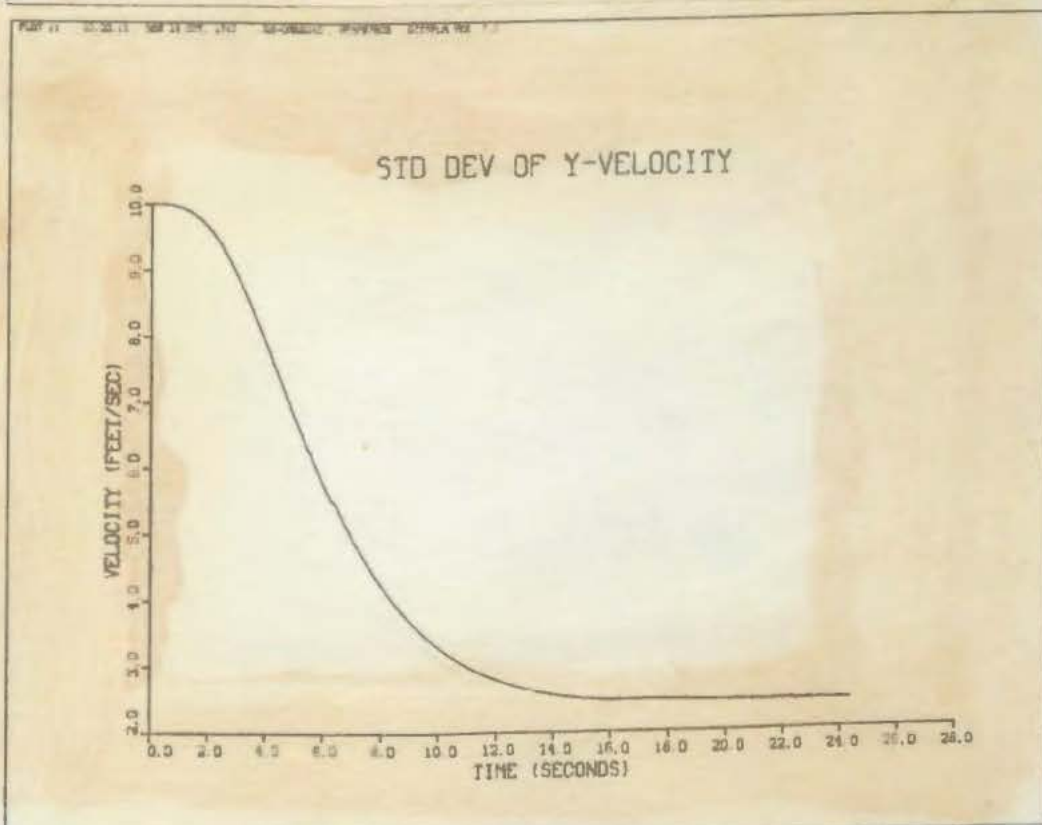
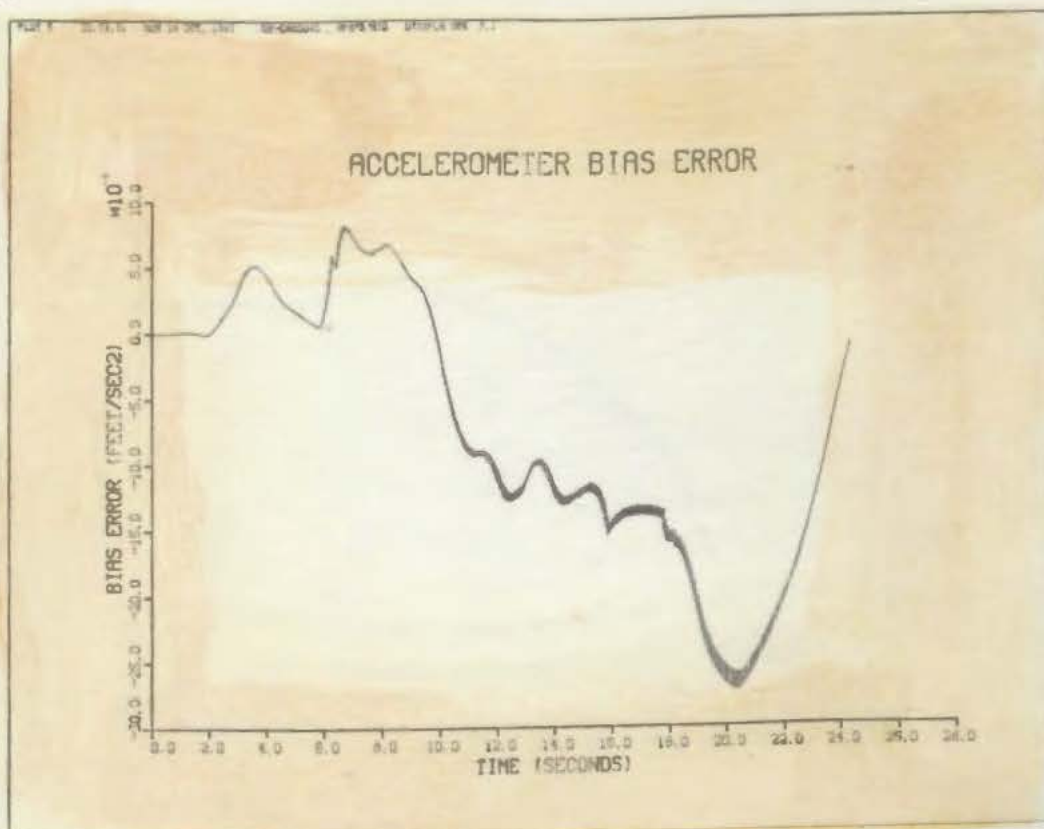


Fig. 4.20(a),(b) Extended Kalman filter - Range and Azimuth

(a)



(b)

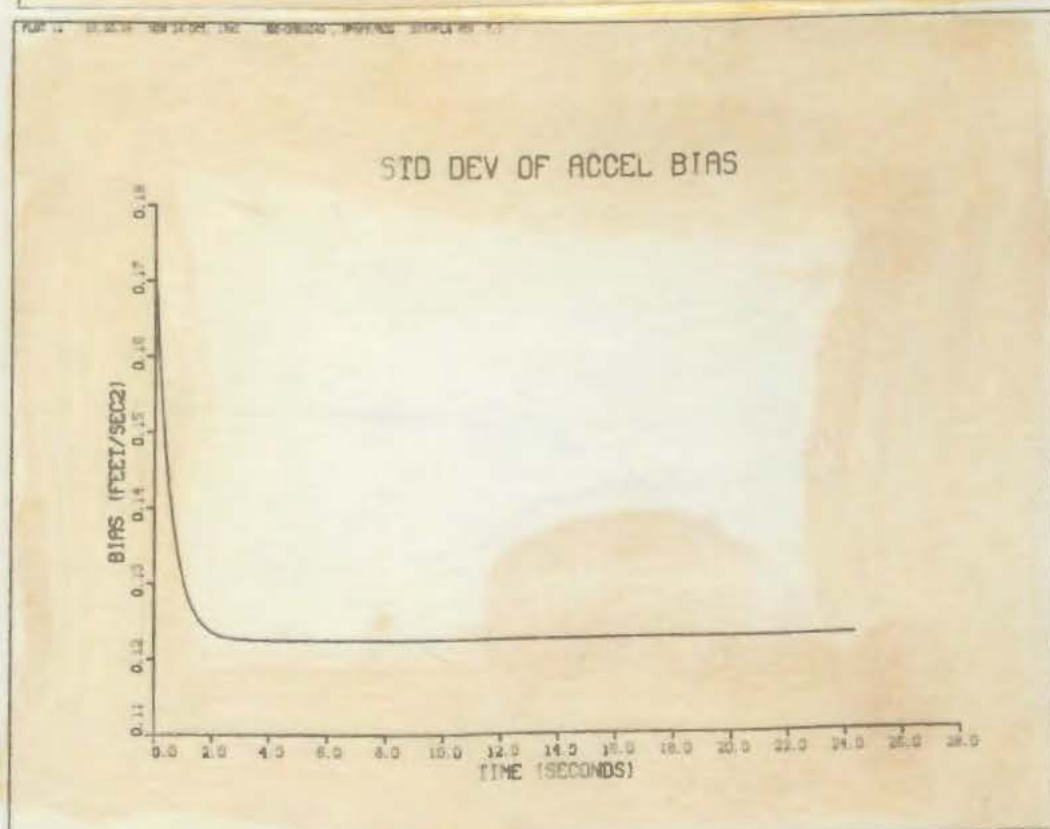
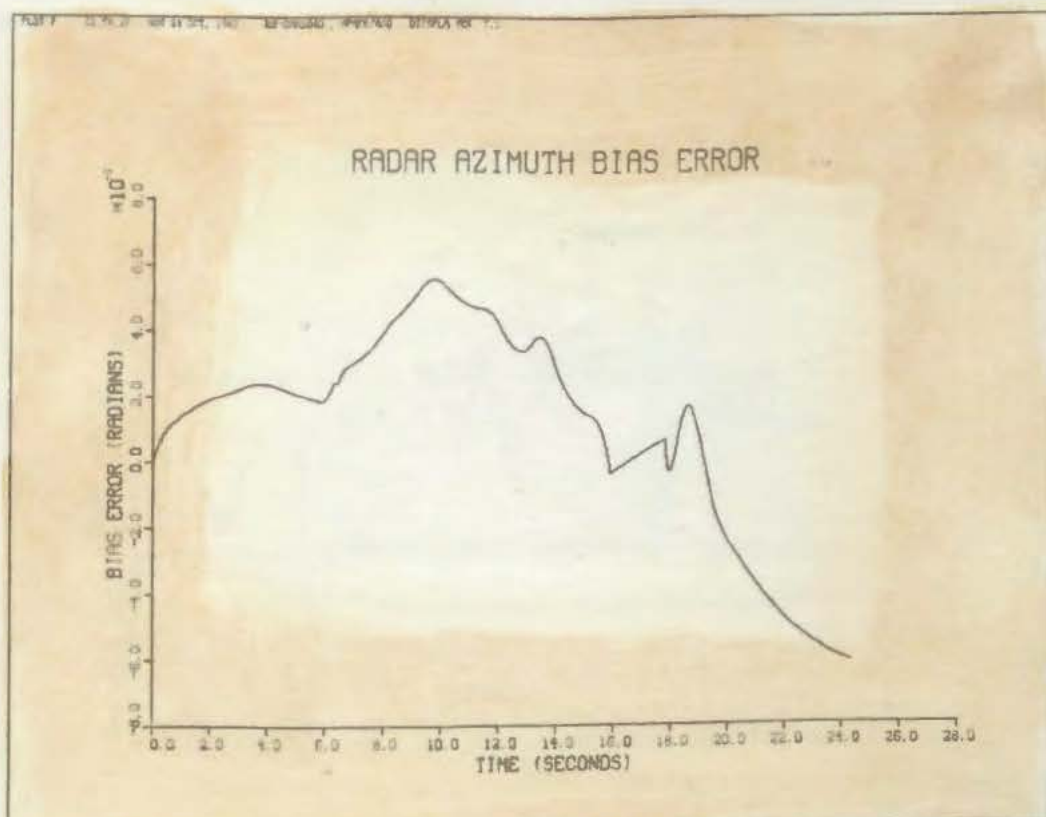


Fig. 4.21(a),(b) Extended Kalman filter - Range and Azimuth

(a)



(b)

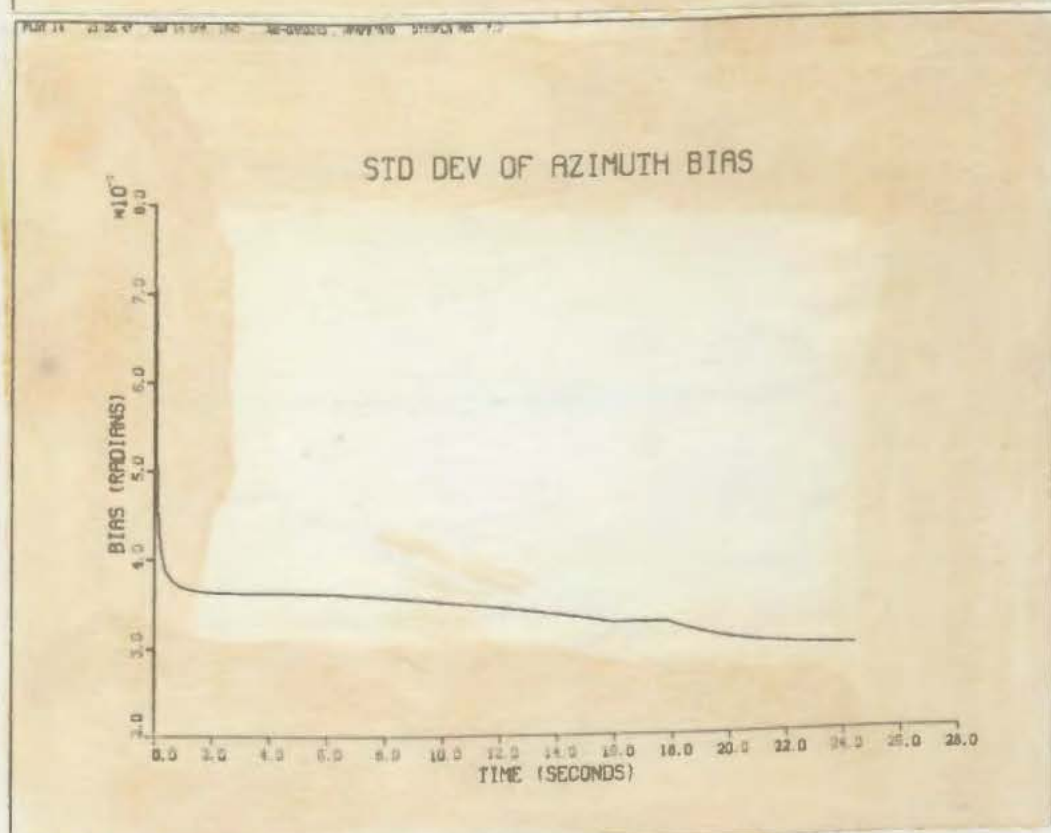
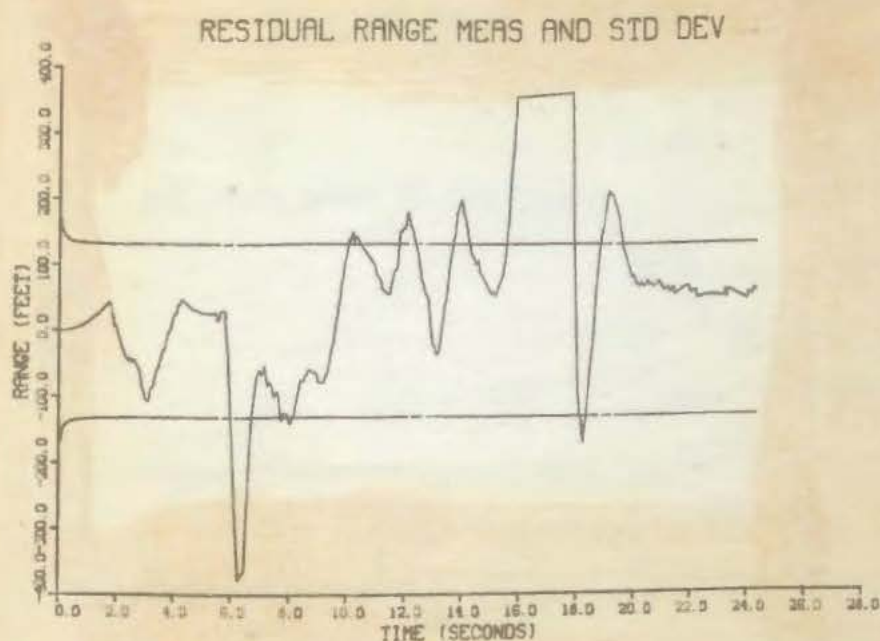


Fig. 4.23(a),(b) Extended Kalman filter - Range and Azimuth

(a)



(b)

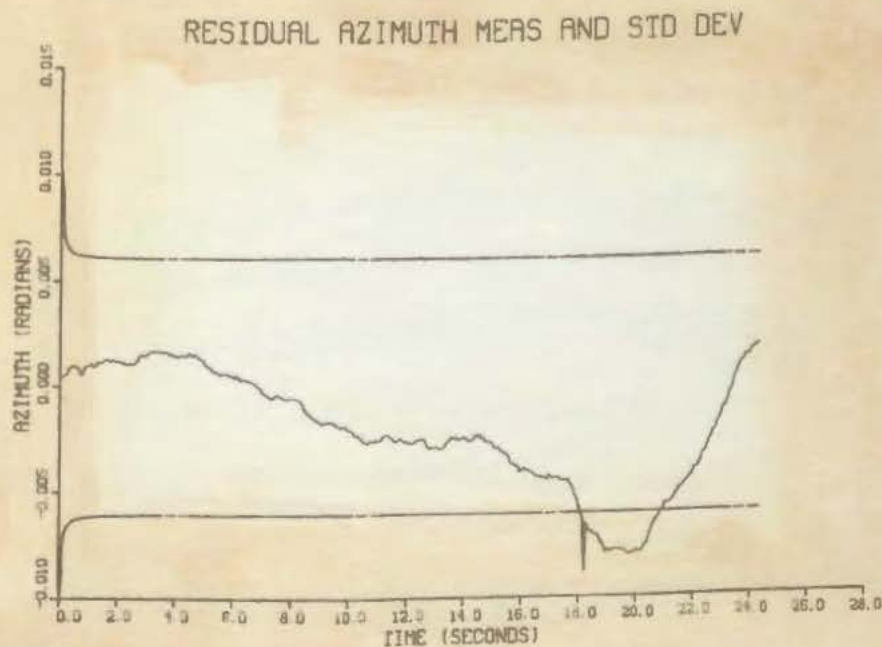
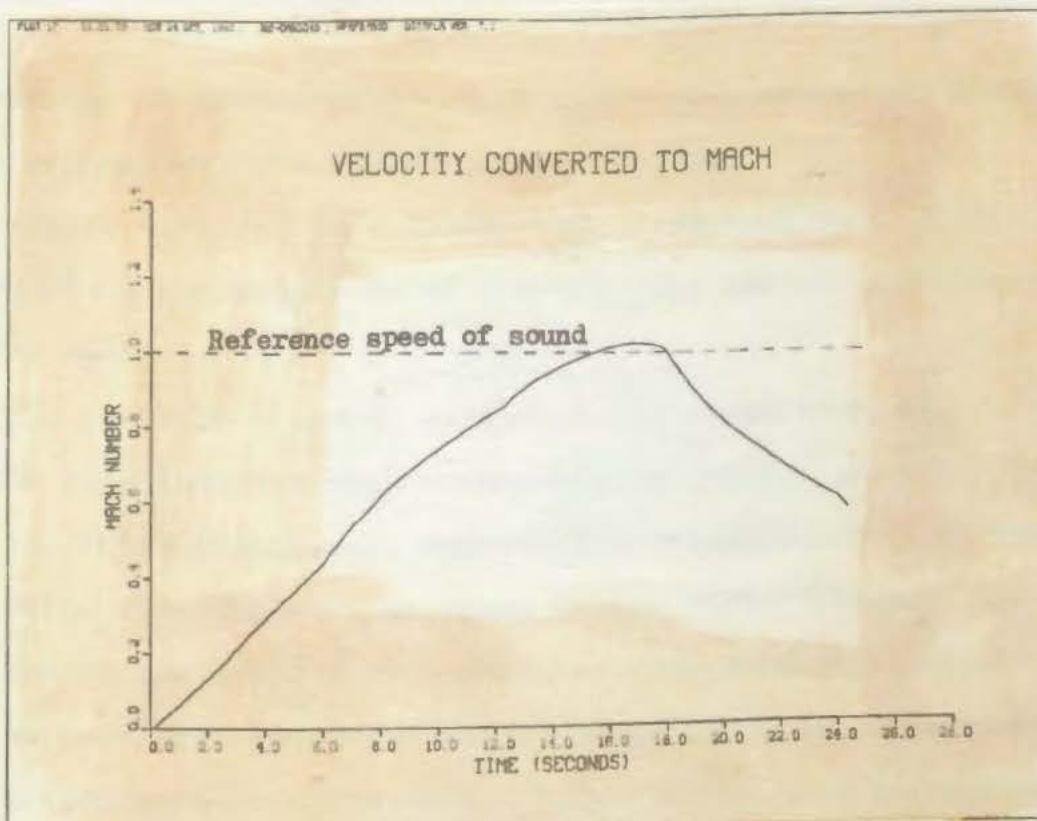


Fig. 4.24(a),(b) Extended Kalman filter - Range and Azimuth

(a)



(b)

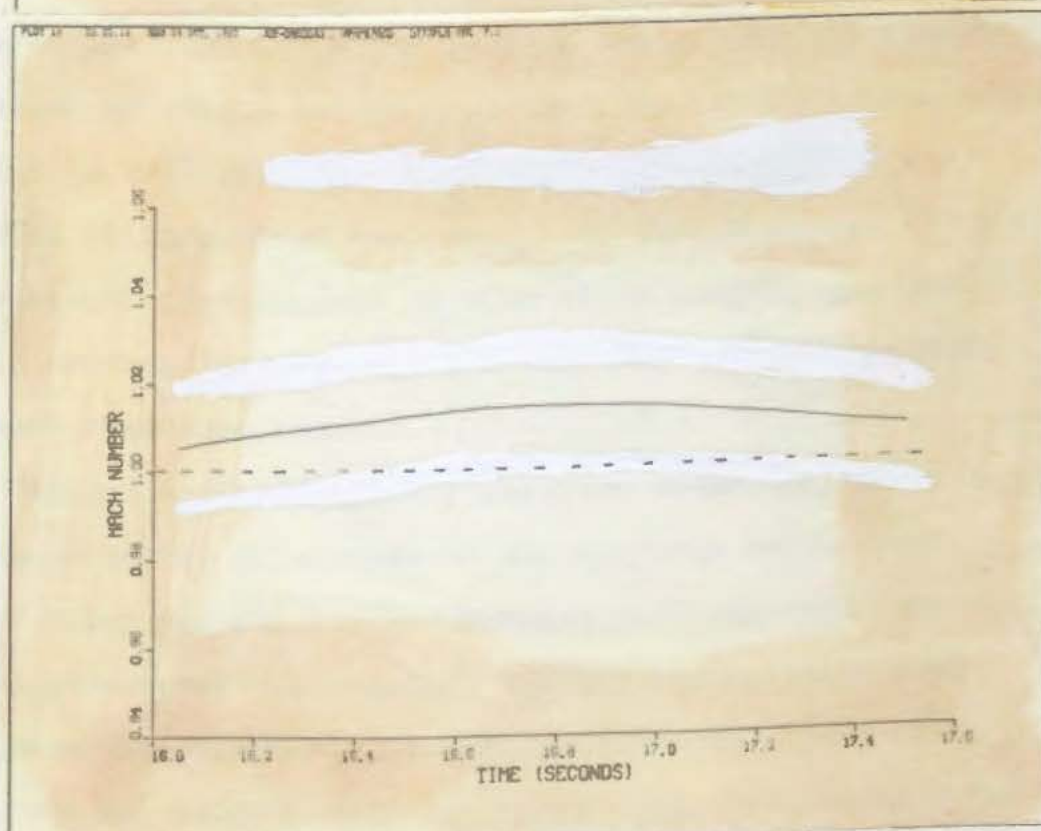


Fig. 4.25(a),(b) Extended Kalman filter - Range and Azimuth

monitoring, 40 measurements between 16-18 seconds, and three measurements near six seconds, are ignored.

Figure 4.25 (b) is a "blown up" version of Fig. 4.25 (a) which is the magnitude of the velocity vector converted to Mach number.

The plots of standard deviation for range bias and azimuth bias indicate weak convergence of the standard deviation for these states. As mentioned previously, this is due to limited observability of these states. The standard deviations of the other state estimates show good convergence and indicate that even the "noisy" range measurement provides some information on state values which can be used to improve state estimation. From the plot of range residual standard deviation it should be apparent that the residual monitoring routine is rejecting measurements of range which have a residual value greater than $3\sigma_{res}$, or approximately 390 feet. The straight line segment between 16-18 seconds and the "spike" at six seconds in Fig. 4.24 (a) show where the range measurements have been ignored.

The large deviation in y position shown in Fig. 4.18 (a) at approximately 10 seconds is due to range measurement errors which are significant between 6-10 seconds. The filter weights these measurements lightly due to relatively high measurement noise, but does not totally reject them. Thus, the estimated y position shows unrealistic values for this state due to inaccuracies in the range measurement. It appears from Fig. 4.11 (b) that during this four second

... ..
... ..

... ..
... ..

... ..
... ..
... ..

... ..
... ..

... ..

... ..

... ..

... ..

... ..

... ..

... ..

... ..

... ..

... ..

... ..

... ..

... ..

... ..

... ..

observability problems previously mentioned associated with estimating x_3 from range measurements. The azimuth only run of the extended Kalman filter indicates the following vehicle performance:

$$\hat{x}_{3\max} = 1080.26 \text{ (16.85 sec)}$$

$$\hat{x}_3 = 977.081 \text{ (18.65 sec, trap entry)}$$

$$\text{Time above Mach 1} = 1.30 \text{ sec}$$

The azimuth only run, however, does not provide very good estimates of y position or velocity due to the observability of these states from azimuth measurements alone. It should be noted, that the apparent error in x velocity caused by observability problems using range measurements is corrected by using the fixed-interval smoother algorithm. The time history of state estimates and error variances from the run of the extended Kalman filter incorporating both measurements is stored for use in the smoother algorithm. The results of the smoother analysis will be presented in the next chapter.

V. Optimal Smoother Results

Chapter II describes the Meditch form of the optimal "fixed-interval" smoother algorithm in detail. A simple FORTRAN program was written by the author to incorporate this smoother algorithm. The output of the extended Kalman filter, detailed in the previous chapter, is stored for use by the smoother program. The FORTRAN code used in the smoother program is listed for reference in Appendix B. The results obtained from this program are presented in this chapter.

The output of the optimal smoother at the initial time, t_0 , is used to correct the initial conditions for another iteration of the forward extended Kalman filter. Such a "forward-backward" iteration scheme is used to correct model errors and initial conditions of the extended Kalman filter. After each iteration of the forward-backward estimator a comparison of state values is made. When the difference in state estimates from one iteration to the next is less than some arbitrarily specified value, ϵ , the estimator is said to have "converged". Since our main area of concern is in the estimate of vehicle speed, we compare the peak estimates of velocity for each run of the smoother. When the difference between peak speed estimates from one iteration to the next is less than 2 ft/sec and the standard deviation of this estimate allows at least a 99 percent confidence that the vehicle exceeded the speed of sound, we stop the iterations. The latter requirement for standard deviation

becomes the driving factor due to time limitations and sufficient confidence after two iterations.

One Iteration of Smoother

The plots of the "smoothed" state estimates after one smoother iteration are presented in Figs. 5.1 (a) to 5.7 (a). The variance for each state estimate calculated by the smoother are presented in Figs. 5.1 (b) to 5.7 (b). Note that the smoother works "as advertised" in reducing the error variance of state estimates when compared to the standard deviation plots of the extended Kalman filter in Chapter IV. Some very interesting results are obtained and need to be discussed. The plot of y position, Fig. 5.2 (a) indicates that the vehicle track is indeed a straight line. However, the figure indicates that y position begins approximately 250 feet east of the assumed origin and decreases in a linear-manner to 60 feet east of centerline. This indicates that the starting position of the vehicle is displaced east of the earth-fixed coordinate frame and that the assumed track heading of 179 degrees true is incorrect by approximately .209 degrees. The smoother estimated state values and variances of x and y position at the start of the run, t_0 , are shown to be

$$\begin{aligned} \hat{x}_1(t_0/t_f) &= 167.78 \text{ ft} & P_{11}(t_0/t_f) &= 3746.5 \text{ ft}^2 \\ \hat{x}_2(t_0/t_f) &= 255.85 \text{ ft} & P_{22}(t_0/t_f) &= 3649.5 \text{ ft}^2 \end{aligned}$$

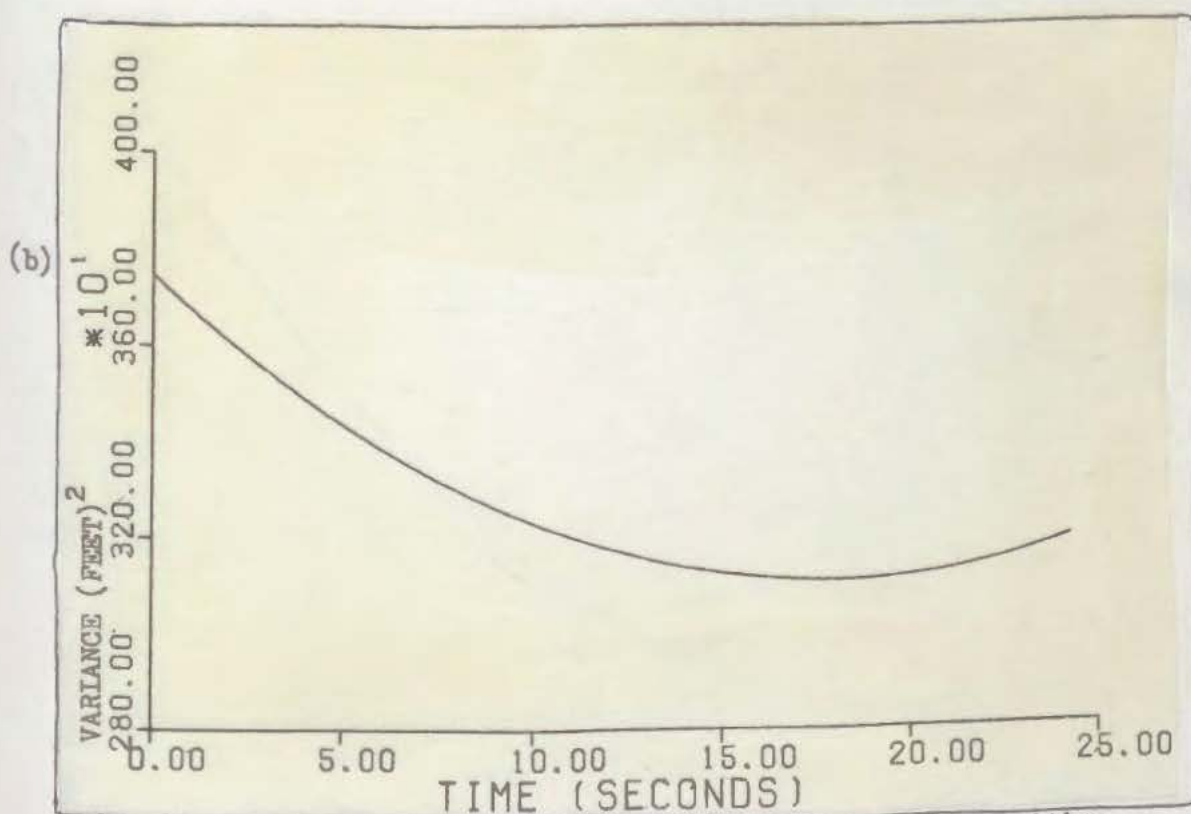
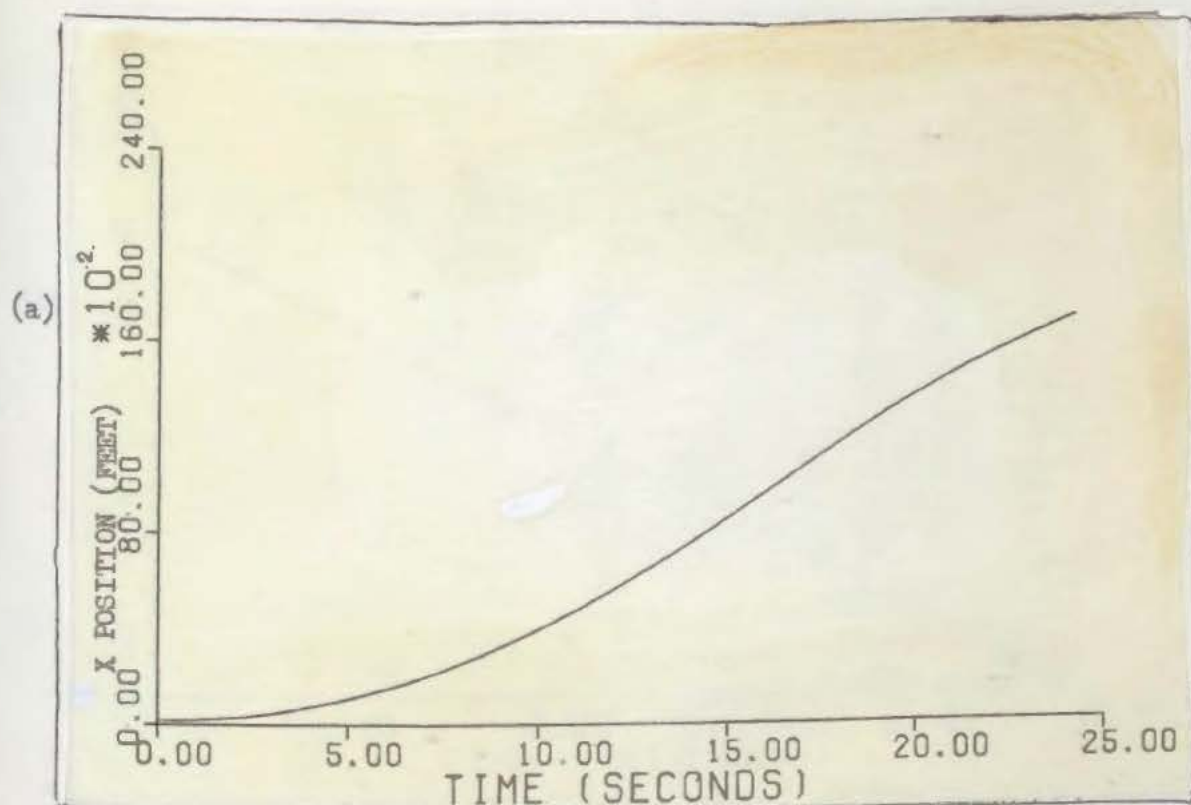
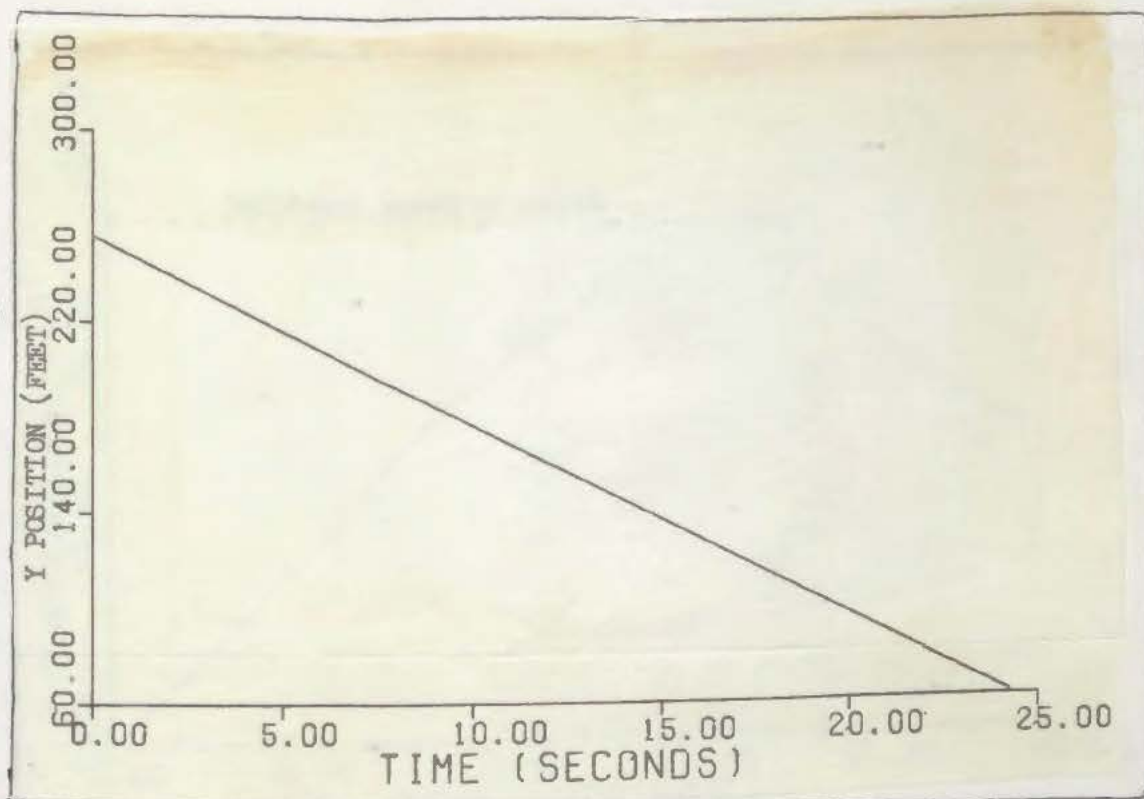


Fig. 5.1(a),(b) Smoother estimate and variance of x-position after one iteration.

(a)



(b)

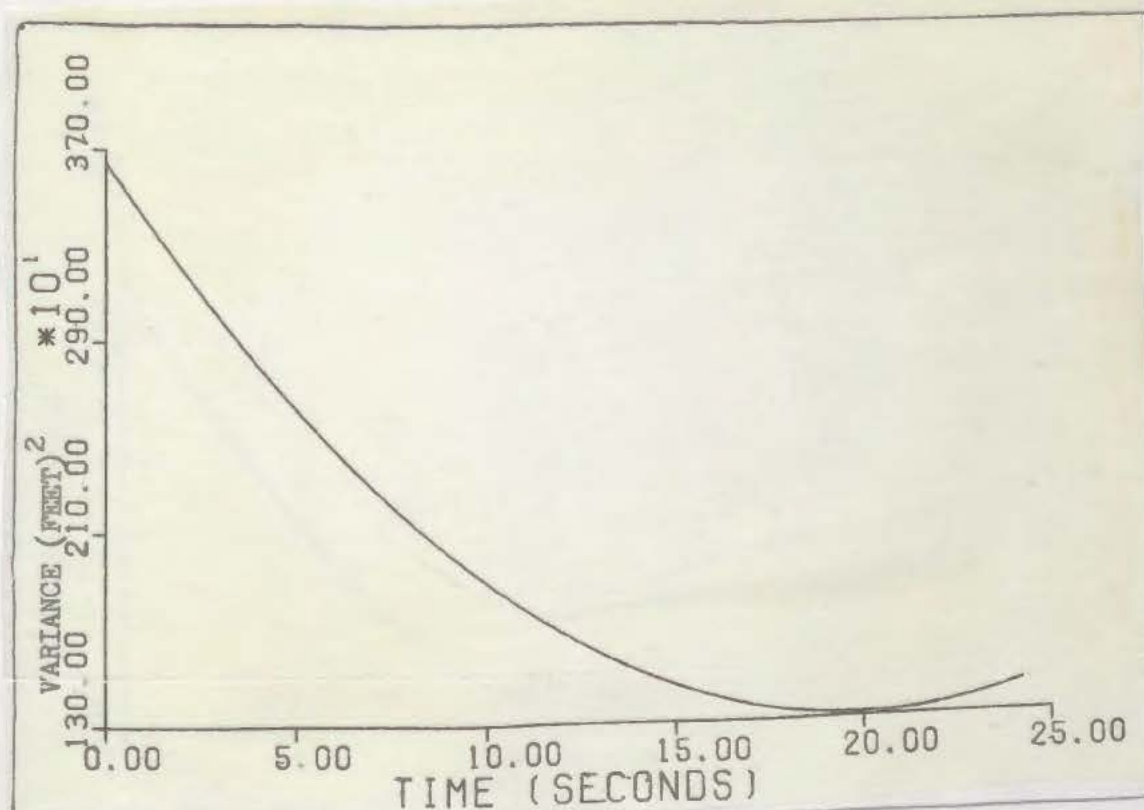


Fig. 5.2(a),(b) Smoother estimate and variance of y-position after one iteration.

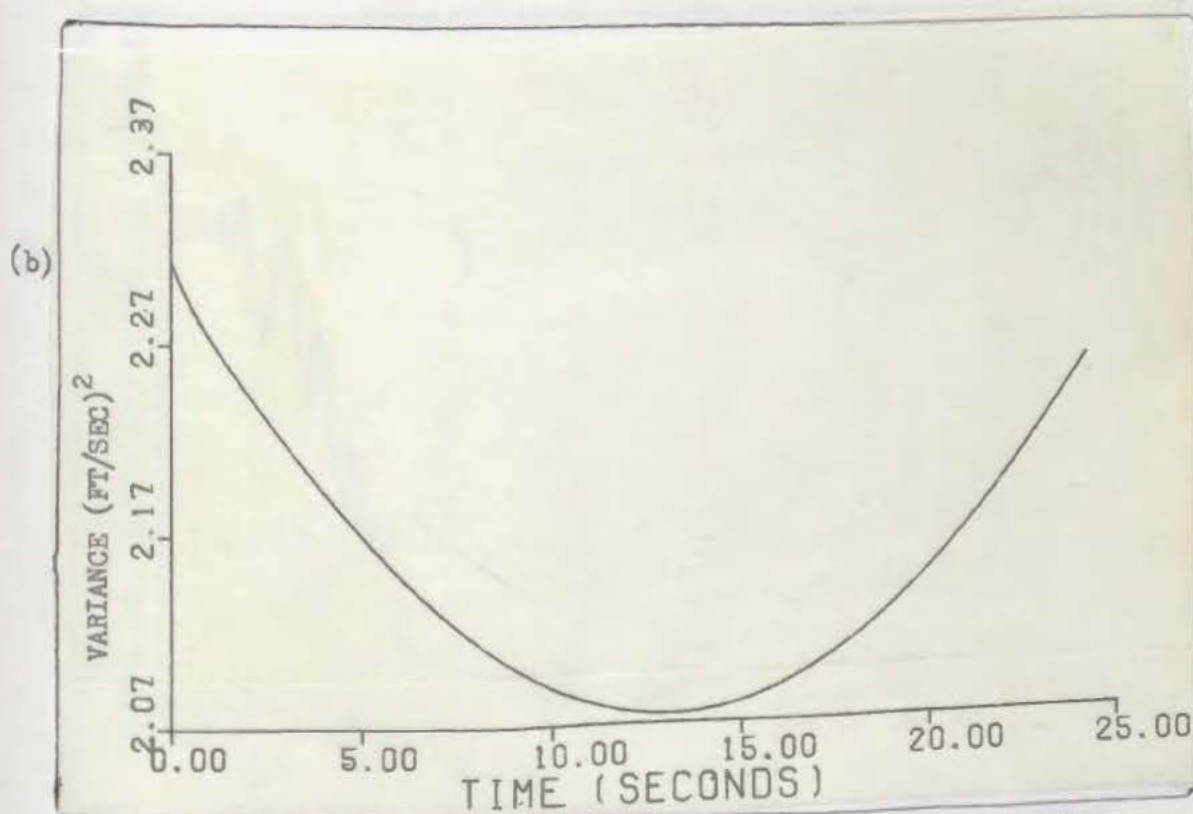
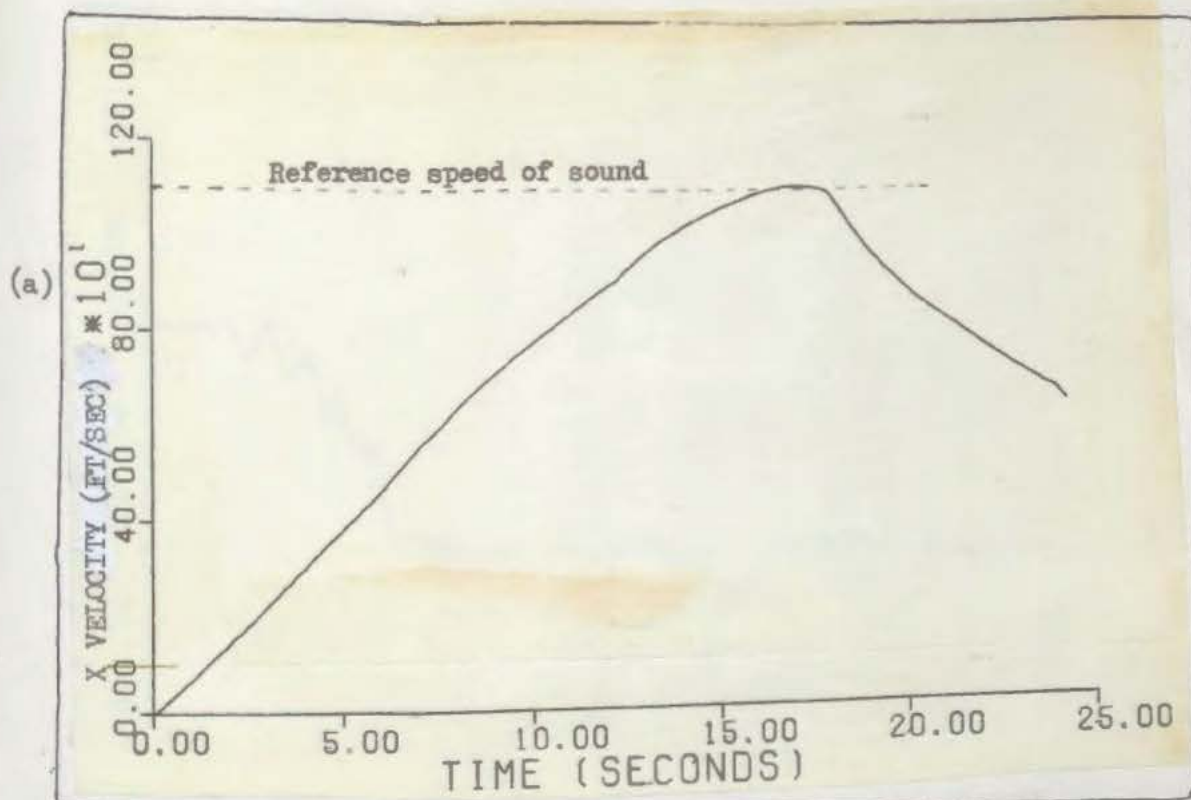


Fig. 5.3(a),(b) Smoother estimate and variance of x-velocity after one iteration.

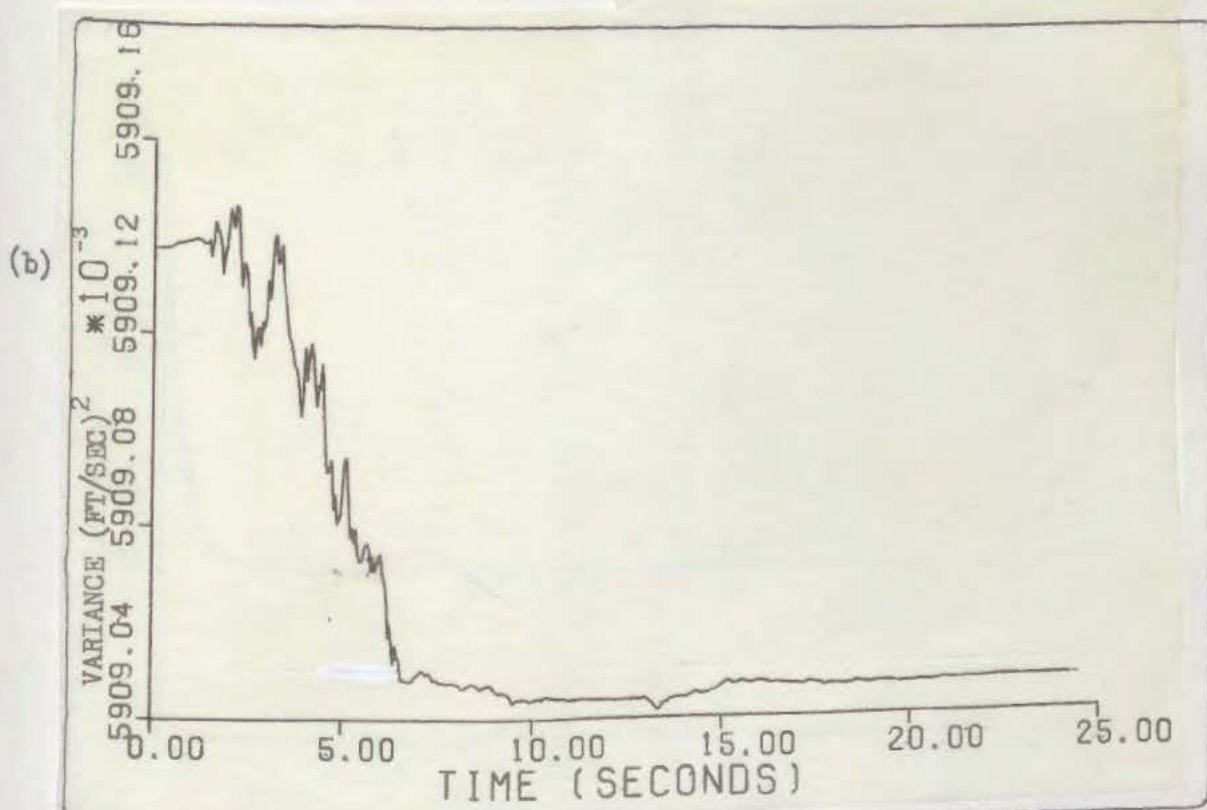
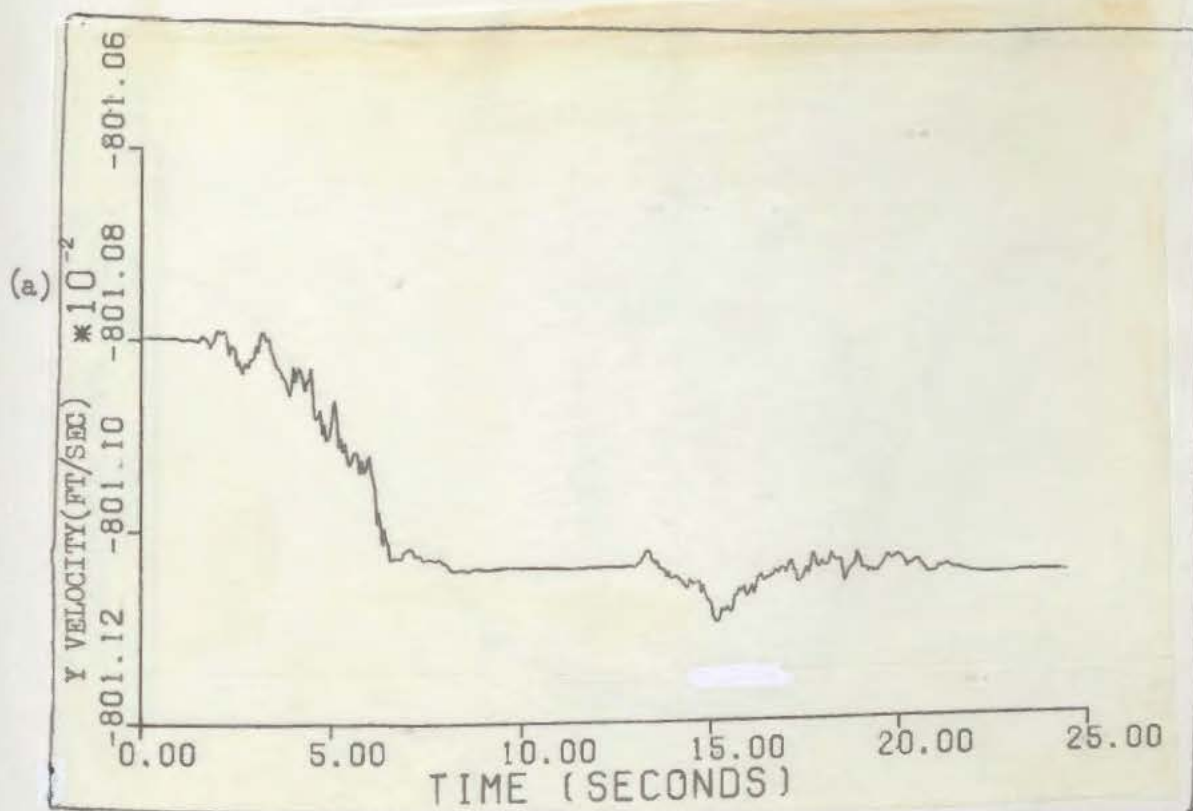


Fig. 5.4(a),(b) Smoother estimate and variance of y-velocity after one iteration.

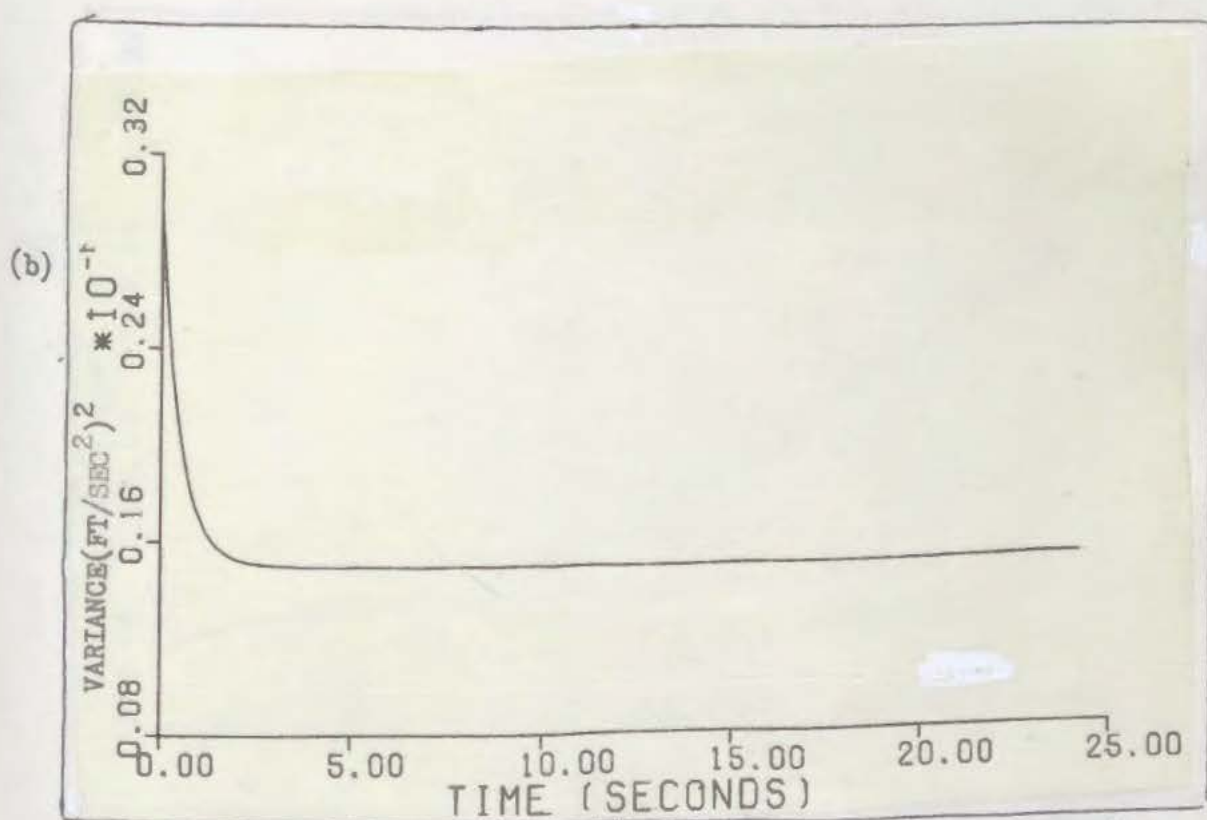
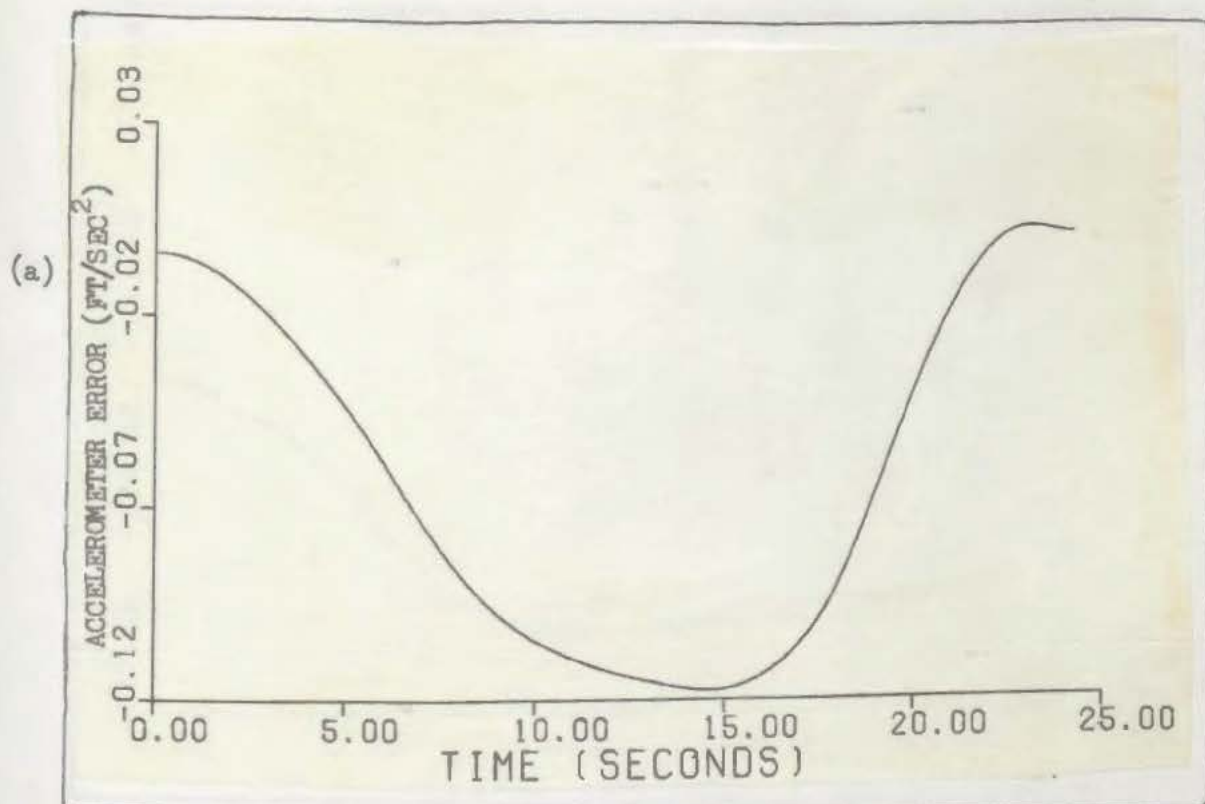
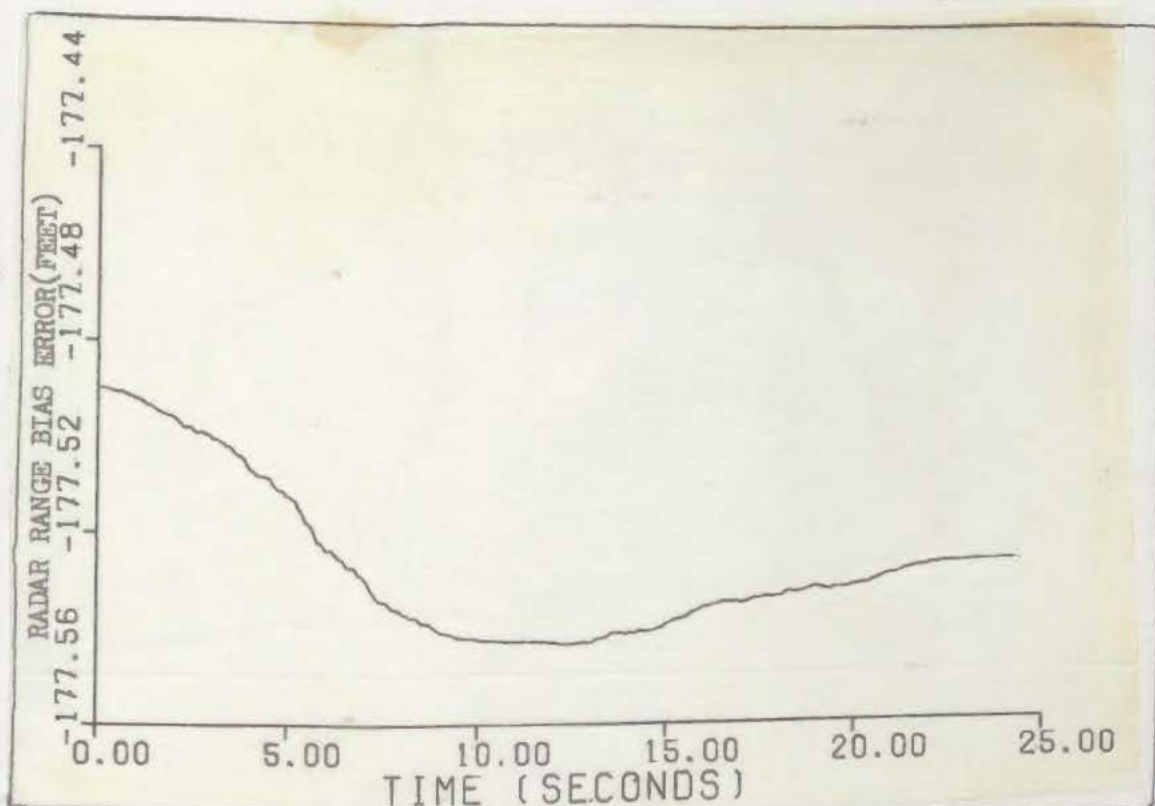


Fig. 5.5(a),(b) Smoother estimate and variance of accelerometer error after one iteration.

(a)



(b)



Fig. 5.6(a),(b) Smoother estimate and variance of range bias error after one iteration.

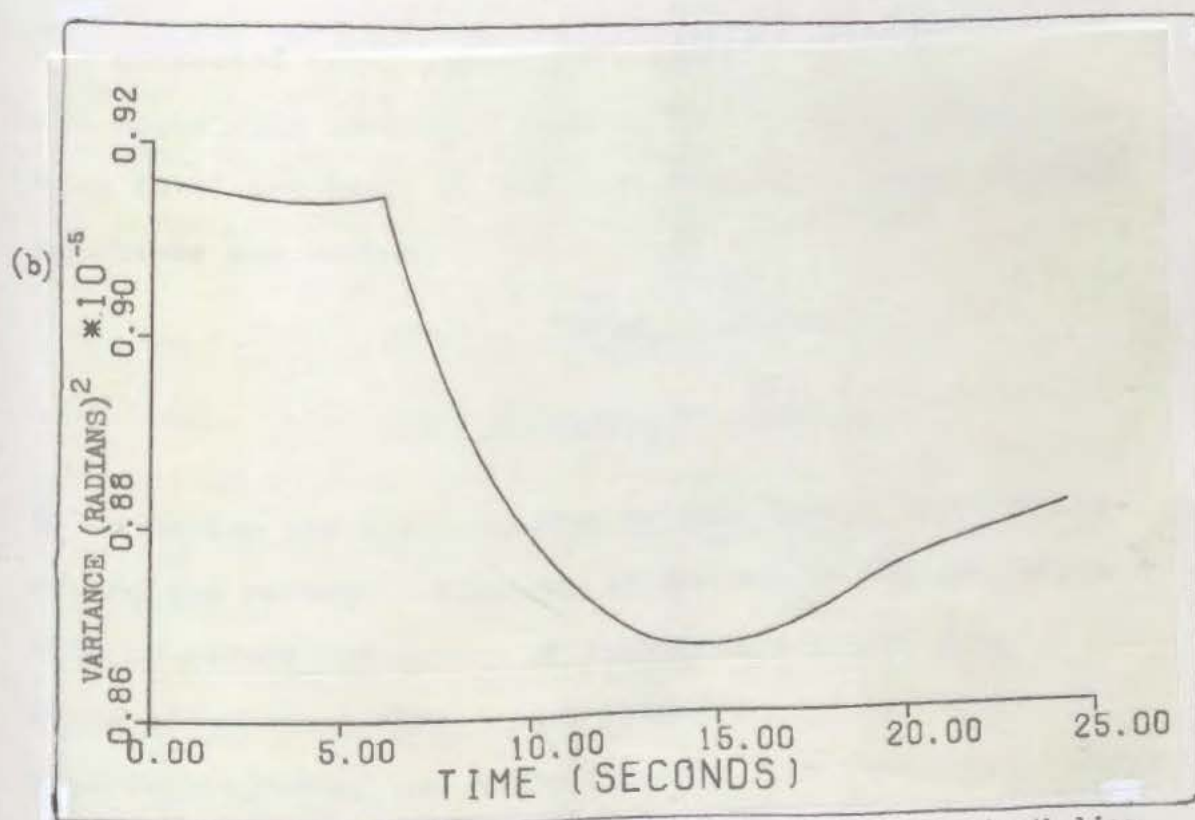
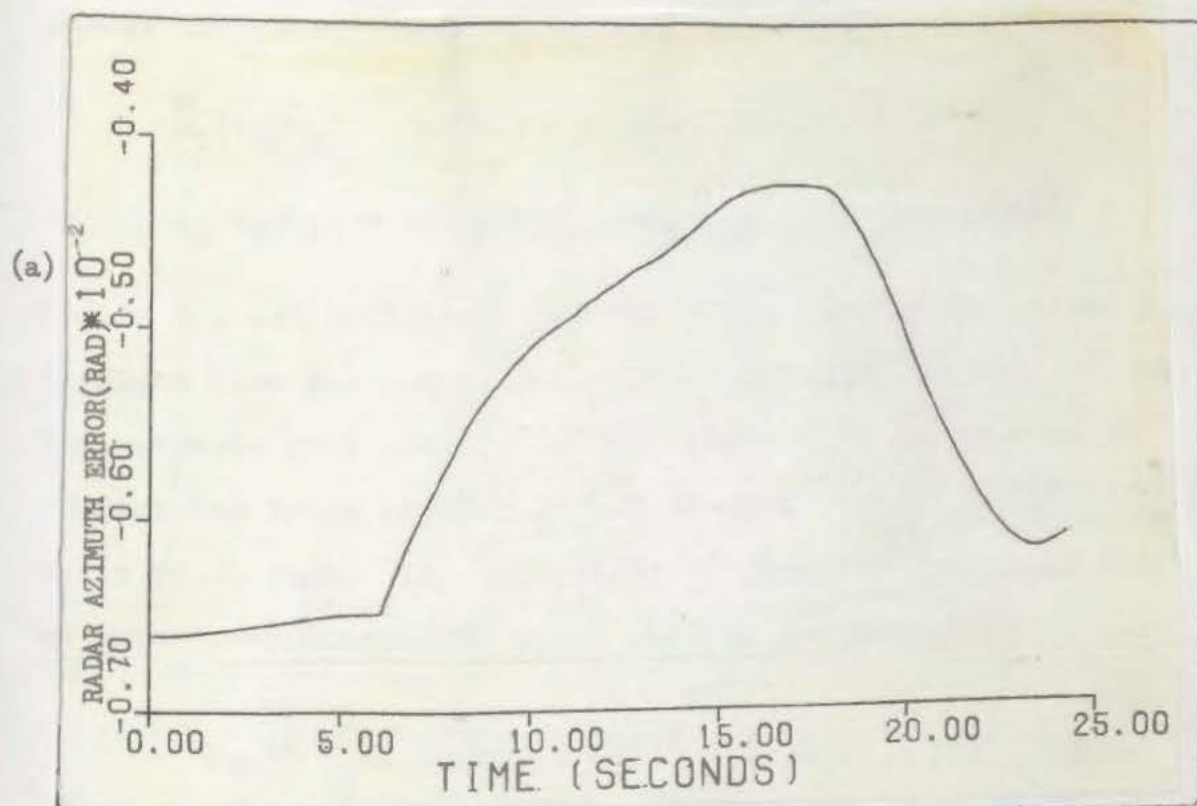


Fig. 5.7(a),(b) Smoother estimate and variance of azimuth bias error after one iteration.

and at the final time, $t_f = 24.3$ seconds:

$$\hat{x}_1(t_f/t_f) = 16771 \text{ ft} \quad P_{11}(t_f/t_f) = 3186.3 \text{ ft}^2$$

$$\hat{x}_2(t_f/t_f) = 61.21 \text{ ft} \quad P_{22}(t_f/t_f) = 1428.0 \text{ ft}^2$$

Figure 5.2 (a) indicates that the vehicle track is indeed a straight line but not aligned with the x-axis we have chosen. The estimate of y position at the final time is used to re-correct the track heading of 179 degrees. The y position at t_f is 61.21 feet. This deviation in position indicates that we have "over-corrected" track heading previously by:

$$\tan^{-1} \left[\frac{\hat{x}_2(t_f/t_f)}{\hat{x}_1(t_f/t_f)} \right] = \tan^{-1} \left[\frac{61.21}{16771} \right] = .209 \text{ degree}$$

The corrected track heading now becomes 179.209 degrees. We can apply this corrected heading to the measurement relation (4-5) and (4-6) so that the bracketed terms in these equations now become:

$$(\text{DELX} - .9999x_1 + .0138x_2)$$

$$(\text{DELY} + .0138x_1 + .9999x_2)$$

By adjusting the track heading by this amount and recalculating the residual variance, as in Chapter IV, we should be able to reduce the amount of measurement noise, $R(t_i)$.

These adjustments should help reconfirm our knowledge of vehicle trajectory and allow the next forward-backward iterations to converge to the "true" state values.

In addition to resetting the initial covariance matrix, \underline{P}_0 , to reflect smoother covariance $\underline{P}(t_0/t_f)$, we also correct the initial conditions of the state vector and adjust the amount of driving noise, $\underline{Q}(t)$. We should note here that several methods are available to adjust $\underline{Q}(t)$. The backward-recursive smoother can be used to generate an estimate of system noise at each sample time, $\hat{\underline{Q}}(t_i/t_f)$ (4). One can also "tune" $\underline{Q}(t)$ in an "off-line" manner and allow the system noise to vary over the time interval of interest. If one has knowledge of the time-varying nature of a particular state, this knowledge can be used to adjust the strength of driving noise. For example, we might desire to relate the amount of driving noise on the azimuth bias error state to incorporate our knowledge of radar operator tracking performance versus vehicle acceleration. As a side note, we should also mention that the smoother algorithm can be used to generate an estimate of the applied controls, $\hat{\underline{u}}(t_i/t_f)$. An estimate of the controls applied to the system at any time, t_i , is not the concern of this analysis. We also choose to iteratively adjust $\underline{Q}(t)$ and use constant noise levels over the time interval of interest. Such an iterative adjustment to $\underline{Q}(t)$ provides adequate smoother performance and simplifies the algorithm.

Figure 5.4 (a) is a plot of the y component of velocity obtained after one iteration of the smoother algorithm. It is apparent from this plot that the y velocity indeed behaves as a constant with a value of approximately -8.0 ft/sec.

This constant negative velocity is caused by the erroneous initial conditions we used in the extended Kalman filter. As seen in Fig. 5.4 (a) the smoother is able to detect small deviations from the constant y velocity. This is seen as small "bumps" in the plot of y velocity. Thus, our model of random walk with small driving noise is reconfirmed and will be used for the next forward-backward iteration.

The smoother estimated value for accelerometer error, $\hat{x}_5(t_i/t_f)$, can be seen in Fig. 5.5 (a). The error appears to grow with time and seems to be related to velocity (i.e., the higher the velocity, the more error). The error does appear to be time-correlated and does not behave as a constant bias error. Thus, the time-correlated model for accelerometer bias appears to be valid. We can, however, adjust the driving noise on the propagation of this state by using the smoother calculated steady state variance. Figure 5.5 (b) shows a constant variance of $0.14937(\text{ft}/\text{sec}^2)^2$ after only a very short transient period. We can adjust the driving noise on this state by using this steady-state variance:

$$q_5 = P_5(\infty)2/T = .029874 (\text{ft}/\text{sec}^2)^2/\text{sec}$$

The initial variance value for this state, P_{05} , is also set to $.014937 (\text{ft}/\text{sec}^2)^2$ to insure a stationary accelerometer error state process.

Figure 5.6 (a) is a plot of smoother estimated radar range bias error, $\hat{x}_6(t_i/t_f)$. This figure indicates that this state indeed behaves as a constant with only slight

variations from the initial estimate, $\hat{x}_6(t_o/t_f) = -177.49$ ft. Thus, a reduction in the amount of driving noise on this state appears valid. We now reduce the strength of driving noise on this state to indicate more confidence in its behavior as a constant. The value of q_6 for the next iteration of the extended Kalman filter-smoother combination is obtained by "tuning" the extended Kalman filter in a sensitivity analysis. The new value for q_6 is determined to be:

$$q_6 = .0001 \text{ ft}^2/\text{sec}$$

This amount of driving noise is two orders of magnitude less than the value used in the first iteration. The new initial variance for x_6 becomes:

$$P_{o6} = 1186.1 \text{ ft}^2$$

and the new initial condition on this state obtained from the smoother becomes:

$$\hat{x}_{o6} = -177.49 \text{ ft}$$

Referring to Fig. 5.7 (a) we see that the azimuth bias error, $\hat{x}_7(t_i/t_f)$, does not behave entirely as a constant. It appears that during the first five seconds of the run the bias error is greatest and reduces to a minimum value as the vehicle achieves peak speed (minimum acceleration). As the vehicle begins to decelerate, the azimuth bias error again grows to a larger value. This result is consistent with our knowledge of radar operator tracking error. The

amount of driving noise on this state appears adequate to allow the filter to track deviations in its value. Thus, q_7 is left unchanged for the next iteration of the forward-backward estimator. We adjust the initial condition and variance of this state, as before:

$$P_{07} = .91619 \text{ E-5 rad}^2$$

$$\hat{x}_{07} = .0066051 \text{ rad}$$

The extended Kalman filter and smoother are used again with new initial conditions on the states and adjusted initial variance. The amount of driving noise on accelerometer error, x_5 , and range bias, x_6 , are also adjusted for the next iteration of the forward-backward estimator. As a result of the first iteration of the smoother we make the following adjustments to our model for measurements and initial conditions:

- 1) The track heading is corrected to 179.209 degrees true.
- 2) Based on the corrected model for measurement incorporation, we recalculate measurement residual variance to reduce the estimate for $\hat{R}(t_i)$, $\hat{R}(t_i)$.
- 3) Initial conditions on the state vector are corrected to reflect the smoother calculation of $\hat{x}(t_o/t_f)$ such that

$$\hat{x}_0 = \begin{bmatrix} 167.78 \\ 255.88 \\ 1.1896 \\ -8.0108 \\ -.003834 \\ -177.49 \\ -.0064 \end{bmatrix}$$

4) The initial covariance matrix, \underline{P}_0 , is adjusted to reflect the smoother calculated value of $\underline{P}(t_0/t_f)$:

$$\underline{P}_0 = \begin{bmatrix} 3746.5 & & & & \\ & 3649.5 & & & \\ & & 2.315 & & 0 \\ & & & 5.91 & \\ 0 & & & .015 & \\ & & & & 1186.1 \\ & & & & & .916E-5 \end{bmatrix}$$

5) Finally, the system noise matrix, $\underline{Q}(t)$ is corrected to indicate increased confidence in our model for range bias, and adjusted steady-state variance on the accelerometer error:

$$\underline{Q}(t) = \begin{bmatrix} 0 & & & & \\ & 0 & & & \\ & & 0 & & 0 \\ 0 & & & .1E-7 & \\ & & & .02987 & \\ & & & & .1E-3 \\ & & & & & .1E-7 \end{bmatrix}$$

The residual variance analysis detailed in Chapter IV now produces an estimated measurement noise matrix, $\hat{\underline{R}}(t_i)$, such that:

$$\hat{\underline{R}}(t_i) = \begin{bmatrix} 16235.4 & 0 \\ 0 & .3900685E-4 \end{bmatrix}$$

The range residual variance is calculated from 415 of 487 total measurements which have a residual magnitude less than 300 feet. These variance values result in calculated RMS errors for the range and azimuth measurements of 127.42 ft and .006245 radian, respectively.

Incorporating updated values for measurement noise, initial state and variance conditions, and system noise, we

rerun the extended Kalman filter. The results of this run are shown in Appendix A. The state and covariance time histories are stored for use in a second iteration of the smoother algorithm.

Second Iteration of Smoother

The second iteration of the optimal smoother algorithm provides refined state estimates as shown in Figs. 5.8 (a) to 5.14 (a). The basic behavior and values of these states remain unchanged from the first iteration of the smoother. The smoother state estimates at the initial time, t_0 , are refined from those obtained in the first iteration.

To illustrate the convergent properties of the smoother, we present a comparison of state estimates and variances between the first and second smoother iterations in Table II. This table includes the percentage difference between the two iterations for each state and variance value and the overall percentage change between the second and first iteration. We choose to compare these values at the time of peak vehicle speed at 16.85 seconds. Table II indicates good reduction in error variance for all the states. This is due to the improved initial conditions supplied to the extended Kalman filter after the first run of the smoother. The smoother is able to reduce error variance from the first to second iterations due to improved state estimates from the forward filter. The convergence of the velocity state estimates and reduction in error variance on these states is

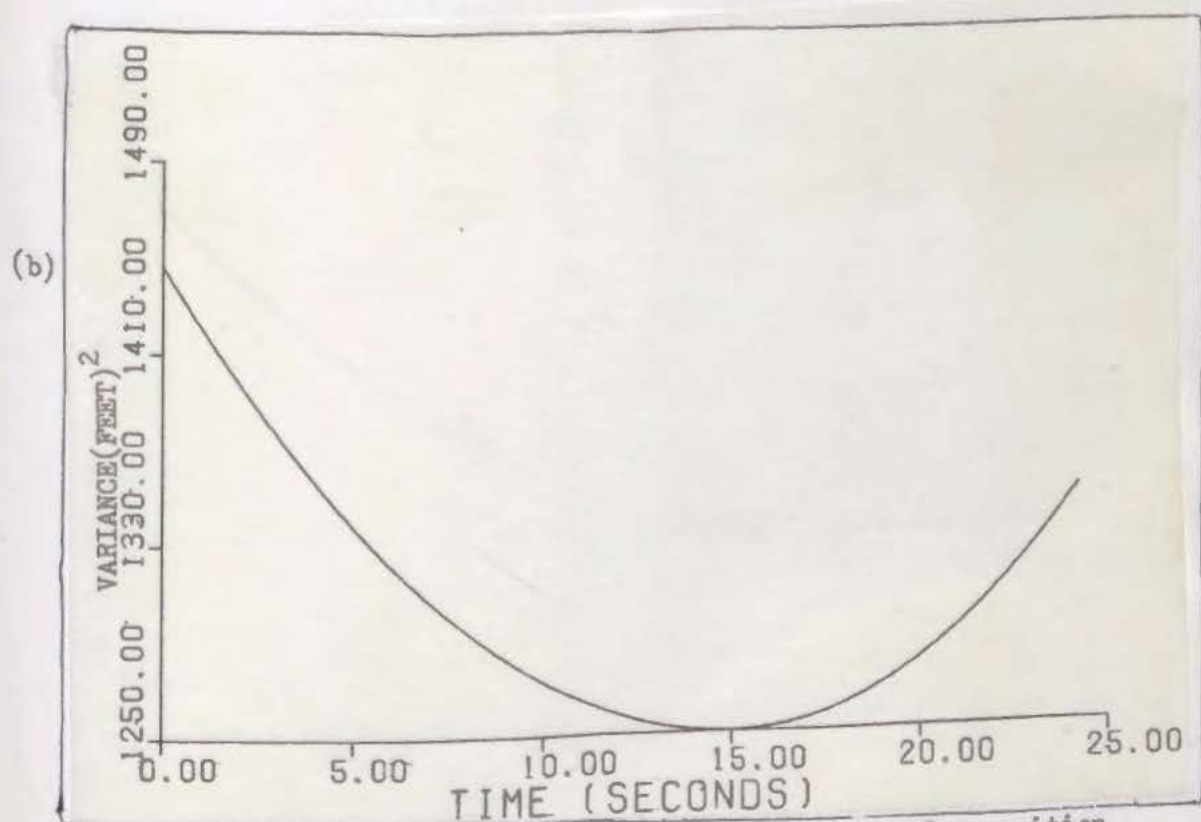
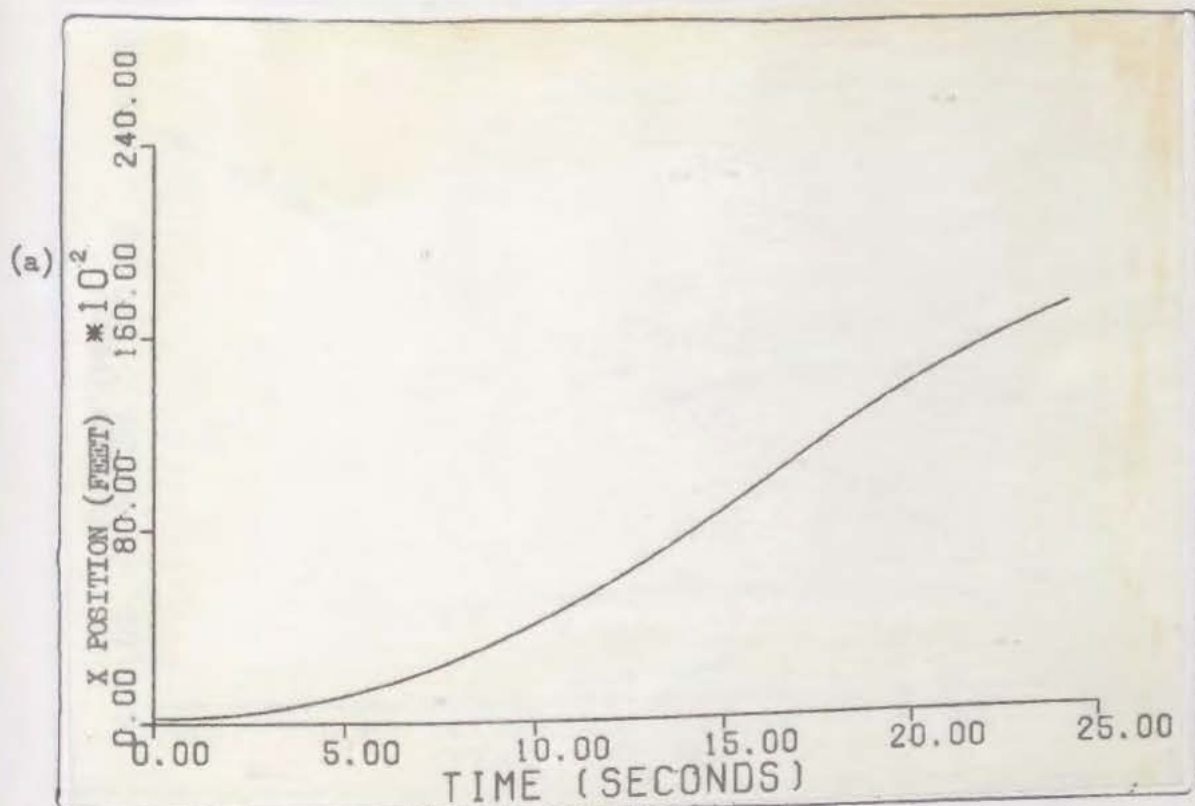


Fig. 5.8(a),(b) Smoother estimate and variance of x-position after two iterations.

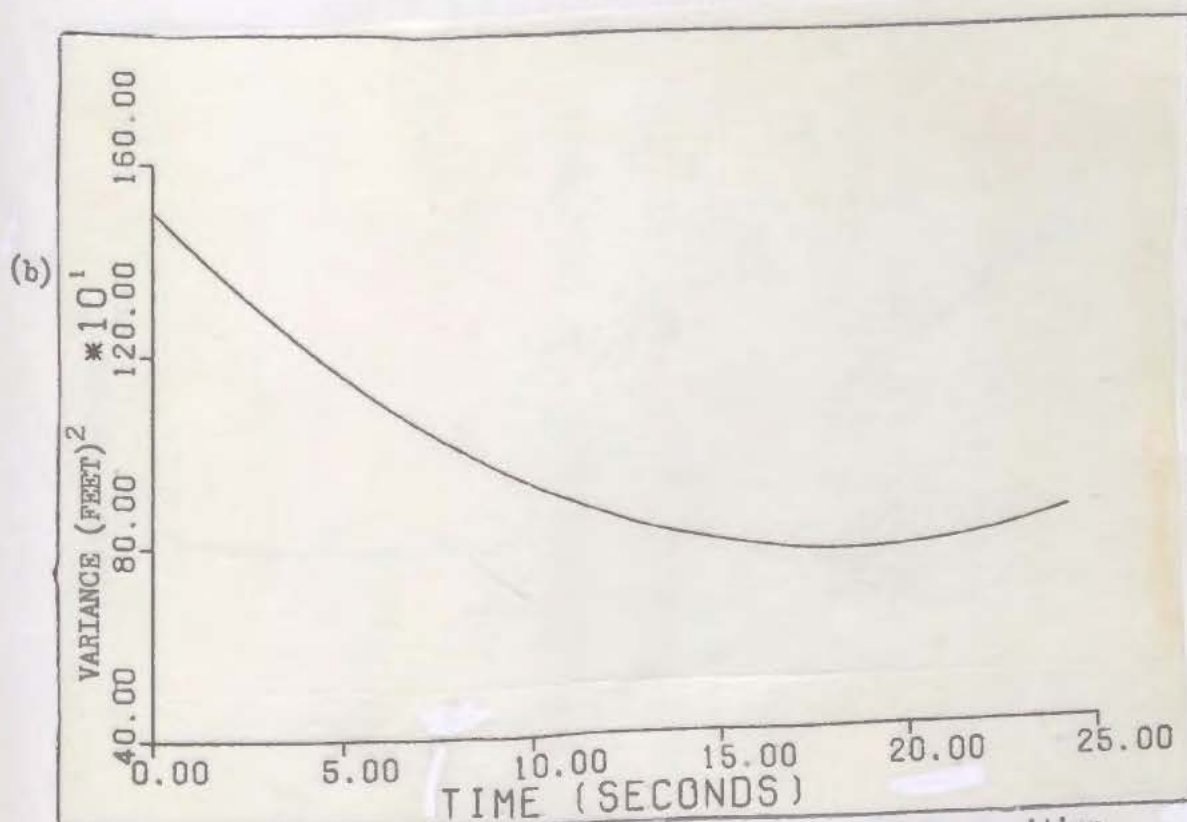
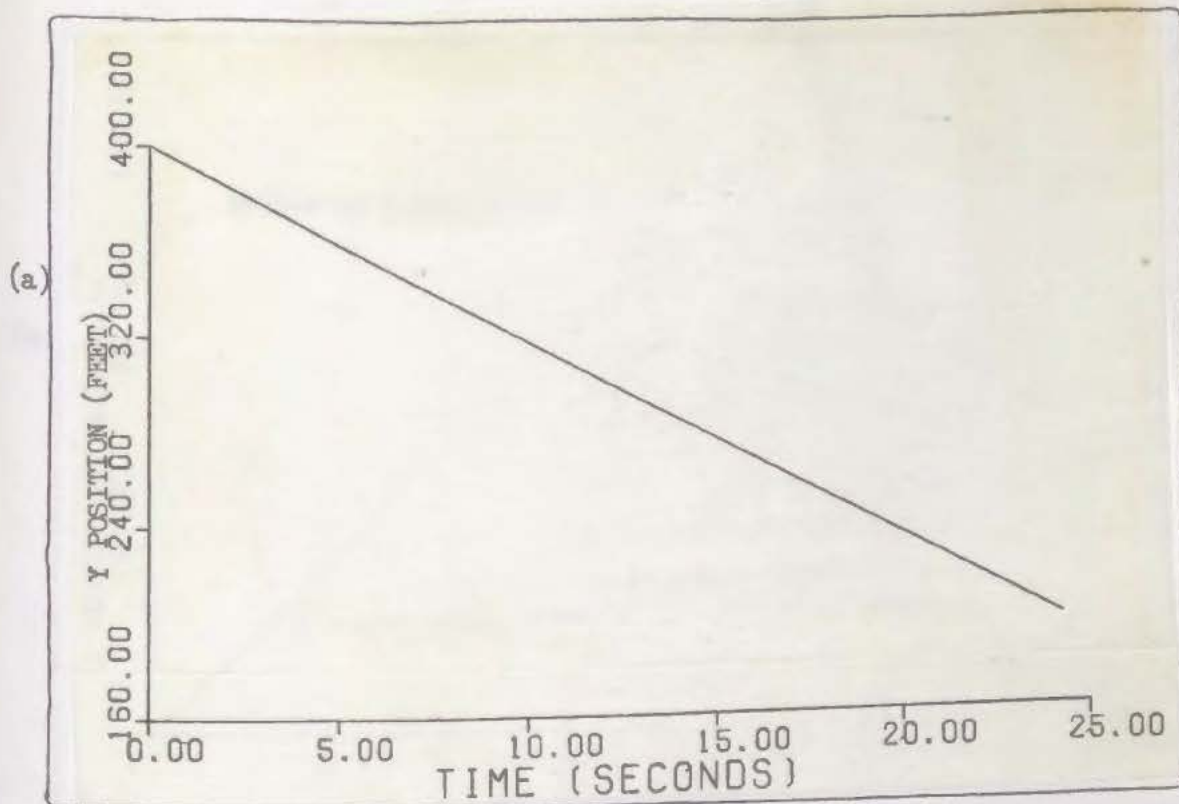
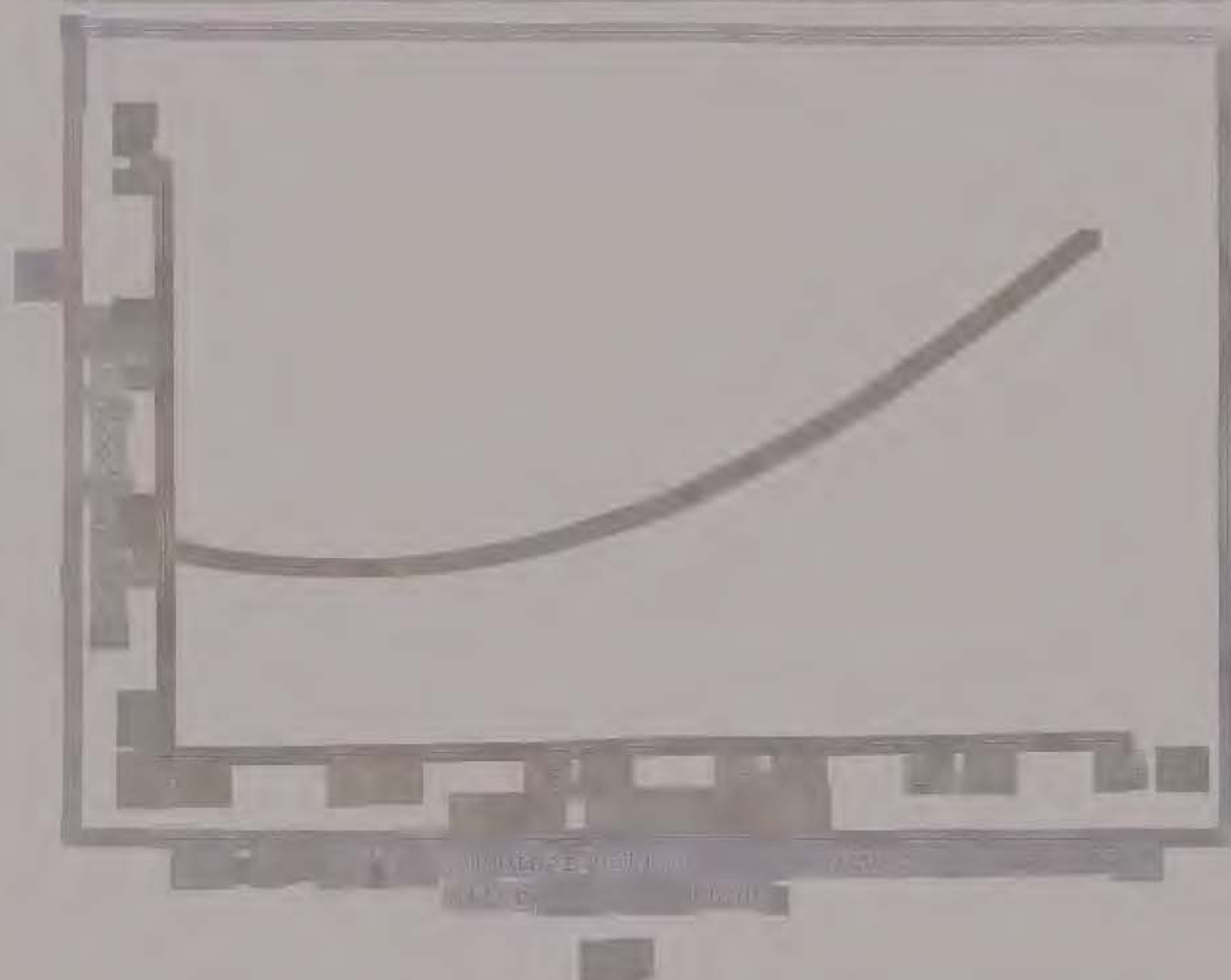
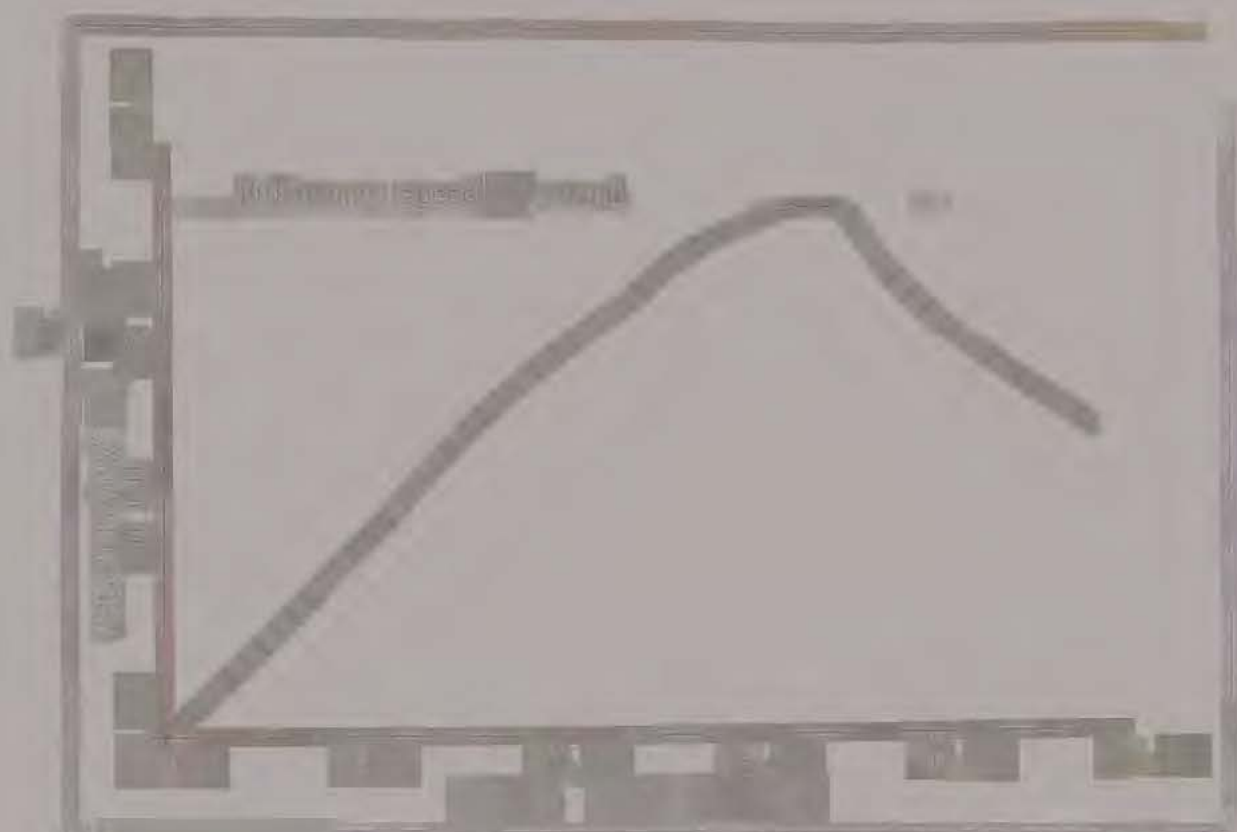


Fig. 5.9(a),(b) Smoother estimate and variance of y-position after two iterations.



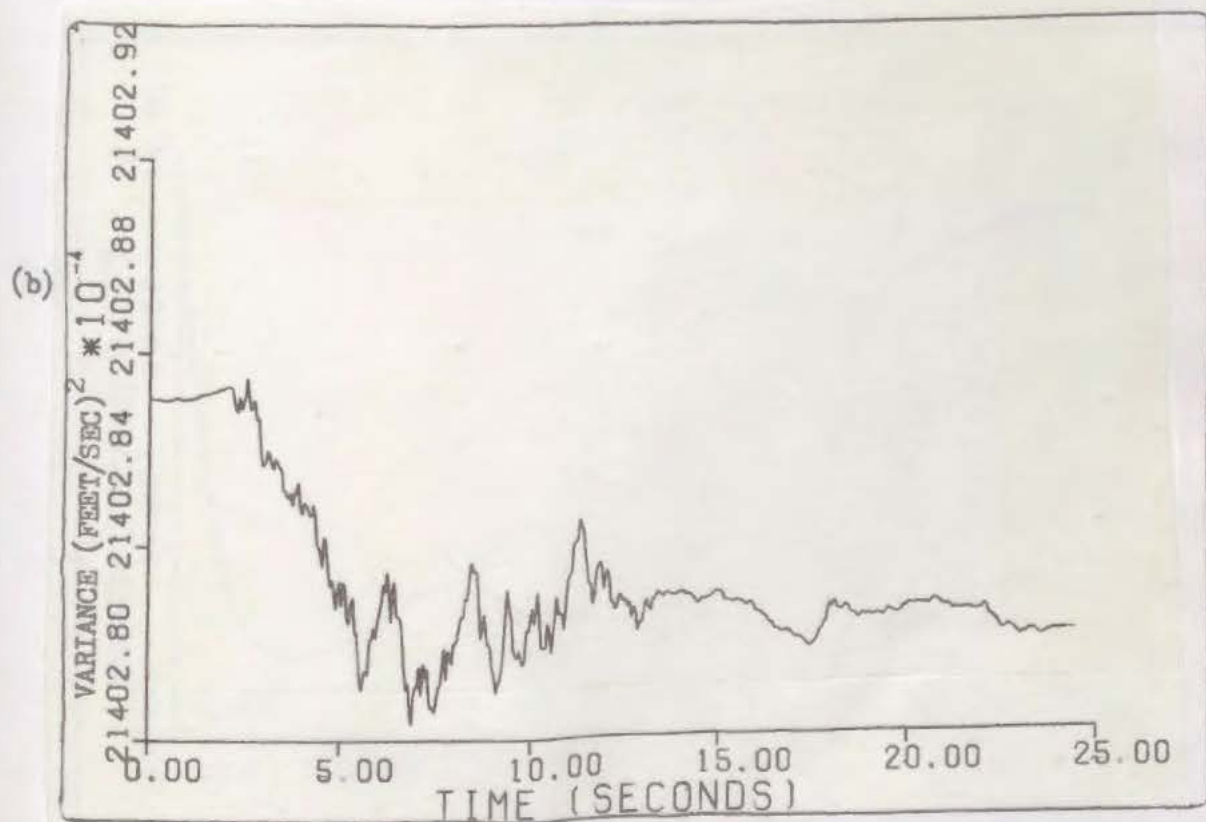
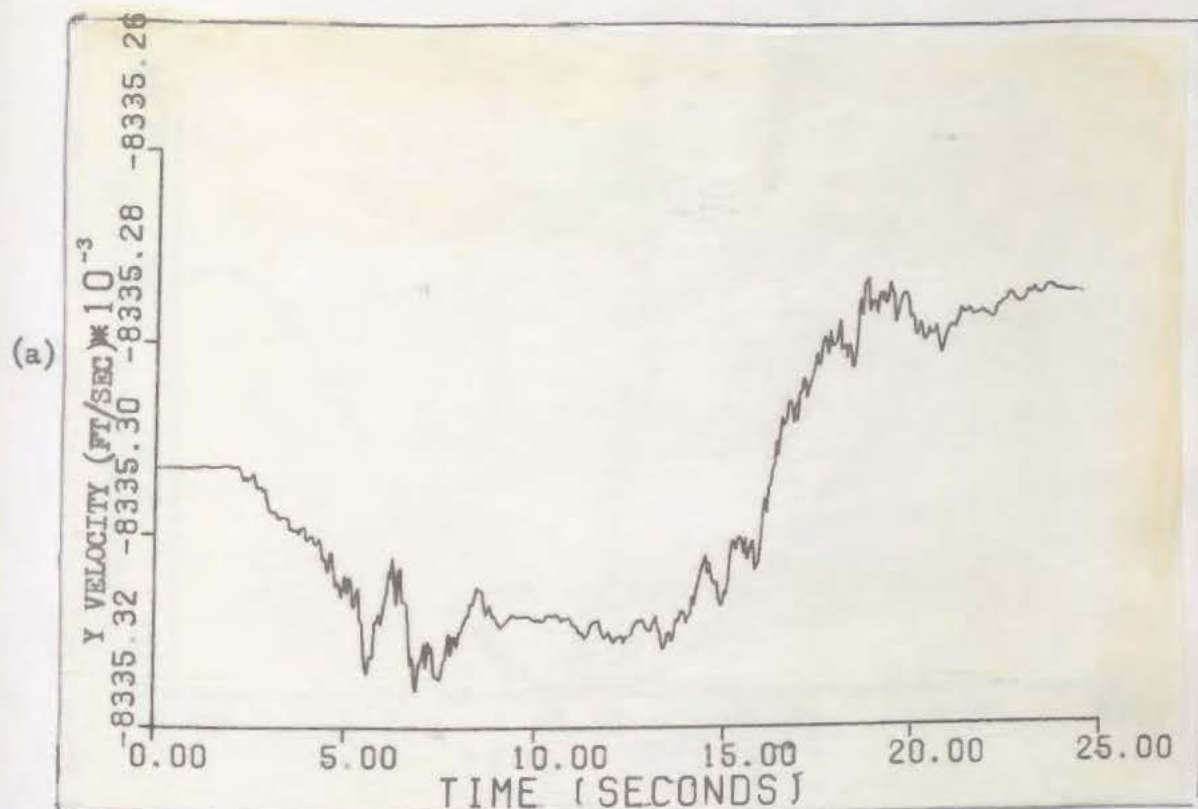


Fig. 5.11(a),(b) Smoother estimate and variance of y-velocity after two iterations.

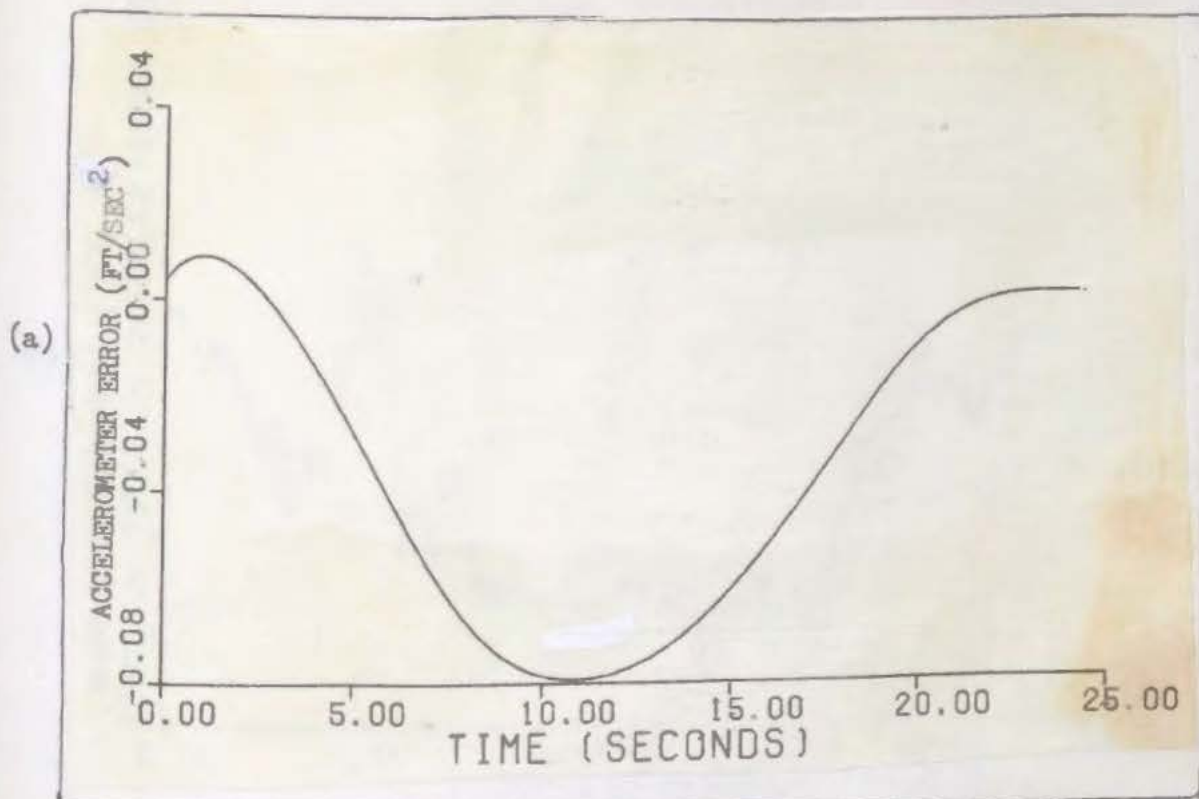


Fig. 5.12(a),(b) Smoother estimate and variance of accelerometer error after two iterations.

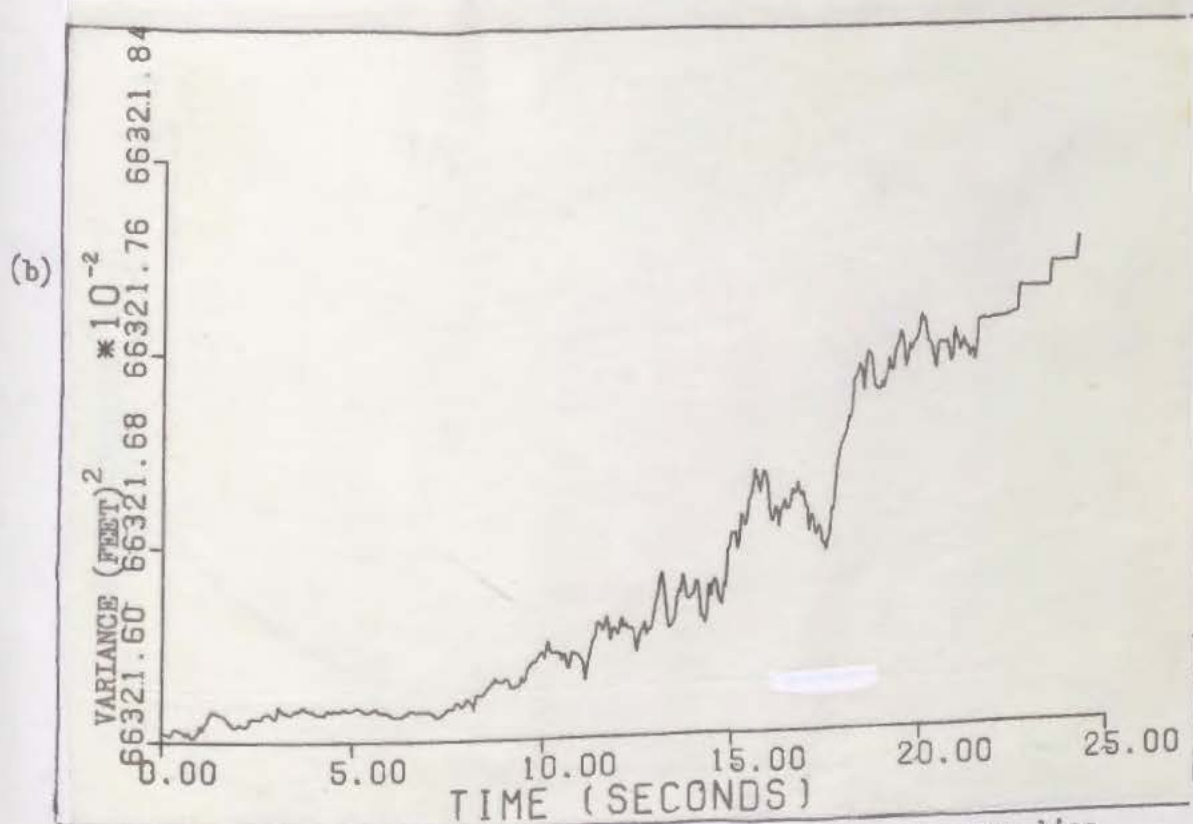


Fig. 5.13(a),(b) Smoother estimate and variance of range bias error after two iterations.

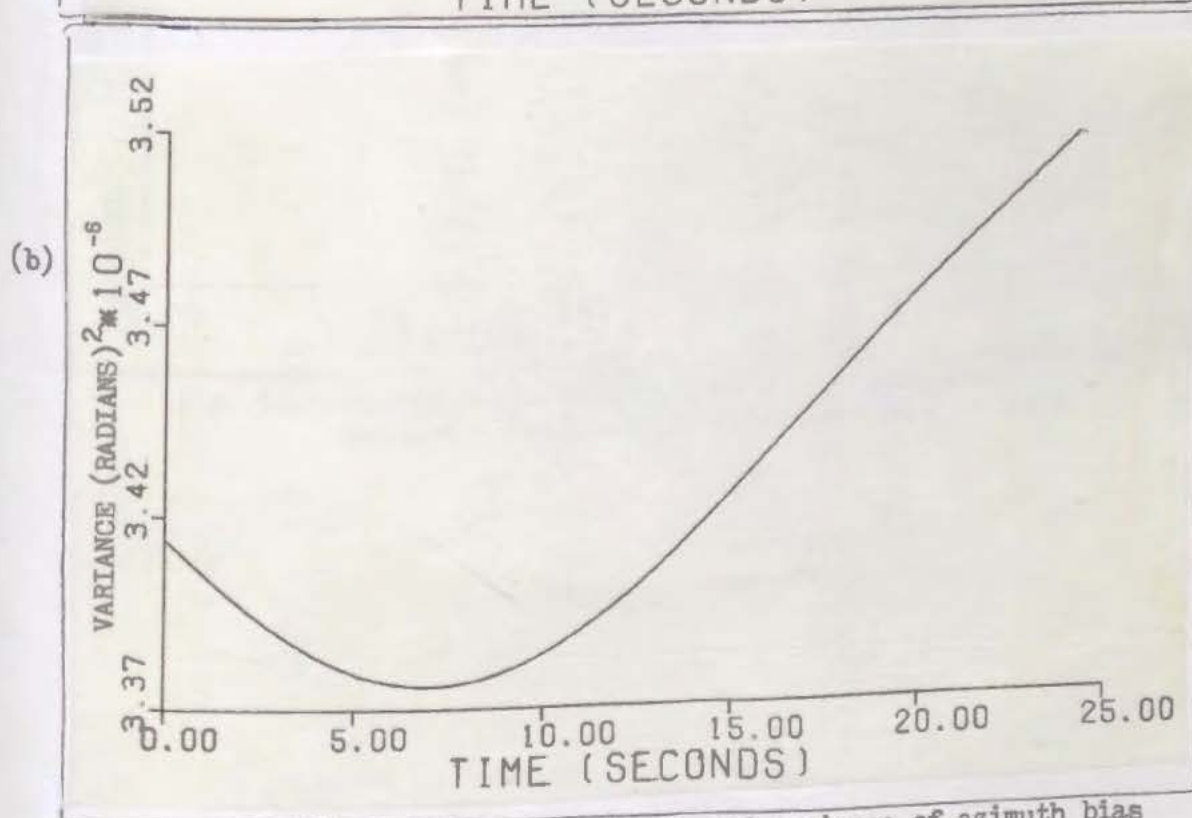
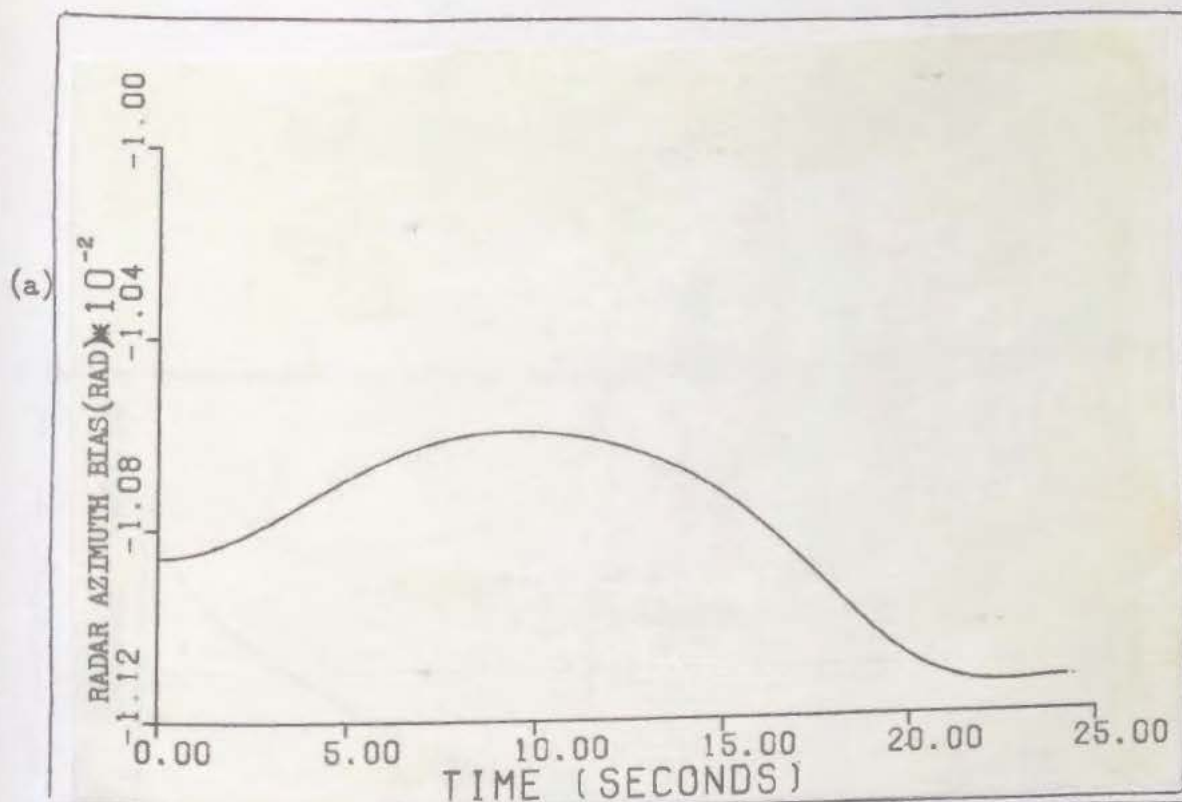


Fig. 5.14(a), (b) Smoother estimate and variance of azimuth bias error after two iterations.



TABLE II

Comparison of First and Second Smoother Iterations

State	$x(16.85/t_f)^*$	$x(16.85/t_f)^{**}$	Difference(%)	$P(16.85/t_f)^*$	$P(16.85/t_f)^{**}$	Difference(%)
x_1	10502.3	10577.3	+.71	3107.5	1254.2	-59.64
x_2	120.89	259.72	+114.84	1367.3	772.7	-43.49
x_3	1080	1082	+.185	2.096	1.117	-46.71
x_4	-8.01	-8.33	-4.0	5.909	2.14	-63.78
x_5	-.1073	-.0427	+60.2	.01488	.01488	0
x_6	-177.53	-255.7	-44.03	1186.2	663.22	-44.08
x_7	-.00429	-.0108	-151.75	.8687E-5	.3444E-5	-60.35

Average change = -3.4%

Average change = -45.44%

* First Iteration

** Second Iteration

st

im mi

ma

5

b

x-axis we have used. However, an exact starting position and track orientation are not the goals of this analysis. Our main interest is to obtain a good estimate of peak vehicle speed along the track. We are not concerned with where this peak speed occurs but more with the value and error of this estimate.

The second iteration of the smoother yields a maximum velocity of 1082.028 ft/sec at 16.85 seconds from chosen initial time. The scalar speed estimate at 18.65 seconds, FIM trap entry time, is 975.043 ft/sec. The reason we do not get better agreement between the smoother and FIM estimates of velocity at the trap is due to the time skew in the radar data previously discussed. The time scale we have used shows trap entry between 18.60 to 18.70 seconds but we are not sure exactly where trap entry occurs in this interval.

The behavior of the error states indicated by the first iteration of the smoother is reconfirmed by the second iteration. The radar range bias error behaves very much as a constant with only slight deviations from a steady value of -255.68 ft. The smoother estimate of range error is plotted in Fig. 5.13 (a). Radar azimuth error in Fig. 5.14 (a) is again shown to be "slowly-varying" over the 24 second interval. Our initial assumptions about the radar operator azimuth tracking error are again reconfirmed. The error in azimuth starts out high as the operator lags behind the vehicle due to rapid acceleration, decreases as the operator "catches up"

to the car near peak speed, and again increases upon vehicle deceleration as the operator "jumps" ahead of the car.

The accelerometer error state estimate shown in Fig. 5.12 (a) indicates that this state varies between approximately 0 to 0.08 ft/sec^2 or 0 to .0025 g's. Maximum error in the accelerometer occurs at approximately ten seconds into the run and the error decreases to near zero by 24 seconds. Perhaps the behavior of this error state can be explained by referring to Fig. 3.2 which is a plot of raw accelerometer data in g's versus time. Figure 3.2 indicates that maximum sustained g's on the vehicle occur between 0 to 10 seconds and slowly decrease from that time on. It appears from Fig. 5.12 (a) that the accelerometer error is a function of the time of application and level of sustained g's on the vehicle. This figure indicates a time-correlated behavior of the accelerometer. Such behavior may have been adequately modeled as a random walk. One way to model this behavior might be to relate the amount of driving noise on the accelerometer error state to the level of acceleration units at any given time. Thus, q_5 , could be modeled as time-varying for use in a random walk model of accelerometer error. Certainly, it can be argued that a correlation time of one second is too short from the behavior of the accelerometer error shown in Fig. 5.12 (a). Nevertheless, the forward-backward iterations have provided better information on the "true" behavior of the states of interest. Another iteration of the smoother could be made with updated initial conditions and perhaps a

different model for accelerometer error, but two iterations have provided sufficient reduction in variance values for our purposes.

Figures 5.8 (b) through 5.14 (b) are plots of smoother calculated error variances for each state. These plots show that the backward filter is able to reduce the errors in state estimates from those obtained from the first iteration of the smoother. After two iterations of the forward-backward estimator, the error in state estimation is reduced by an average of 45% over that obtained in the first iteration of the smoother.

The results of this second iteration of the smoother are now used to test the hypothesis that the rocket car did, in fact, exceed the reference speed of sound. This will be shown in detail in the next chapter.

VI. Hypothesis Testing

The previous chapter presented the results of the extended Kalman filter - fixed interval smoother estimation scheme. The resulting state estimates and error covariance after two iterations of the smoothing method will now be evaluated to yield the best estimate of peak rocket car speed and a confidence level for this estimate. Before we can analyze a hypothesis test of the peak vehicle speed, it is necessary to calculate the scalar speed estimate standard deviation.

Development of Scalar Speed Standard Deviation

The values for x_3 and x_4 , x and y velocity, are given in terms of mean values, $\hat{x}_3(t_i/t_f)$ and $\hat{x}_4(t_i/t_f)$ and variances $P_{33}(t_i/t_f)$ and $P_{44}(t_i/t_f)$ and the covariance $P_{34}(t_i/t_f)$. Under our assumptions of approximately Gaussian error models, these mean and variance values completely describe a two-dimensional Gaussian probability density function which propagates forward in time from the initial to final time. The state estimates of x and y velocity provide the components of a two-dimensional conditional mean vector, \underline{m} , the magnitude of which is the estimate of scalar speed at any time, t_i . This mean vector in the x - y plane, shown in Fig. 6.1, locates the peak of the density function. Surfaces of "constant likelihood" (4) are generated by passing planes through the density function parallel to the x - y plane. These surfaces are

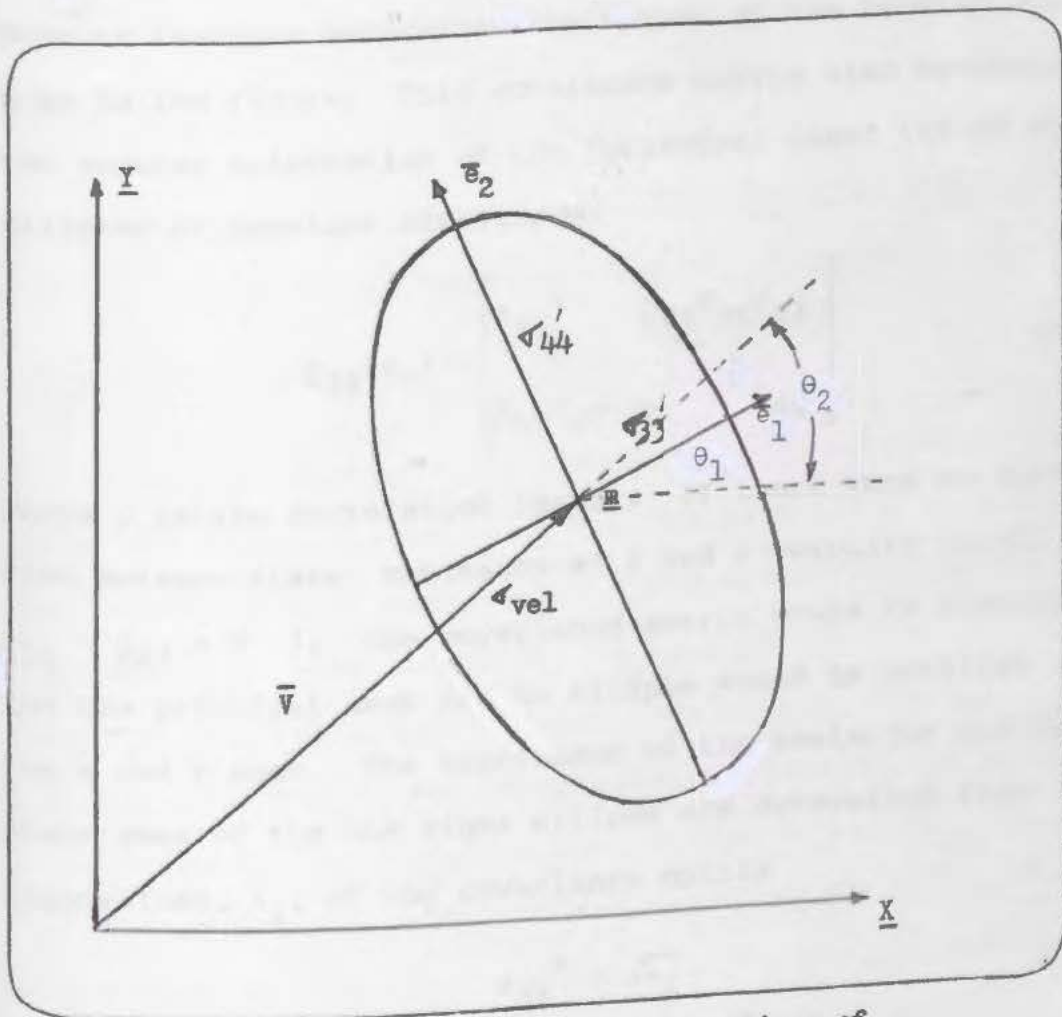


Fig. 6.1 Velocity vector and one sigma ellipse of constant likelihood

ellipses parallel to the x-y plane and when viewed from above, the one sigma surface of constant likelihood appears as in Fig. 6.1.

The covariance matrix for the two-dimensional velocity density function determines the spread of the density about \underline{m} as in the figure. This covariance matrix also determines the angular orientation of the "principal axes" (4) of the ellipses of constant likelihood.

$$\underline{P}_{34}(t_i) = \begin{bmatrix} \sigma_{33}^2 & \rho_{34}\sigma_{34}\sigma_{43} \\ \rho_{43}\sigma_{43}\sigma_{34} & \sigma_{44}^2 \end{bmatrix} \quad (6-1)$$

where ρ is the correlation factor. If there were no correlation between state estimates of x and y velocity (i.e., $\rho_{34} = \rho_{43} = 0$), the covariance matrix would be diagonal, and the principal axes of the ellipse would be parallel to the x and y axes. The magnitudes of the semimajor and semiminor axes of the one sigma ellipse are determined from the eigenvalues, λ_i , of the covariance matrix

$$\sigma_{33}' = \sqrt{\lambda_1} \quad (6-2)$$

$$\sigma_{44}' = \sqrt{\lambda_2} \quad (6-3)$$

where the primed notation indicates the lengths are defined in the principal axes frame of reference. We desire to relate the calculated scalar speed estimate from the optimal smoother:

$$|\bar{v}(t_i/t_f)| = [(\hat{x}_3(t_i/t_f))^2 + (\hat{x}_4(t_i/t_f))^2]^{\frac{1}{2}} \quad (6-4)$$

[REDACTED]

[REDACTED]

[REDACTED]

[REDACTED]

e_1

\bar{e}_2

[REDACTED]

he

[REDACTED]

hi

[REDACTED]

[REDACTED]

[REDACTED]

7

[REDACTED]

P₄₃

[REDACTED]

[REDACTED]

$$|\lambda \underline{I} - \underline{P}| = \begin{vmatrix} \lambda - P_{33} & -P_{34} \\ -P_{43} & \lambda - P_{44} \end{vmatrix} = \lambda^2 - (P_{33} + P_{44})\lambda + (P_{33}P_{44} - P_{34}P_{43}) \quad (6-8)$$

This "characteristic polynominal" is set equal to zero and the resulting roots are the eigenvalues, λ_1 and λ_2 , of the velocity covariance matrix. Noting that this covariance matrix is symmetric so that:

$$P_{34} = P_{43} \quad (6-9)$$

we define the characteristic polynominal as:

$$\lambda^2 - (P_{33} + P_{44})\lambda + (P_{33}P_{44} - P_{34}^2) = 0 \quad (6-10)$$

The resulting eigenvalues are

$$\lambda_{1,2} = [(P_{33} + P_{44}) \pm \sqrt{(P_{33} + P_{44})^2 - 4(P_{33}P_{44} - P_{34}^2)}] / 2 \quad (6-11)$$

Substituting these eigenvalues, λ_i , into the matrix $[\lambda_i \underline{I} - \underline{P}]$ and noting that the eigenvectors are in the "null space" of this matrix, so that

$$\begin{bmatrix} \lambda_i - P_{33} & -P_{34} \\ -P_{34} & \lambda_i - P_{44} \end{bmatrix} \begin{bmatrix} e_{i1} \\ e_{i2} \end{bmatrix} = \underline{0} \quad (6-12)$$

results in two equations for each eigenvector of the form:

$$a e_{i1} + b e_{i2} = 0 \quad (6-13)$$

either one of which is related to the other by a constant.

Thus, we have one equation and two unknowns from which to solve for the eigenvector, \bar{e}_i , for a given eigenvalue, λ_i .

We need another relation between the components of the eigenvector in order to solve for the individual elements. Noting that the "normalized" eigenvector is the unit vector we find the other equation:

$$e_{i1}^2 + e_{i2}^2 = 1 \quad (6-14)$$

With two equations and two unknowns we can solve for the individual components of each eigenvector.

The resulting eigenvectors determine the angular orientation of the principal axes of the one sigma ellipse. The angle, θ_1 , between the x-axis and the semiminor axis of the ellipse (associated with x velocity error variance) can be found from:

$$\theta_1 = \tan^{-1} (e_{12}/e_{11}) \quad (6-15)$$

where e_{12} and e_{11} are the components of the eigenvector which describes the orientation of the semiminor axis. This angle specifies a coordinate transformation matrix, \underline{L} , for a rotation about the z axis, such that:

$$\underline{L} = \begin{bmatrix} \cos\theta & \sin\theta & 0 \\ -\sin\theta & \cos\theta & 0 \\ 0 & 0 & 1 \end{bmatrix} \quad (6-16)$$

This coordinate transformation matrix is used to relate the orientation of the normalized velocity vector to the principal axes of the one sigma ellipse. Transforming this velocity unit vector into the frame of reference of the principal axes, we obtain a length from ellipse center to the one sigma ellipse in the direction of the velocity vector. It is the magnitude of this length, σ_{vel} in Fig. 6.1, which determines scalar speed standard deviation.

Calculation of Peak Scalar Speed and Standard Deviation

After two iterations of the smoother algorithm we arrive at the following estimates of x and y velocity at 16.85

seconds. As in the previous iteration, this time is found to be the point at which peak x velocity is obtained. The associated error variances and covariances for x_3 and x_4 at this time are also given:

<u>Velocity State Estimates</u>	<u>Covariances</u>
$\hat{x}_3(16.85/t_f) = 1081.996 \text{ fps}$	$P_{33} = 1.117148 (\text{fps})^2$
$\hat{x}_4(16.85/t_f) = -8.335287 \text{ fps}$	$P_{44} = 2.140282 (\text{fps})^2$
	$P_{34} = P_{43} = .071 (\text{fps})^2$

The magnitude of the velocity vector or scalar speed estimate is:

$$|\bar{v}| = 1082.028 \text{ fps} \quad (6-17)$$

From the covariances for the velocity state estimates at 16.85 seconds we form the two-dimensional covariance matrix:

$$P_{34} = \begin{bmatrix} 1.117148 & .071 \\ .071 & 2.140282 \end{bmatrix} \quad (6-18)$$

The eigenvalues and associated eigenvectors for this matrix are found from (6-11), (6-13), and (6-14):

$$\begin{aligned} \lambda_1 &= 1.11328 & \bar{e}_1 &= \begin{bmatrix} .99852 \\ .0544 \end{bmatrix} \\ \lambda_2 &= 2.14453125 & \bar{e}_2 &= \begin{bmatrix} .06894 \\ .99762 \end{bmatrix} \end{aligned} \quad (6-19)$$

The lengths of the semiminor and semimajor axes of the one sigma ellipse of constant likelihood become:

[REDACTED]
[REDACTED]

[REDACTED]

[REDACTED]
[REDACTED]
[REDACTED]

[REDACTED]

[REDACTED]

[REDACTED]

[REDACTED] 74 ⇒ [REDACTED]

in [REDACTED] ex [REDACTED]

[REDACTED]

[REDACTED] .99852
[REDACTED] 0544

[REDACTED]

an [REDACTED]

[REDACTED]
[REDACTED]

[REDACTED]

[REDACTED]

[REDACTED]

[REDACTED]

[REDACTED]

[REDACTED] 1 [REDACTED]

[REDACTED]

[REDACTED] t [REDACTED]

[REDACTED]

Subtracting (6-26) from (6-21) we find the angle between the \bar{e}_1 eigenvector and the velocity vector in the principal axes frame:

$$\theta_1 - \theta_2 = .44172 \text{ degrees} \quad (6-27)$$

This knowledge will become helpful in a moment.

We need to find the distance from the one sigma ellipse center to the ellipse itself, in the direction of the velocity vector, $\bar{v}_{\bar{e}_1 \bar{e}_2}$. To accomplish this, we have the general equation for any point (x_1, x_2) on the ellipse:

$$\frac{x_1^2}{\lambda_1} + \frac{x_2^2}{\lambda_2} = c \quad (6-28)$$

where c is a constant. For the one sigma ellipse c is equal to one. We also have the familiar relationship between two vectors $\underline{v}_1, \underline{v}_2$:

$$\frac{\bar{v}_1 \bullet \bar{v}_2}{|\bar{v}_1| |\bar{v}_2|} = \cos \gamma \quad (6-29)$$

where γ is the angle between the vectors. Let x_1 and x_2 describe the coordinates of the point where the line from ellipse center in the direction of the transformed velocity unit vector intersects the ellipse. We apply (6-28) and (6-29) to the point on the ellipse described by these points x_1 and x_2 . In (6-29) we are interested in the \bar{e}_1 eigenvector direction of length $\sqrt{\lambda_1}$, and the transformed velocity vector

$$\bar{v} = x_1 \bar{e}_1 + x_2 \bar{e}_2 \quad (6-30)$$

of length $\sqrt{x_1^2 + x_2^2}$. It is this length which describes the one sigma deviation of the scalar speed estimate. From (6-28)

$$\frac{x_1^2}{\lambda_1} + \frac{x_2^2}{\lambda_2} = 1 \quad (6-31)$$

and from (6-29)

$$\frac{\sqrt{\lambda_1} \bar{e}_1 \cdot [x_1 \bar{e}_1 + x_2 \bar{e}_2]}{|\sqrt{\lambda_1} \bar{e}_1| |x_1 \bar{e}_1 + x_2 \bar{e}_2|} = \cos \gamma = \cos(.44172) = .99997$$

$$\frac{x_1}{\sqrt{x_1^2 + x_2^2}} = .99997$$

$$x_1 = 129.095572 x_2 \quad (6-32)$$

From (6-31)

$$\frac{16665.67 x_2^2}{\lambda_1} + \frac{x_2^2}{\lambda_2} = 1 \quad (6-33)$$

we find

$$x_2 = .008173$$

and from (6-32)

$$x_1 = 1.055098$$

Thus,

$$\sqrt{x_1^2 + x_2^2} = 1.05513 \quad (6-33)$$

This value is the standard deviation of the scalar speed estimate, 1082.028 ft/sec. Note that we expected the standard deviation of the velocity estimate to be only slightly higher than the one sigma deviation of the x velocity estimate due

to the small off-diagonal terms of the P_{34} matrix, and relative magnitudes of the x and y velocities.

Hypothesis Test of Peak Speed and Confidence Level

We are now prepared to apply a hypothesis test of the peak vehicle speed. We wish to test the hypothesis that the peak speed estimate is above the reference speed of sound, a:

$$a = 1073.536213 \text{ fps}$$

From our assumptions of Gaussian models, the estimate of peak speed and associated covariance describe a conditional normal distribution. The appropriate one-sided "confidence interval" (8) for this hypothesis test is given by (8):

$$\bar{x} - z (\text{confidence level}) \sigma(\bar{x}) \geq \mu \quad (6-34)$$

where

\bar{x} - mean of normal distribution = 1082.028

z - area under the standard normal distribution curve

$\sigma(\bar{x})$ - standard deviation of normal distribution = 1.05513

μ - lower bound of confidence interval = 1073.536213

For $\bar{x} = 1082.028 \text{ fps}$, $\mu = 1073.536213$, $\sigma(\bar{x}) = 1.05513$:

$$z(\text{confidence}) = \frac{\bar{x} - \mu}{\sigma} = 8.048 \quad (6-35)$$

To eight significant figures (6-35) yields a probability that the vehicle was below Mach one of:

$$1 - P(x) = 3.4346578 \text{ E-15} \quad (6-36)$$

from which $P(x)$, the probability that the vehicle was above Mach one, is found to be:

$$P(x) = .99999999999999965653422 \quad (6-37)$$

For all intents and purposes, we have achieved a probability or confidence level of one that the vehicle exceeded the reference speed of sound. Of course, this confidence level is based on the assumptions and modeling techniques we have used in this analysis. Such a high confidence after only two iterations of the forward-backward estimator illustrates the power of optimal smoothing theory in post-run data analysis.

101

i

mp

mg

see exact correlation between filter estimated velocity and FIM trap speed at 18.65 seconds. On the time scale we have used, the FIM trap occurs somewhere between 18.60 and 18.70 seconds. In spite of this time skew, the estimated values are close enough to trap speed to allow the comparison shown in Table III.

The actual starting position of the vehicle is really not the information we desire. We set out primarily to get the best estimate possible of peak vehicle speed no matter at what time or where on the track this occurs. In terms of vehicle velocity, the smoothing algorithm used in this analysis after two iterations has provided excellent convergence to the "true" peak speed.

We also have come close to the maximum velocity estimate obtained on the day of the run from AFFTC radar data analysis. It appears that the AFFTC method used to correct erroneous range data was valid and even averaging only three radar points came very close to the "true" peak speed. We now summarize the estimates obtained of the peak vehicle speed by AFFTC, accelerometer data only, and one and two iterations of the forward-backward smoothing method incorporating range and azimuth measurements. These velocity estimates are converted to Mach number using the calculated reference speed of sound of 1073.536213 ft/sec. These results are summarized in Table IV.

Two iterations of the optimal smoother also provide some information on the behavior of the error states of the

TABLE III

Speed Estimate at FIM Trap (18.65 seconds)

Method	Feet/sec	MPH
FIM Recorded Speed	977.1432	666.234
Accelerometer Data Only	978.582	667.215
First Run of Extended Kalman Filter	979.22	667.649
First Run of Smoother	972.91	663.35
Second Run of Extended Kalman Filter	978.568	667.206
Second Run of Smoother	975.043	664.802

TABLE IV

Peak Scalar Speed Estimates

Method Used	Feet/sec	MPH	MACH	Time Above Mach 1
AFFTC Computer Analysis of Corrected Radar Data	1084.835	739.66	1.0105	N/A
Integration of Longitudinal Accelerometer Data	1080.05	736.4	1.006	1.25 sec
First Run of Extended Kalman Filter	1089.5	742.84	1.0149	2.0 sec
First Run of Smoother	1080.006	736.34	1.006	1.25 sec
Second Run of Extended Kalman Filter	1086.71	740.94	1.0123	1.8 sec
Second Run of Smoother	1082.028	737.75	1.008	1.4 sec

accelerometer and radar. The accelerometer error varies between 0 and $.08 \text{ ft/sec}^2$ (0 to $.0025 \text{ g's}$) during the 24 second time interval of interest, achieving its maximum value at approximately ten seconds into the run. From ten seconds on, this error slowly decreases to approximately zero by 24 seconds. The sustained g's on the vehicle are fairly high (Fig. 3.2) up to ten seconds and then begin to decrease after this time. It would appear the accelerometer error is a function of the length of time sustained g's are applied to the accelerometer and the magnitude of these acceleration units. Depending on one's definition of "slowing-varying", one could make a case for using a random walk model for the accelerometer error. Certainly, it could be argued that a correlation time of one second is too short for the behavior of this error. Another study of the rocket car data could use on-line "tuning" of the system noise matrix, $Q(t)$, by allowing the smoother to calculate an estimate of its value over time, $\hat{Q}(t_i/t_f)$. One could also calculate smoother estimated inputs $\hat{u}(t_i/t_f)$. In terms of the rocket car analysis, such estimation of accelerometer input at any time t_i based on the entire measurement time history would yield improved state estimation. Nevertheless, the smoother has provided a better "glimpse" of the "true" behavior of this state than is available from a forward filter only, especially without more knowledge about inherent accelerometer errors.

The random walk models for radar range and azimuth bias errors prove to be very adequate. These errors are shown as

nearly constant over the 24 second interval with only slow changes from the behavior of true constants. Certainly, we are somewhat surprised at the magnitude of the radar range bias error. Considering the size of the vehicle being tracked, lack of transponder, ground clutter, and distance from the radar site, it is conceivable that the radar range has a large inherent error. The azimuth bias error behaves as we expected based on our knowledge of operator tracking performance. Perhaps "bias" is a misnomer, as most of the error in azimuth is operator-induced. The azimuth error shows that the operator lags behind the vehicle initially but is able to regain good tracking as the acceleration decreases. After engine "flame-out" at approximately 18 seconds, the azimuth error again increases, indicating the operator has probably "jumped" ahead of the vehicle. For another iteration of the estimator, a better description of the azimuth error could be used. One could relate the strength of driving noise on this state, q_7 , to the acceleration of the vehicle. When acceleration is high q_7 would be increased. The amount of driving noise would decrease as vehicle acceleration decreases.

This analysis has shown that state estimation can be significantly improved if the estimation algorithm has access to future measurements. This is the real benefit of a smoother algorithm in post-run data analysis. The method used in this analysis requires a straightforward incorporation of existing theory and available software with only limited additional programming required. The forward-backward

iteration scheme is a simple yet effective way to provide improved state estimates in an "off-line" application. It can be applied to almost any system of interest no matter what dimension, with only computer workload becoming a driving factor. Good dynamical and error models are a requirement, but not a necessity. The iterative method used in this analysis can help "fine-tune" very simplified models to provide improved state estimates.

The reader familiar with estimation of unknown parameters using a "maximum likelihood" estimation technique may wonder if such a technique could have been employed in this analysis. The answer is a guarded "yes" if we can make some valid assumptions. The inherent assumption in maximum likelihood estimation is that the parameters to be identified can be accurately modeled as constants over some time interval of interest. In this analysis, we are concerned with accurate estimates of state values at discrete points in time (i.e., peak speed at some time, t_1). If we assume the parameters affecting this problem, such as accelerometer and radar errors, are constant over time, a maximum likelihood estimation algorithm will yield a best fit of a constant to the data. If the parameters are not true constants, a better (non-constant) model would inherently allow better estimation accuracy. This analysis has shown that the error states do not behave as constants. Therefore, one cannot accurately model these errors as constant unknown parameters for implementation in a maximum likelihood estimation algorithm without non-negligible

estimation performance degradation. Without a priori information on the behavior of the errors to be modeled, the decision was made to model the errors as states in the forward extended Kalman filter-backward smoother estimator.

If there is a "bottom-line" to this analysis it has to do with the peak speed of the Budweiser Rocket Car on 17 December 1979. Rather than "eyeballing" the peak speed of the car based on poor data, we are able to provide an estimate of the speed and a confidence level for our estimate. In fact, after only two iterations of the forward-backward smoothing technique, we can state with probability of nearly one that the vehicle did achieve the reference speed of sound, based on the assumptions and modeling techniques used in this analysis.

Recommendations

The position estimates and off-zero velocities calculated by the smoother at the initial time, t_0 , indicate a rather poor choice of origin for the vehicle frame of reference. Relying on the radar to provide a good initial "fix" of vehicle position, no matter how long the radar is aimed at the vehicle, is only "wishful thinking". Perhaps a better origin could have been located at remote camera site A8 shown in Fig. 1.1. This point has been surveyed and "exact" latitude and longitude coordinates of both A8 and the radar site are known. Using these coordinates one could calculate a much better DELX and DELY from which to reference changing

radar measurements to vehicle motion in the frame of reference. If the information on track alignment with respect to A8 is correct, a frame of reference at A8 should indicate a vehicle track parallel to the x-axis. The starting position of the vehicle within a frame of reference centered at A8 is still unknown, however, and only iterative methods could "zero-in" on the "true" starting position.

An adjustment could be made in the initial time chosen in the radar data to find the "true" sample time as the vehicle starts to move. At 20 samples per second, however, one can only get within 0.05 second accuracy. Also, the radar data is constant until the azimuth suddenly increases very rapidly. We chose one sample time before the first change in azimuth as the initial time. One could "back-up" the radar data until the smoother estimate of x-velocity at t_0 approaches zero.

Other possibilities for further study include some off-line tuning of system noise to account for the time-varying nature of accelerometer and azimuth errors. One way to accomplish this might be to use the smoother estimate of system noise, $\hat{Q}(t_i/t_f)$, based on the measurement data to provide a time history of driving noise for each of the affected states. This would provide the forward extended Kalman filter with improved knowledge of state behavior.

Finally, it might be beneficial to allow the smoother to calculate an estimate of the applied controls, in this case accelerometer specific force. This smoother estimated

control input, $\hat{u}(t_i/t_f)$, could be used to better determine accelerometer errors and improve state estimation. These possibilities were not explored in this analysis due to time limitations and a feeling that confirmation of peak vehicle speed was the critical area of concern.

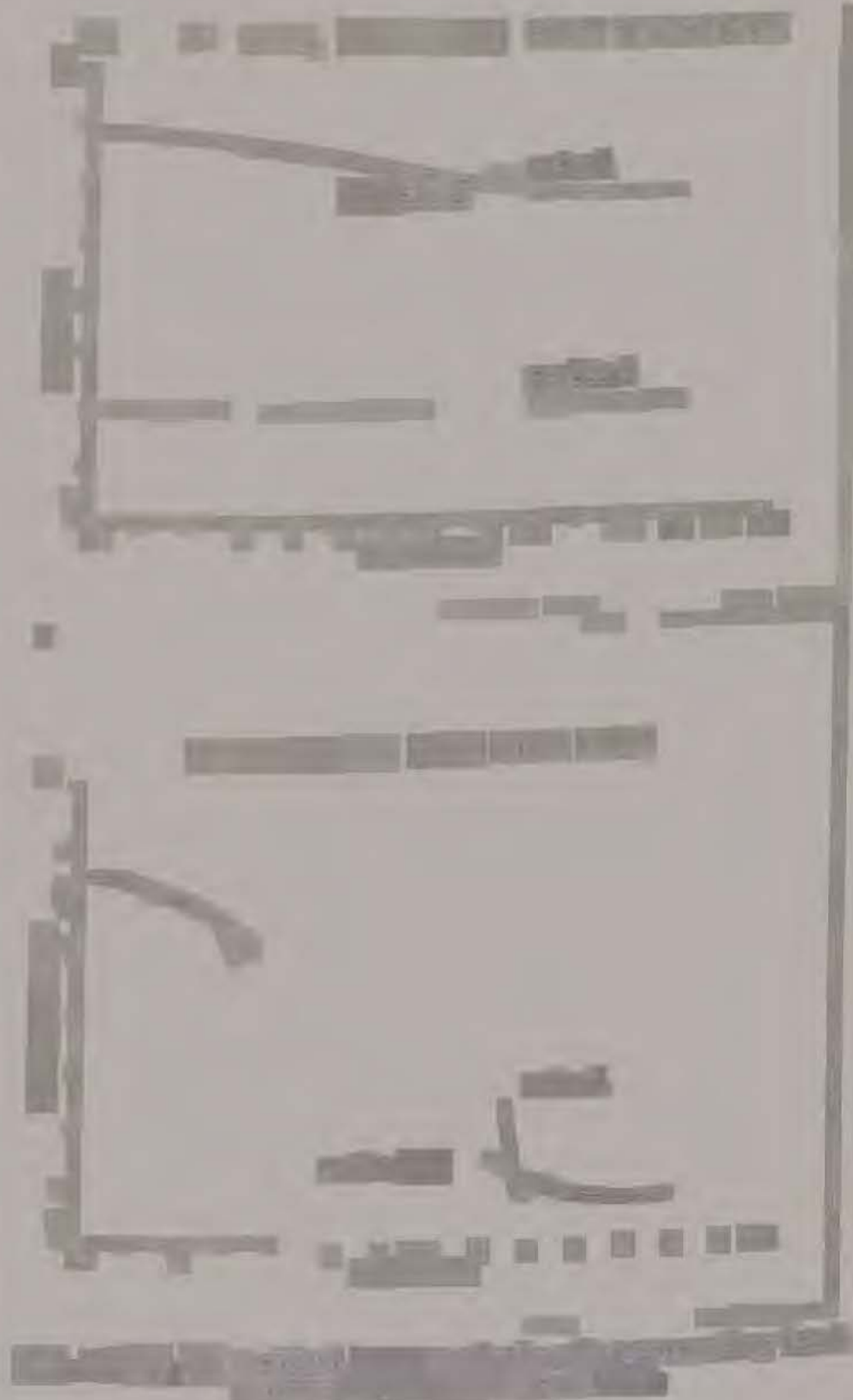
Appendix A. Plots from Second Iteration of Extended Kalman Filter

This section presents the results of the second iteration of the extended Kalman filter developed in Chapter III and IV. State estimates and error variances at the initial time from the first iteration of the Meditch (5) smoothing algorithm are used to update the initial conditions of the extended Kalman filter for this run. In addition, a slight correction to the assumed test track heading provides closer filter correlation to range and azimuth measurements, allowing a reduction in the estimated measurement noise for radar range.

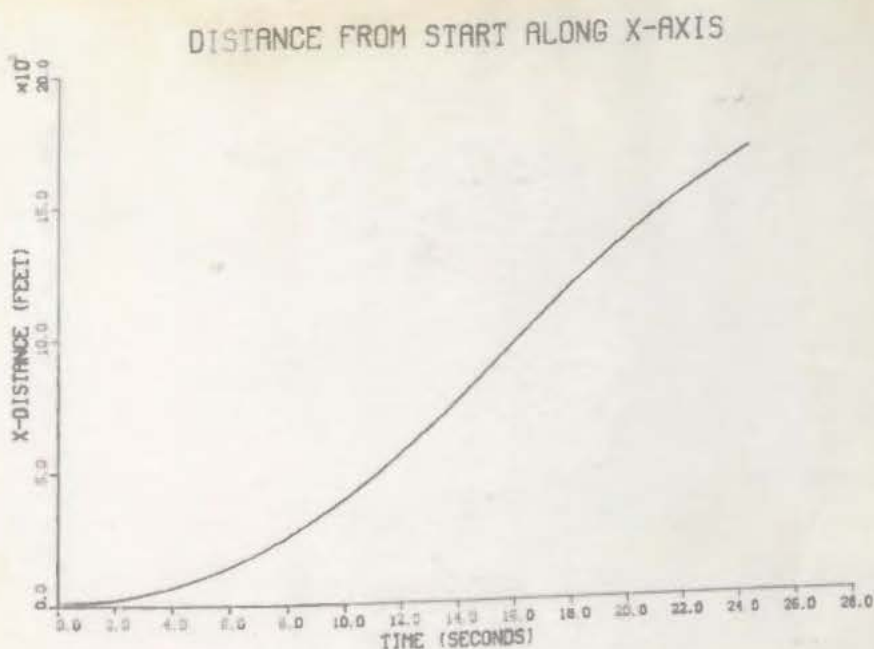
Figure A.1 shows a plot of estimated and actual radar range obtained with the corrected test track heading. This figure indicates that the divergence of actual and estimated range between 20 to 24 seconds has been removed.

The extended Kalman filter shows improved convergence of the standard deviations of the state estimates due to improved initial conditions from the smoother. This can be seen by comparing to part (b) of Figs. A.2 through A.8 to part (b) of Figs. 4.17 to 4.23. Figures A.9 (a) and A.9 (b) are plots of the range and azimuth measurement residuals bracketed by the residual standard deviations. From Fig. A.9 (a) it is apparent when the residual monitoring routine bypasses range measurements in excess of three times the residual standard deviation. Figure A.10 (b) is an expanded

version of Fig. A.10 (a) which is the scalar speed estimate
(magnitude of the velocity vector) converted to Mach number.



(a)



(b)

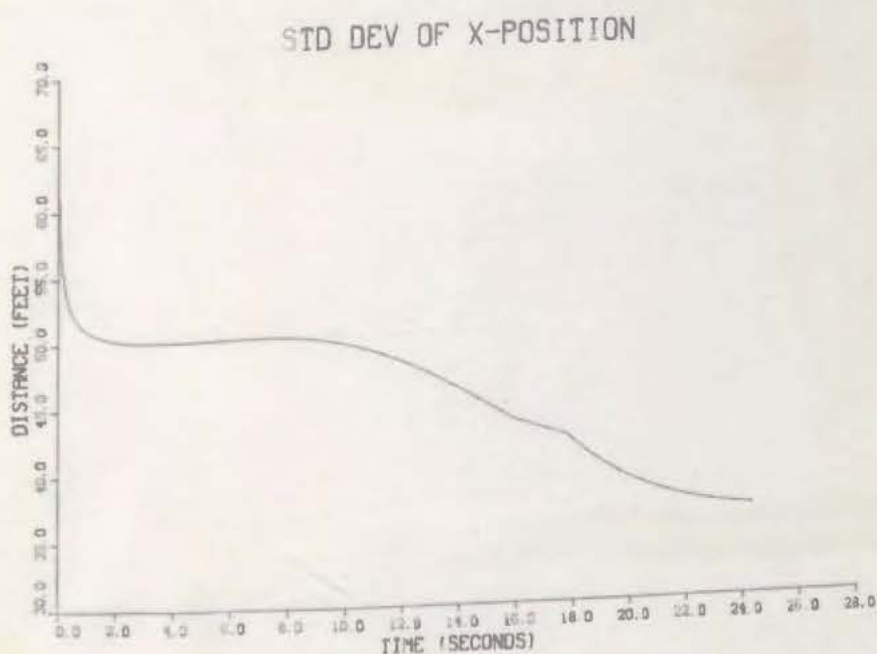
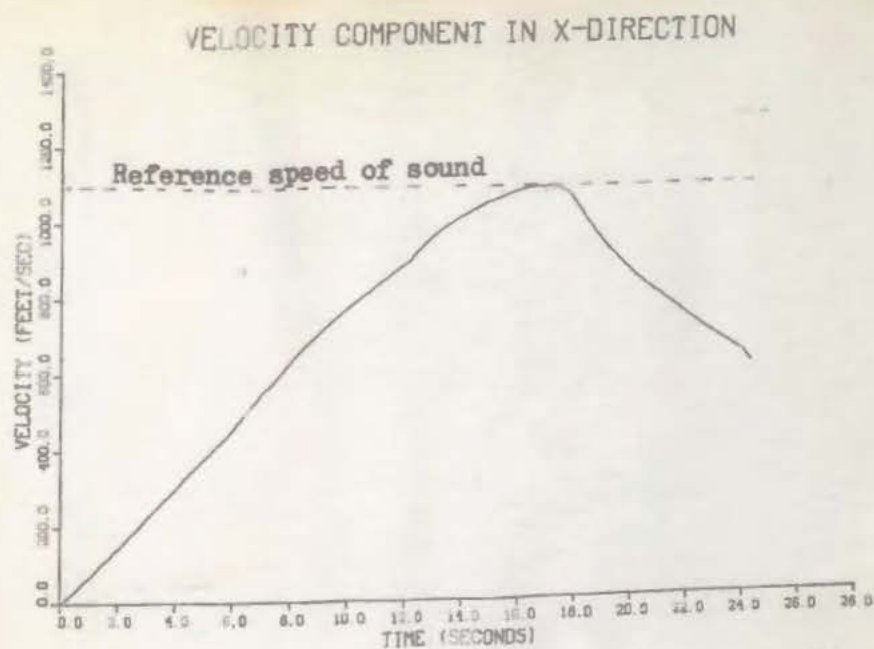


Fig. A.2(a),(b) Extended Kalman filter state estimate and standard deviation after two iterations



(a)



(b)

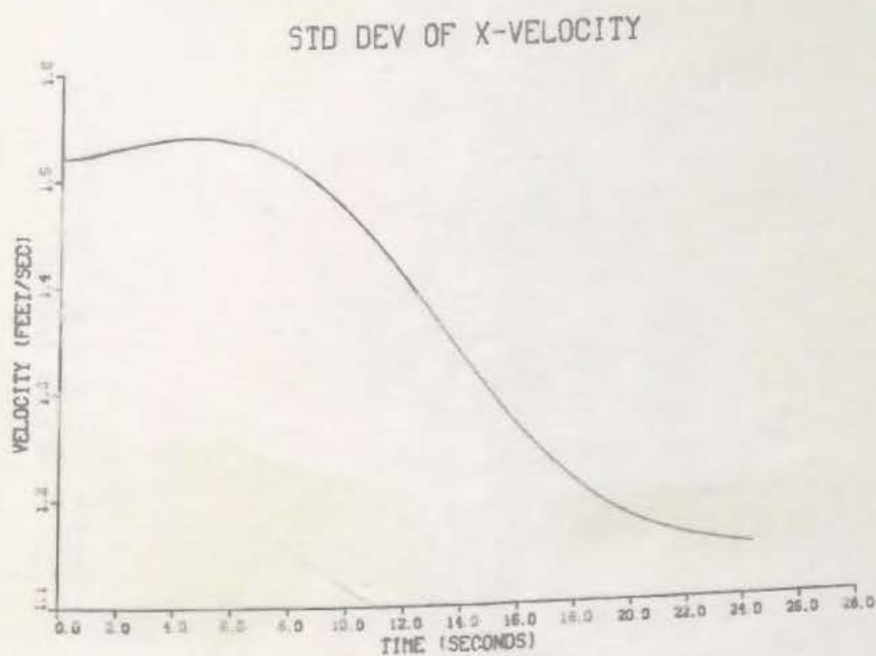
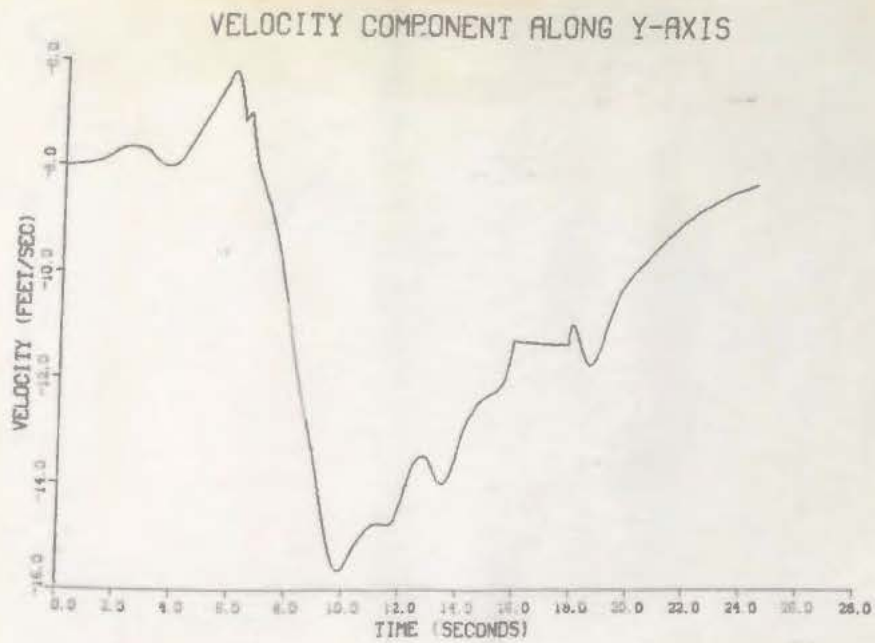


Fig. A.4(a),(b) Extended Kalman filter state estimate and standard deviation after two iterations

(a)



(b)

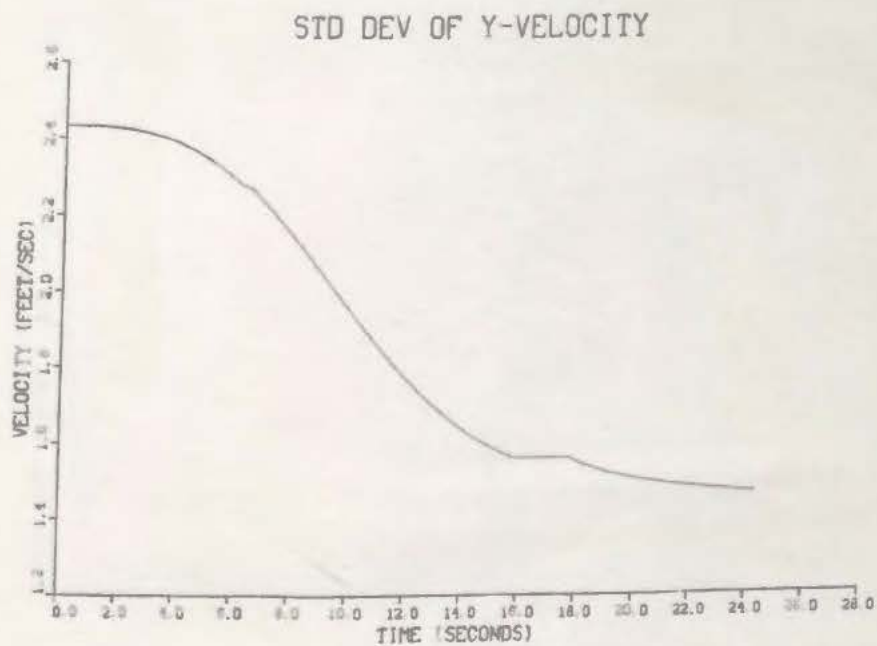
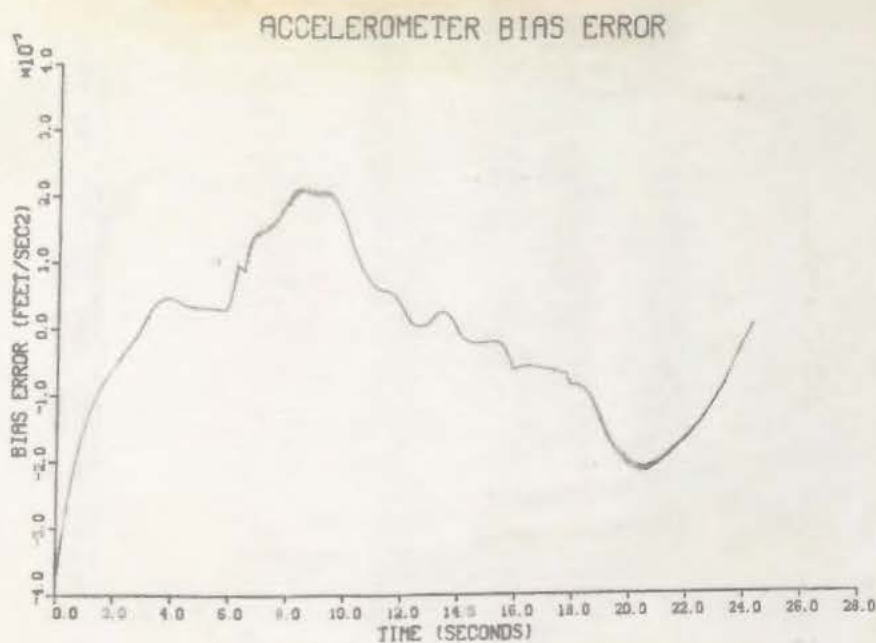


Fig. A.5(a),(b) Extended Kalman filter state estimate and standard deviation after two iterations

(a)



(b)

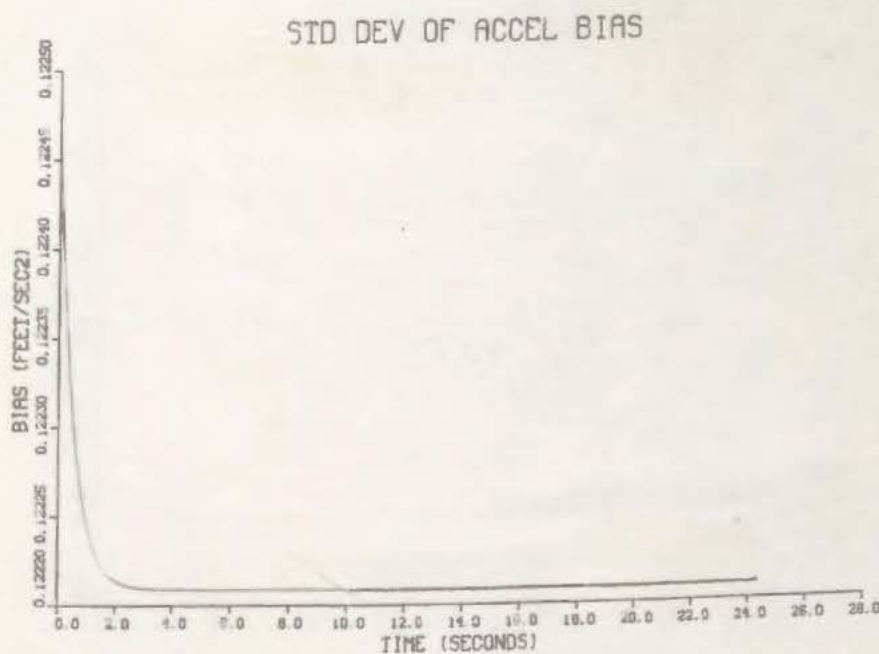
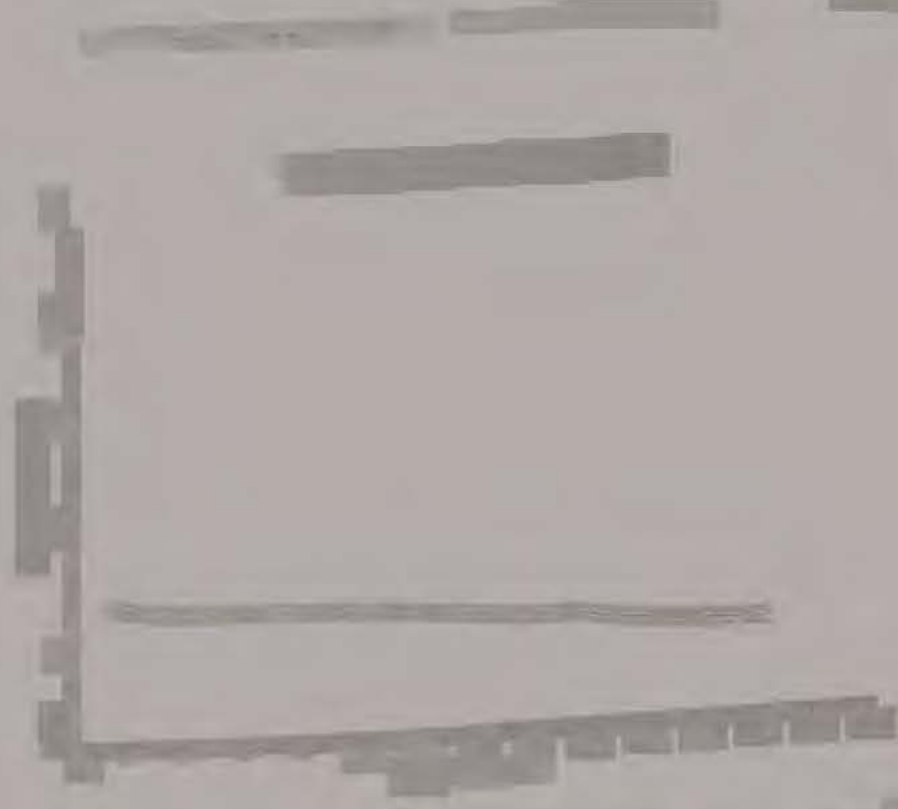
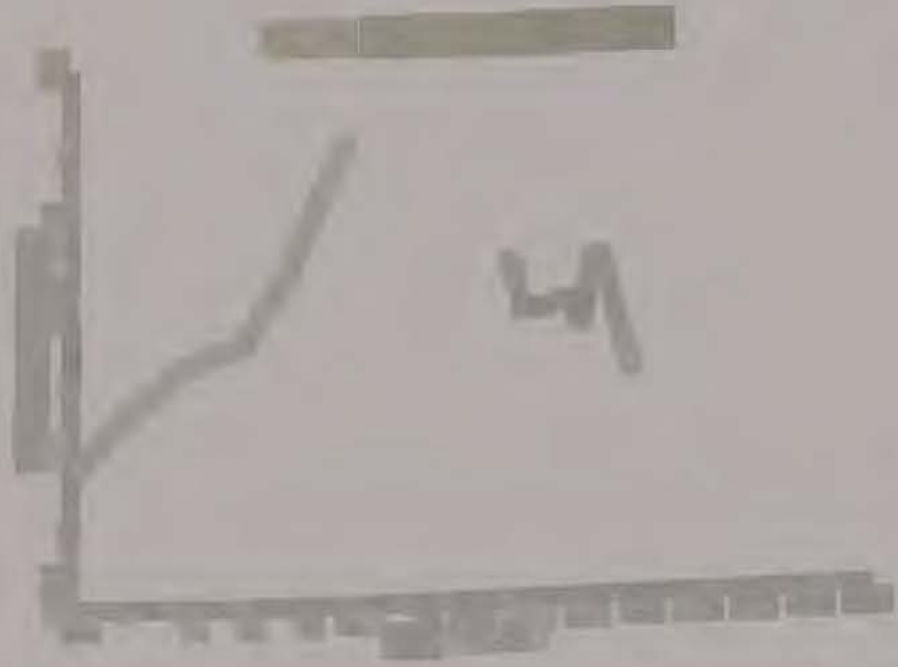


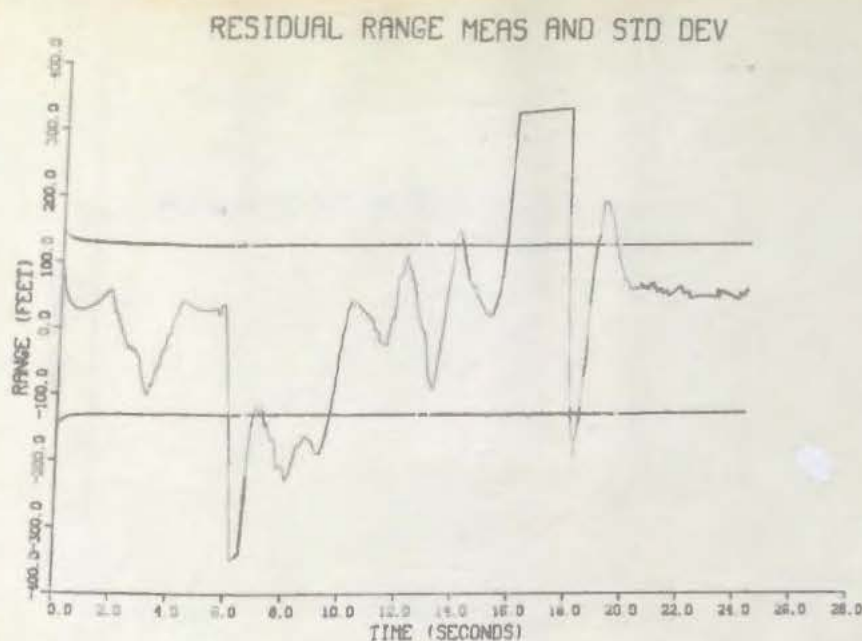
Fig. A.6(a),(b) Extended Kalman filter state estimate and standard deviation after two iterations





Copyright © 2000 by John Wiley & Sons, Inc.

(a)



(b)

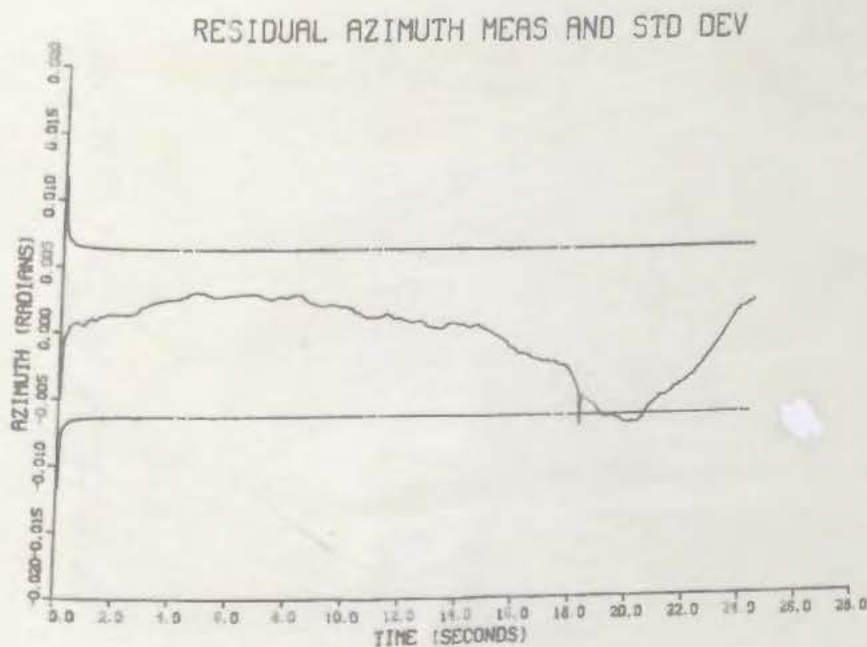
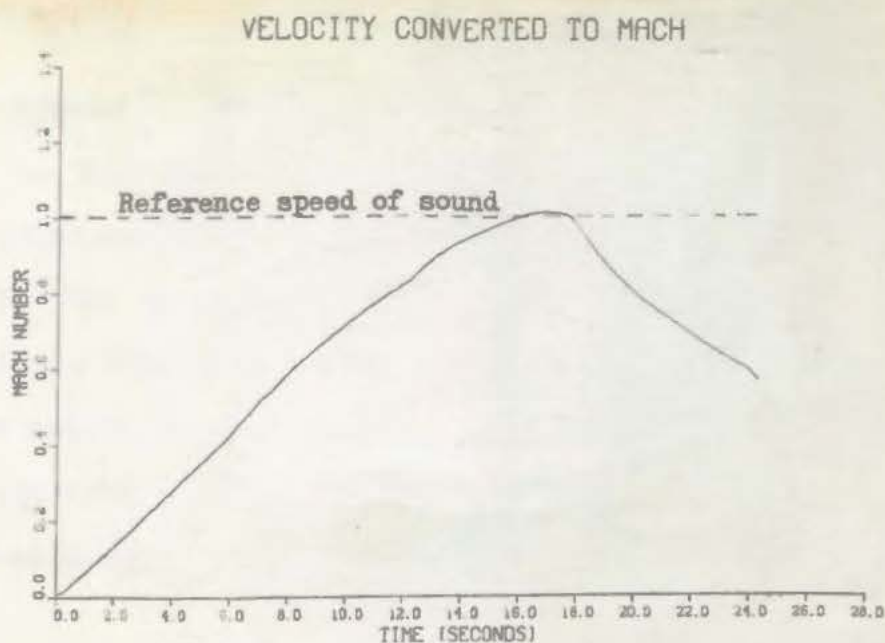


Fig. A.9(a),(b) Range and Azimuth residuals and standard deviations after two iterations.

(a)



(b)

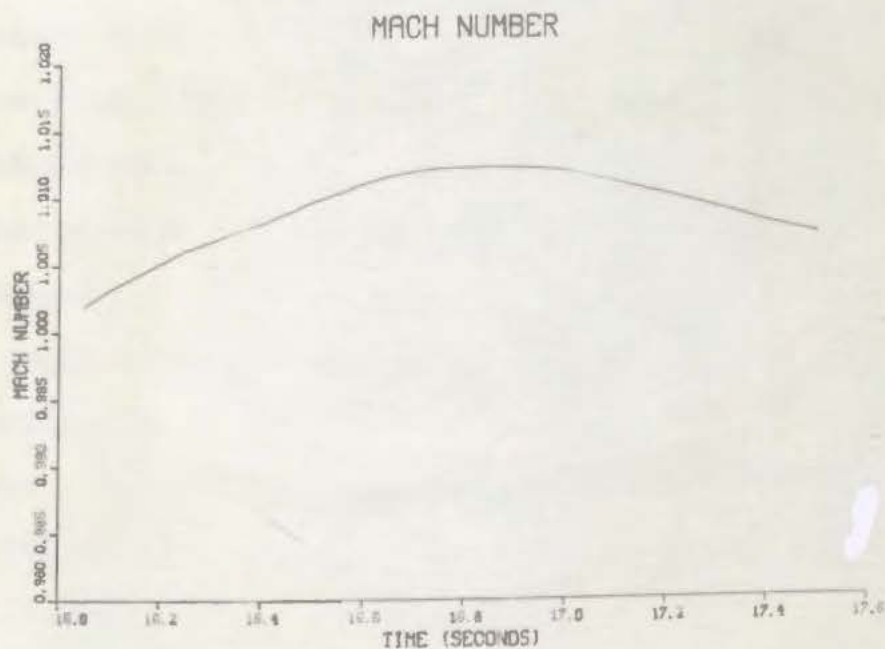


Fig. A.10(a),(b) Velocity converted to Mach number after two iterations of the Extended Kalman filter.

Appendix B. Optimal Smoother Computer Program

This appendix includes a listing of the computer program used to incorporate the Meditch (5) backward-recursive optimal linear smoother algorithm described in detail in Chapter II. The data required for this program includes the current sample time, t_i , state estimate vector before update, covariance matrix before update (stored in upper triangular form), state estimate vector after update, and covariance matrix after update (stored in upper triangular form) from t_0 to t_f .

For this analysis the state estimates and covariance before and after each measurement update are stored as a result of one run of the extended Kalman filter implemented in SOFE. A short data reformatting program was used to put the data at the final time first and the remaining data records in backward-recursive form to the initial time. This enables the smoother program to read forward through the data but actually compute quantities "backward" in time. The Meditch algorithm requires $\hat{x}(t_i^+)$ and $\hat{x}(t_{i+1}^-)$ for one calculation at each sample time. The data was put in the following order to allow for a step-by-step "read" of the required quantities for each time of calculation. Each data record contains the following information in the order shown:

1. time, t_i
2. state vector at time t_i after update, $\hat{x}(t_i^+)$

3. covariance matrix at time t_i after update, $\underline{P}(t_i^+)$
4. state vector at time t_i before update, $\hat{\underline{x}}(t_i^-)$
5. covariance matrix at time t_i before update, $\underline{P}(t_i^-)$

The order of the system used in the rocket car analysis allowed for storage of formatted records. A higher order system will probably require more efficient data storage and improved formatting of smoother printed output.

1 PROGRAM SMOOTH(INPUT,OUTPUT,TAPE5=INPUT,TAPE6=OUTPUT,TAPE7,
- TAPE8,TAPE9)

C

5

C

THIS IS THE EXECUTIVE ROUTINE OF A FIXED INTERVAL
SMOOTHER ALGORITHM. THE DEVELOPMENT OF THE ALGORITHM
IS THE RESULT OF WORK DONE BY J. S. MEDITCH AND
PUBLISHED IN INFORM AND CONTROL, 1967.

C

10

C

THIS ALGORITHM USES THE OUTPUT OF A FORWARD RUNNING
KALMAN FILTER (IN THIS CASE AN EXTENDED FILTER). IT
PROPAGATES A SMOOTHED ESTIMATE OF THE STATE VECTOR AND
COVARIANCE MATRIX BACKWARD FROM AN INITIAL CONDITION
AT THE FINAL TIME OF THE FORWARD FILTER. THIS RESULTS
IN AN IMPROVED STATE ESTIMATE AND LOWER COVARIANCE.

15

C

DATA FROM THE FORWARD FILTER IS STORED ON MAGNETIC TAPE
IN THE FOLLOWING FORMAT FOR EACH RECORD:

C

1. TIME

20

C

2. XFMINUS - VECTOR OF STATE ESTIMATES BEFORE
MEASUREMENT UPDATE

C

3. PFM - UPPER TRIANGULAR COVARIANCE MATRIX
BEFORE MEASUREMENT UPDATE (STORED IN THIS
MANNER FOR COMPACTNESS)

C

4. XFPLUS - VECTOR OF STATE ESTIMATES AFTER
MEASUREMENT UPDATE

25

C

5. PFP - UPPER TRIANGULAR COVARIANCE MATRIX
AFTER MEASUREMENT UPDATE

C

DEFINITION OF VARIABLES IN MEDITCH ALGORITHM

30

C

XFMINUS - VECTOR OF (NS) STATES BEFORE UPDATE

C

XFPLUS - VECTOR OF (NS) STATES AFTER UPDATE

C

XFTF - SMOOTHED ESTIMATE OF STATE VECTOR

C

PFMINUS - COVARIANCE MATRIX BEFORE UPDATE

C

PFPLUS - COVARIANCE MATRIX AFTER UPDATE (NSXNS)

35

C

PFTF - SMOOTHED COVARIANCE

C

AMAT - SMOOTHING ESTIMATOR GAIN MATRIX (NS X NS)

C

PHI - STATE TRANSITION MATRIX FOR ADJOINT SYSTEMS

C

$PHI = EXP(F * T)$ (TRANPOSED)

C

STARTING CONDITION FOR SMOOTHER

40

C

$XFTF(TF) = XFPLUS(TF)$

C

$PFTF(TF) = PFPLUS(TF)$

C

PROPAGATION OF STATE ESTIMATE

C

$XFTF(TI) = XFPLUS(TI) + AMAT(TI)(XFTF(TI+1) - XFMINUS(TI+1))$

45

C

$AMAT(TI) = PFPLUS(TI) * PHI(TI+1, TI) * PFMINUS(TI+1) ** -1$

C

$PFTF(TI) = PFPLUS(TI) + AMAT(TI)(PFTF(TI+1) - PFMINUS(TI+1)) * AMAT(TI) TRANSPOSED$

C

IN ADDITION TO THE ROUTINES HERE, THE DAVID L. KLEINMAN
LIBRARY OF LINEAR SYSTEMS PROGRAMS IS USED TO PROVIDE
VECTOR AND MATRIX OPERATIONS.

50

C

C

C

COMMON /MAIN1/ NDIM,NDIM1,COM1(10,10)

COMMON /MAIN2/ COM2(10,10)

COMMON /INOU/ KIN,KOUT,KPLOT,KDATA,KUSER

COMMON /DIM/ NS,NTR,NSEC,NSAMP,NSTEP

COMMON /PHI/ PHI(10,10)

55

```

COMMON /XFP/ XFPLUS(10)
COMMON /XFM/ XFMINUS(10)
60 COMMON /PFPV/ PFP(55)
COMMON /PFMV/ PFM(55)
COMMON /PFP/ PFPLUS(10,10)
COMMON /PFM/ PFMINUS(10,10)
COMMON /A/ AMAT(10,10)
65 COMMON /XFTF/ XFTF(10)
COMMON /PFTF/ PFTF(10,10)
COMMON /HEADING/ TITLE(20),ADATE,ATIME
COMMON /TIME/ T,T0,TF
LOGICAL PLOTEM,DATACHK,USEROUT
70 NAMELIST /IN/ NS,NTR,NSAMP,T0,TF,DATACHK,PLOTEM,USEROUT
DATA NDIM,NDIM1/10,11/
DATA KIN,KOUT,KPLOT,KDATA,KUSER/5,6,7,8,9/

```

```

C
C
C INITIALIZE AND READ IN VARIABLES FROM INPUT FILE

```

```

75
NS=0
NTR=0
NSAMP=0
NSEC=0
80 T0=0.
TF=0.
T=0.
USEROUT=.FALSE.
DATACHK=.FALSE.
85 PLOTEM=.FALSE.
NSTEP=0

```

```

C
C
C READ TITLE AND PRINT TO OUTPUT

```

```

90 CALL DATE(ADATE)
CALL TIME(ATIME)
READ(KIN,1000) TITLE
WRITE(KOUT,1001)TITLE,ADATE,ATIME

```

```

C
95 READ(KIN,IN)
WRITE(KOUT,IN)

```

```

C
NSTEP=INT(NSAMP*(TF-T0))+1

```

```

C
C
C INITIALIZE COMMON BLOCKS AND FIND FINAL TIME CONDITION

```

```

CALL ONCE(DATACHK)

```

```

C
C
C LOOP FOR SMOOTHER CALCULATIONS

```

```

105
10 CALL GETMINS
CALL GETPLUS
CALL MAKEA
CALL SMOOTHX
CALL SMOOTHP
110 CALL OUT(PLOTEM,USEROUT)
IF(T.EQ.T0) GOTO 20
GOTO 10

```

```

C

```

115

```
1000 FORMAT(20A4)
1001 FORMAT("1SMOOTHER1",10X,20A4,10X,2A10)
20 STOP "SMOOTHER1 FINISHED"
END
```

.158

```
1      SUBROUTINE ONCE(DATACHK)
      C
      C      CALLED ONLY ONCE PER RUN TO INITIALIZE ALL
      C      MATRICES AND FIND THE FINAL TIME CONDITION.
      C      CAN BE USED TO READ IN A TIME-INVARIANT MATRIX.
      C
      COMMON /MAIN1/ NDIM,NDIM1,COM1(10,10)
      COMMON /MAIN2/ COM2(10,10)
      COMMON /INOU/ KIN,KOUT,KPLOT,KDATA,KUSER
10     COMMON /DIM/ NS,NTR,NSEC,NSAMP,NSTEP
      COMMON /PHI/ PHI(10,10)
      COMMON /XFP/ XFPLUS(10)
      COMMON /XFM/ XFMINUS(10)
      COMMON /PFMV/ PFM(55)
15     COMMON /PFPV/ PFP(55)
      COMMON /PFM/ PFMINUS(10,10)
      COMMON /PFP/ PFPLUS(10,10)
      COMMON /A/ AMAT(10,10)
      COMMON /XFTF/ XFTF(10)
20     COMMON /PFTF/ PFTF(10,10)
      COMMON /TIME/ T,TO,TF
      LOGICAL DATACHK
      C
      C      ZERO ALL REQUIRED MATRICES AND VECTORS
      C
159 25     CALL ZROIZE(NS,NS,PHI)
      CALL ZROIZE(1,NS,XFPLUS)
      CALL ZROIZE(1,NS,XFMINUS)
      CALL ZROIZE(1,NTR,PFM)
30     CALL ZROIZE(1,NTR,PFP)
      CALL ZROIZE(NS,NS,PFPLUS)
      CALL ZROIZE(NS,NS,PFMINUS)
      CALL ZROIZE(NS,NS,AMAT)
      CALL ZROIZE(1,NS,XFTF)
35     CALL ZROIZE(NS,NS,PFTF)
      CALL ZROIZE(NDIM,NDIM,COM1)
      CALL ZROIZE(NDIM,NDIM,COM2)
      C
      C      READ IN TIME-INVARIANT PHI MATRIX
      C      IN THIS CASE, PHI WAS SIMPLY SET IN THE SUBROUTINE
      C
      DO 10 I=1,NS
      PHI(I,I)=1.0
10     CONTINUE
45     PHI(3,1)=0.05
      PHI(4,2)=0.05
      PHI(5,5)=.9512
      PHI(5,1)=.001229
      PHI(5,3)=.04877
50     C
      C      SEARCH DATA FILE FOR FINAL TIME AND SET INITIAL
      C      CONDITION FOR BACKWARD PROPAGATION
      C
      READ(KDATA,90) T,(XFTF(J),J=1,NS),(PFP(J),J=1,NTR)
55     90  FORMAT(F6.2,7E15.7,4(/7E15.7))
      C
      CALL MAKEP(NS,PFP,PFTF)
```



```

C
C   PRINT FINAL TIME CONDITIONS
60  C
      WRITE(KOUT,1000) T
      WRITE(KOUT,1001)
      DO 50 I=1,NS
        WRITE(KOUT,1002) I,XFTF(I)
65    50 CONTINUE
      WRITE(KOUT,1003)
      DO 60 I=1,NS
        WRITE(KOUT,1004) (PFTF(I,J),J=1,NS)
70    60 CONTINUE
      C
      1000 FORMAT("1SMOOTHER INITIAL CONDITION AT TF=",F6.2,".")
      1001 FORMAT("0STATE VECTOR AT FINAL TIME:")
      1002 FORMAT("0ELEMENT(",I2,")=" ,E13.5)
      1003 FORMAT("//,"0COVARIANCE MATRIX AT FINAL TIME:")
75    1004 FORMAT(1H010E13.5)
      C
      IF (DATACHK) STOP "FORMAT CHECK OF DATA COMPLETE"
      RETURN
      END
```

```
1      SUBROUTINE GETMINS
      C
      C      READS DATA FILE AND FINDS XFMINUS VECTOR AND
      C      PFM VECTOR. FILLS PFMINUS MATRIX.
5      C
      COMMON /XFM/ XFMINUS(10)
      COMMON /PFMV/ PFM(55)
      COMMON /PFM/ PFMINUS(10,10)
      COMMON /INOU/ KIN,KOUT,KPLOT,KDATA,KUSER
10     COMMON /DIM/ NS,NTR,NSEC,NSAMP,NSTEP
      COMMON /TIME/T,T0,TF
      C
      READ (KDATA,91) (XFMINUS(I),I=1,NS),(PFM(I),I=1,NTR)
      91  FORMAT(7E15.7,4(/7E15.7))
15     C
      C      FILL PFMINUS MATRIX
      C
      CALL MAKEP(NS,PFM,PFMINUS)
      C
20     RETURN
      END
```

```
1      SUBROUTINE GETPLUS
      C
      C      READS DATA FILE AND FINDS XFPLUS AND PFPLUS
      C      FOR PREVIOUS SAMPLE TIME. FILLS IN PFPLUS MATRIX.
5      C
      COMMON /INOU/ KIN,KOUT,KPLOT,KDATA,KUSER
      COMMON /DIM/  NS,NTR,NSEC,NSAMP,NSTEP
      COMMON /XFP/  XFPLUS(10)
      COMMON /PFPV/ PFP(55)
10     COMMON /PFP/ PFPLUS(10,10)
      COMMON /TIME/ T,T0,TF
      C
      READ (KDATA,92) T, (XFPLUS(I),I=1,NS),(PFP(I),I=1,NTR)
      92  FORMAT(F6.2,7E15.7,4(/7E15.7))
15     C
      C      FILL IN PFPLUS MATRIX
      C
      CALL MAKEP(NS,PFP,PFPLUS)
      C
20     RETURN
      END
```

```
1      SUBROUTINE MAKEA
      C
      C      COMPUTES SMOOTHER GAIN MATRIX, A
      C      REQUIRES A MATRIX INVERSE ROUTINE
5      C      AND A MATRIX MULTIPLICATION ROUTINE.
      C
      COMMON /MAIN1/ NDIM,NDIM1,COM1(10,10)
      COMMON /INOU/ KIN,KOUT,KPLOT,KDATA,KUSER
10     COMMON /DIM/ NS,NTR,NSEC,NSAMP,NSTEP
      COMMON /PHI/ PHI(10,10)
      COMMON /PFP/ PFPLUS(10,10)
      COMMON /PFM/ PFMINUS(10,10)
      COMMON /A/ AMAT(10,10)
      C
15     DIMENSION PFINV(10,10), A1(10,10), A2(10,10)
      C
      C      EQUATE DUMMY MATRIX WITH PFMINUS
      C
      CALL EQUATE(A1,PFMINUS,NS,NS)
20     C
      C      INVERT PFMINUS, PRINT ERROR MESSAGE IF PFMINUS
      C      IS OF DEFICIENT COMPUTATIONAL RANK TO INVERT
      C
      MT=1
25     CALL GMINV(NS,NS,A1,PFINV,MR,MT)
      C
      C      MULTIPLY PHI MATRIX BY PFINV
      C
      CALL MAT1(PHI,PFINV,NS,NS,NS,A2)
30     C
      C      COMPUTE AMAT MATRIX (AMAT=PFPLUS*A2)
      C
      CALL MAT1(PFPLUS,A2,NS,NS,NS,AMAT)
      C
35     RETURN
      END
```


1 SUBROUTINE MAKEP(N,PIN,POUT)
C
C FILLS IN FULL MATRIX FROM A VECTOR MATRIX
C STORED IN UPPER TRIANGULAR FORM.
5 C PIN IS STORED IN THE FOLLOWING ORDER:
C
C PIN(1)=P(1,1)
C PIN(2)=P(1,2)
10 C PIN(3)=P(2,2)
C
C .
C ETC.
C
C DIMENSION PIN(55), POUT(10,10)
15 C
C ICOL=1
C N1=1
20 DO 10 I=1,ICOL
C POUT(I,ICOL)=PIN(N1)
C N1=N1+1
20 10 CONTINUE
C IF (ICOL.EQ.N) GOTO 30
C ICOL=ICOL+1
C GOTO 20
25 C
30 C N1=1
C N2=2
60 DO 40 J=N2,N
C POUT(J,N1)=POUT(N1,J)
30 40 CONTINUE
C IF (N2.EQ.N) GOTO 50
C N1=N1+1
C N2=N1+1
C GOTO 60
35 C
50 C RETURN
C END

1 SUBROUTINE SMOOTHX
C
C COMPUTES THE "SMOOTHED" ESTIMATE OF STATE VECTOR
C AS IT PROPAGATES BACKWARD IN TIME.
5 C REQUIRES VECTOR ADDITION AND VECTOR MULTIPLICATION
C ROUTINES TO BE USED.
C
COMMON /DIM/ NS,NTR,NSEC,NSAMP,NSTEP
COMMON /XFP/ XFPLUS(10)
10 COMMON /XFM/ XFMINUS(10)
COMMON /A/ AMAT(10,10)
COMMON /XFTF/ XFTF(10)
C
C DIMENSION A(10), B(10), C(10)
15 C
C EQUATE A DUMMY VECTOR A TO XFTF
C AND FIND THE DIFFERENCE BETWEEN XFTF AND
C XFMINUS
C
20 DO 10 I=1,NS
A(I)=XFTF(I)
10 CONTINUE
CALL VADD(NS,-1.0,A,XFMINUS)
C
25 C COMPUTE AMAT TIMES VECTOR DIFFERENCE
C
CALL VMAT1(AMAT,A,NS,NS,B)
C
C COMPUTE NEW XFTF VECTOR(SMOOTHED ESTIMATE)
30 C
DO 20 I=1,NS
C(I)=XFPLUS(I)
20 CONTINUE
CALL VADD(NS,1.0,C,B)
35 C
C SET NEW ESTIMATE
C
DO 30 I=1,NS
XFTF(I)=C(I)
40 30 CONTINUE
C
RETURN
END

1 SUBROUTINE SMOOTHP
C
C COMPUTES THE "SMOOTHED" COVARIANCE MATRIX AS
C IT PROPAGATES BACKWARD IN TIME.
5 C REQUIRES MATRIX ADDITION AND MULTIPLICATION
C ROUTINES TO BE USED.
C
COMMON /MAIN1/ NDIM,NDIM1,COM1(10,10)
COMMON /DIM/ NS,NTR,NSEC,NSAMP,NSTEP
10 COMMON /PFP/ PFPLUS(10,10)
COMMON /PFM/ PFMINUS(10,10)
COMMON /A/ AMAT(10,10)
COMMON /PFTF/ PFTF(10,10)
C
15 DIMENSION PDIFF(10,10), APAT(10,10)
C
C COMPUTE DIFFERENCE BETWEEN PFTF AND PFMINUS
C
CALL MADD1(NS,NS,PFTF,PFMINUS,PDIFF,-1.0)
20 C
C COMPUTE MATRIX PRODUCT AMAT*PDIFF*AMAT(T)
C
CALL MAT3(NS,NS,AMAT,PDIFF,APAT)
C
25 C COMPUTE NEW VALUE FOR PFTF
C
CALL MADD1(NS,NS,PFPLUS,APAT,PFTF,1.0)
C
30 RETURN
END

[REDACTED]
[REDACTED]

[REDACTED]
[REDACTED]
[REDACTED]

[REDACTED]

[REDACTED]
[REDACTED]

[REDACTED]

[REDACTED]
[REDACTED]

[REDACTED]

[REDACTED]

[REDACTED]

[REDACTED]
[REDACTED]

[REDACTED]
[REDACTED]

[REDACTED]

CARD NR.	SEVERITY	DETAILS	DIAGNOSIS OF PROBLEM
41	I	23 CD 42	TOTAL RECORD LENGTH IS GREATER THAN 137 CHARACTERS. IT MAY EXCEED THE I/O DEVICE CAPACITY.
43	I	56 CD 43	FIELD WIDTH IS GREATER THAN 137 CHARACTERS. IT MAY EXCEED THE I/O DEVICE CAPACITY.
43	I	59 CD 43	TOTAL RECORD LENGTH IS GREATER THAN 137 CHARACTERS. IT MAY EXCEED THE I/O DEVICE CAPACITY.
44	I	20 CD 45	FIELD WIDTH IS GREATER THAN 137 CHARACTERS. IT MAY EXCEED THE I/O DEVICE CAPACITY.
44	I	23 CD 45	TOTAL RECORD LENGTH IS GREATER THAN 137 CHARACTERS. IT MAY EXCEED THE I/O DEVICE CAPACITY.

```
1      SUBROUTINE ZROIZE(M,N,A)
      C
      C      ZEROS AN M X N MATRIX, A
      C
5      C      DIMENSION A(10,10)
      C
      DO 10 I=1,M
      DO 20 J=1,N
      A(I,J)=0.
10      20 CONTINUE
      10 CONTINUE
      C
      RETURN
      END
```

Bibliography

1. Fraser, D.C. A New Technique for the Optimal Smoothing of Data, Ph.D. Dissertation, Massachusetts Institute of Technology, Cambridge, June 1967.
2. Fraser, D.C. and J.E. Potter. "The Optimum Linear Smoother as a Combination of Two Optimum Linear Filters." IEEE Transactions on Automatic Control VII, 4: 387-390. (1969).
3. Hamilton, D.E. Evaluation of the Land Speed of Sound Record Attempt by the Budweiser Rocket Car, unpublished historical report, Edwards AFB, CA, July 1982.
4. Maybeck, P.S. Stochastic Models, Estimation, and Control, Volume I and II, Wright-Patterson AFB, OH, 1982.
5. Meditch, J.S. "On Optimal Linear Smoothing Theory," Information and Control, XX, 598-615. (1967).
6. Musick, S.H. "SOFE: A Generalized Digital Simulation for Optimal Filter Evaluation, User's Manual," Technical Report, AFWAL-TR80-1108, Wright-Patterson AFB, OH, October 1980.
7. Musick, S.H. et. al. "SOFEPL: A Plotting Postprocessor for SOFE User's Manual," Technical Report, AFWAL-TR-80-1109, Wright-Patterson AFB, OH, November 1981.
8. Neter, J. et. al. Applied Statistics, Boston, 1978.

VITA

Captain David A. Reinholz was born on [REDACTED] n [REDACTED]. He graduated from high school in Delavan, Wisconsin, in 1970 and attended the United States Air Force Academy from which he received a Bachelor of Science in Aeronautical Engineering in June 1974. He completed pilot training and received his wings in August 1975. He served as a C-130 pilot in the 41st Tactical Airlift Squadron, Pope AFB, North Carolina from January 1976 to April 1979. From May 1979 to April 1982 he served as an instructor pilot and Undergraduate Pilot Training Class Commander in the 47th Flying Training Wing, Laughlin AFB, Texas. He entered the School of Engineering, Air Force Institute of Technology, in June 1982.

Permanent address: [REDACTED]